BETA 1 INTEGRINS IN BONE FORMATION DURING DEVELOPMENT AND ENGINEERED INTEGRIN-SPECIFIC HYDROGELS FOR ENHANCED BONE HEALING IN SEGMENTAL DEFECTS

A Dissertation
Presented to
The Academic Faculty

by

Asha Shekaran

In Partial Fulfillment
of the Requirements for the Degree
Doctor of Philosophy in the
Wallace H. Coulter School of Biomedical Engineering

Georgia Institute of Technology
May 2013

THE ROLE OF BETA 1 INTEGRINS IN BONE FORMATION AND ENGINEERED INTEGRIN-SPECIFIC HYDROGELS FOR ENHANCED BONE HEALING IN SEGMENTAL DEFECTS

Approved by:

Dr. Andrés J García, Advisor
School of Mechanical Engineering
Georgia Institute of Technology

Dr. Todd McDevitt
Department of Biomedical Engineering
Georgia Institute of Technology

Dr. Barbara D Boyan
School of Engineering
Virginia Commonwealth University

Dr. Julie Champion
School of Chemical and Biomolecular Engineering
Georgia Institute of Technology

Dr. Robert Guldberg
School of Mechanical Engineering
Georgia Institute of Technology

Date Approved: February 28, 2013

To my family and friends.

ACKNOWLEDGEMENTS

I would first like to thank my advisor Andrés García for his scientific guidance, unwavering support, contagious excitement about research, inspiring pep talks and commitment to always making time for his students. I've learned many important science and life lessons from Andrés such as: silicone grease will fix anything, the experiment can always be done by yesterday, always look for the 'parsimonious' explanation, and most importantly, the numerous reasons for which "that's why I'm the PI!" Andres, it's been a pleasure working in your lab, and thank you for your mentorship and encouragement!

I would also like to thank the members of my thesis committee for sharing their expertise with me and for providing valuable feedback and guiding my graduate work as well. My thanks to Dr Barbara Boyan, who guided me on important aspects of bone biology and BMP-2 therapies, Dr Bob Guldberg for his invaluable expertise on segmental defect animal models, bone healing in response to BMP-2-based biomaterial therapies and analyses for the bone defect studies, Dr Todd McDevitt for his keen insight on stem cells and regenerative medicine strategies and Dr Julie Champion for her expert advice on drug delivery and therapeutic biomaterials.

I also want to thank all the members of the Garcia lab, both past and present, for showing me the ropes, helping me in lab, sharing their ideas, assisting me in my surgeries, for random time-wasting discussions and/or funny video watching in the lair of inefficiency, and fun times together on Carver's runs, zombie apocalypse training sessions or at conferences. I'm very thankful that I had the opportunity to work in a lab

where the people are energetic, smart, motivated, fun and interesting in many different ways. The brilliant Abbey Wojtowicz and Tim Petrie taught me to harvest primary cells, perform surgery, operate the SPR (aka Tim's girlfriend), set up SAMs and of course, to work with GFOGER! Dave Dumbauld is a meticulous scientist and was my wonderful next-desk buddy who would lend a helping hand me whenever I had to reach something on a high shelf and was always happy to teach me new lab techniques (thanks, Dave!). Kellie Templeman is of course, indispensable to this lab. She's super-efficient, organized, a great friend and completely hilarious. Kellie, thanks for all your help with surgeries, with ordering, for the million other things you do and for the great lunch-time conversations! I've also been extremely fortunately to work with and mentor very hardworking and talented undergraduate students. Thanks to Nick Cheng for his excellent work on bone IHC and radial mechanical testing. And Taylor Kavanaugh is a brilliant student who juggles classes, research, RA responsibilities and work in the PRL with enviable ease. Taylor has worked with me on many surgeries and developed a transgenic system to image osteoprogenitor invasion into the radial defect. Taylor, thank you for all your help. I know you have a promising career in science ahead of you, and good luck in your senior year! Other lab mates who have made our lab a wonderful place to work in include Sean Coyer, who always had a good story to tell, Ed Phelps, a natural-born (zombie) killer and our PEG-maleimide hydrogel pioneer, Rachel Whitmire, our type-A personality lab cleanup-organizer and the only person who could sing "Happy Birthday" in tune, and Ram Selvam, our ever-so-quotable and perpetually cheerful IVIS king. I must also thank Susan Lehman (phage-girl), our resident microbiologist for her help on numerous surgeries and for her hard work in trying to destroy the bone healing response

of my biomaterial with bacteria. Imen is a wonderfully helpful lab mate and I've had fun times working with her on cell isolations. To our lab's dynamic duo, Ankur Singh and Shalu Suri, thanks for sharing your delicious home-cooked Indian food with me and for offering me great scientific advice. I have to especially thank Ankur who is an inspiring and brilliant postdoc for always showing me pictures of food in the morning and making me hungry way before lunch time, as well as for all the valuable career advice he's given me. I also want to thank the current members of this lab have made my time in graduate school a truly wonderful experience. Nduka Enemchukwu is the kindest, most warm-hearted person I know and I have to thank him for many thought-provoking science or philosophy discussions while doing tissue culture. Our lab is blessed with many talented and enthusiastic bakers, but foremost among them is Stacie Gutowski (who is incidentally and unbelievably also Andrés' personality twin). Stacie, thanks for all the amazing cakes, cupcakes and cookies you've brought to lab for birthdays, proposals, defenses to make those events feel more special, for fun evenings watching plays at Woodruff, and for your help with my surgeries. Chi-Chi is an energetic and efficient organizer and was my co-committee chair for both the BBUGS Research Committee and the Technique Symposium. Ted Lee is our smart, fun, loud, and opinionated Mr Fix-it who also has an impressive ability to spend large sums of money on fancy new lab equipment. Thanks Ted, for ensuring that I would never have to manually back up the computers ever again. Amy Cheng is a talented researcher who has helped me on many surgeries. She is also an excellent surgeon and now guardian of the bone cutters. Apoorva is ambitious, multitalented and can Gangnam Style like no other! Devon is a doer and a unique personality even within a lab of very unique people. Devon, thanks for attempting

to teach me to whistle, although I never figured it out (good thing I have a PhD!) Jose is always upbeat, a veteran assistant for my surgeries (thanks!), master of the thin gels and a quick study, which is probably why he also serves as a living repository of specialized protocols from all graduating PhD students. Efrain is witty and funny and a great lab mate to have around. To honorary and visiting members of the lab who were around for a short while, but left a big impression, I enjoyed getting to know you too. Thanks to Julia Henkels and Patricia Pacheco for brining/roasting thanksgiving turkeys, organizing girls' night parties, baking chocolate flan and for evenings watching plays and musicals at the Woodruff Arts Center. Simone Weis works constantly and with a passion and says the most hilarious things without even meaning to. In her time here, she dominated the quote board. Nina Dinjasky is cheerful and her interesting presentations (together with Susan's) have made me a fan of microbiology.

Outside of the Garcia Lab, I want to thank other people without whom my work would not have been possible. Thanks to Angela Lin, the microCT and mechanical testing expert, for going out of her way with help and advice on how to set up scans or tests and how best to analyze data. Dr Yuhong Fan provided me with valuable advice on lab techniques as well as experimental design in my work with transgenic animals. JT Shoemaker provided me with valuable assistance with embryo dissections and I especially want to thank all the members of the PRL staff including Andrea Gibson, Odell Neal, Ogeda Blue, Altair Rivas, Josh Scarborough, Kim Benjamin as well as Dr O'Farrell for their hard work and help which was essential to all my in vivo work. I'd like to also thank all the members of Wing 2D including Nick Willett, Brent Uhrig, Ashley Allen, Chris Dosier, Tanu Tote, Alice Li, Jason Wang, David Reese, Laxmi Krishnan,

Lauren Priddy, Albert Cheng and Hazel Stevens for their help, advice, and for helping make the lair of inefficiency live up to its name. Aqua Asberry's histology expertise was also crucial to my work. Megan McDevitt and Colly Mitchell were great resources when I was organizing events for BBUGS and Sally Gerrish and Shannon Sullivan made sure that I was on track and submitting the right forms to fulfill the BME program requirements.

To my friends in Atlanta, thanks for all the great times here and helping make grad school more fun! I have to thank the Sunday dinner/ Dim sum/ Singaporeans andfriends group for all the times spent over delicious Buford Highway food – Vivek Kumar, Peng Meng Kou, Robert Lychev, Ji Han, Taylor Choi, Weiyin Xu, YS, Julia Raykin, Jeannie Lee, Danny Lee and Gopi Jayaprakash. I'd like to also acknowledge Julia Raykin for her Matlab program for analyzing mechanical testing data. My next special mention goes out to all the past and present members of my pool team for many fun Monday nights and weekend lunch pool at Mr Cues including Steve Feng, Aaron Harris, Darshini Nanavati, Jake Laas, Will Mathurin, Rob Lesesne, Risa Lin, and Ashley Rice, Ryan Hooper and Ben Roller. Thanks also to the second-generation poker group for allowing me to take your money every now and then, for fun discussions, and for reminding me that in no limit hold'em, as in life, intimidation is more important than math skills. I've also received constant encouragement from my best friend since first grade, Divya Pradha and my college roommate from Northwestern, Ritu Chaturvedi. I'd also like to thank some of my close friends in the A*STAR fellowship program for their scientific advice, for commiserating about graduate school, and for random vacations

together around Thanksgiving or Christmas when most students would go home, and for inspiring me by publishing in say, Nature.

I would especially like to thank Daniel Keeney for his support, encouragement, open and adventurous spirit, humor and excellent taste in tv shows. Daniel is remarkably decisive and purposeful, yet also warm, relaxed and unflappable in the face of challenges. Daniel has been a source of calm and goofy jokes in times when research was stressful. I would also like to thank Daniel's family for their support and kindness and for making me a part of their holiday season celebrations.

And finally, I am blessed with a wonderful family who has given me their love and unconditional support throughout my life. My parents L Shekaran and Kana Gopal have raised me and given everything I could possibly want growing up, and they've always trusted my judgment and supported all my decisions unreservedly. I can't thank them enough for that. I also want to thank my awesome twin brother Anand Shekaran for always making me laugh. I enjoyed seeing Anand when he was in Atlanta for a semester and I'm lucky to have an irreverent, funny brother who is always there for me. Finally, I want to thank my grandparents Lutchumanan, Devanai, Gopal and Manomany, who I always admired for embodying the humble, disciplined, hard-working, and self-sacrificing family values that are typical of immigrants. Their advice to me in Tamil as a girl was always "Study hard." My grandparents never wanted expensive things for themselves; they worked hard to ensure that their children and grandchildren would have the educational opportunities they never had. I miss my grandparents most at major milestones in my life such as this one because I think they would have felt very proud to see me now. I dedicate this work most of all to the memory of my grandparents.

TABLE OF CONTENTS

LIST OF TABLES

LIST OF FIGURES

LIST OF SYMBOLS AND ABBREVIATIONS

Itgβ1	beta 1 integrin
ECM	extracellular matrix
BMP	bone morphogenetic protein
rhBMP-2	recombinant human bone morphogenetic protein 2
CT	computed tomography
DBM	demineralized bone matrix
FAK	focal adhesion kinase
OSX	osterix, also known as Sp7
OCN	osteocalcin
TW2	Twist 2, also known as Dermo 1
ERK	extracellular-signal related kinase
hMSC	human mesenchymal stem cell
PEG	polyethylene glycol
GFOGER	synthetic triple helical ligand containing ‘GFOGER’ hexapeptide sequence
RGD	GRDGSPC adhesive peptide
VPM	bi-cysteine peptide crosslinker containing MMP-sensitive cleavage site
ICM	inner cell mass
WT	wild-type
cKO	conditional knockout
MUP	Methylumbelliferyl phosphate
FMT	Fluorescence molecular tomography
PCL	Polycaprolactone

itgβ1$^{cKO\ (TW2)}$ conditional beta 1 integrin knockout under the twist 2 promoter, itgβ1$^{fl/fl}$-TW2cre genotype

het itgβ1$^{cKO\ (TW2)}$ heterozygous for conditional beta 1 integrin knockout under the twist 2 promoter, itgβ1$^{fl/+}$- TW2cre genotype

itgβ1$^{cKO\ (OSX)}$ conditional beta 1 integrin knockout under the osterix promoter, itgβ1$^{fl/fl}$-OSX-cre genotype

het itgβ1$^{cKO\ (OSX)}$ heterozygous for conditional beta 1 integrin knockout under the twist 2 promoter, itgβ1$^{fl/+}$- OSXcre genotype

itgβ1$^{cKO\ (OCN)}$ conditional beta 1 integrin knockout under the osteocalcin promoter, itgβ1$^{fl/fl}$- OCN-cre genotype

het itgβ1$^{cKO\ (OCN)}$ heterozygous for conditional beta 1 integrin knockout under the twist 2 promoter, itgβ1$^{fl/+}$- OCNcre genotype

SUMMARY

Bone formation is a complex physiological process which is orchestrated by multiple microenvironmental cues such as soluble factors, cell-cell interactions and the extracellular matrix. Integrins are heterodimeric transmembrane receptors consisting of α and β subunits which mediate cell interactions with the extracellular matrix. Beta 1 integrins encompass the majority of integrins and represent the main integrin binding partners of collagen I, the most abundant extracellular matrix component of bone. The central goals of this dissertation project were to elucidate the role of β1 integrins on bone development and healing *in vivo*, and to design biomimetic α2β1 integrin-specific polyethylene glycol hydrogels to enhance bone healing within segmental bone defects.

Because global β1 knockout mice are embryonically lethal, in order to study the role of β1 integrins *in vivo*, we used the Cre-Lox system to generate mice with conditional beta 1 integrin deletions in osteolineage cells at three stages: (1) mesodermal cells [under Twist 2/Dermo 1], (2) osteoprogenitors [under the osterix promoter] and (3) mature osteoblasts and osteocytes [under the osteocalcin promoter]. We found that β1 integrin deletion in mesodermal cells severely impaired pre-natal skeletal mineralization, particularly in the calvarium, and also resulted in late-stage embryonic lethality. In contrast, β1 integrin deletion in pre-osteoblasts resulted in viable but runted mice with decreased cranial mineralization, tooth defects, impaired femur development and some perinatal mortality. Finally, mice with β1 integrin null osteoblasts and osteocytes displayed very mild bone phenotypes with no change in femur fracture healing capacity. Taken together, these results suggest that β1 integrins play an important role in

the early bone formation process but are not essential for the function of mature osteoblasts and osteocytes.

We also sought to engineer a biomimetic bone graft substitute by incorporating the following two bioactive components into a matrix metalloproteinase (MMP)-sensitive synthetic polyethylene glycol (PEG) hydrogel: (1) the collagen I-mimetic triple-helical synthetic ligand GFOGER, which specifically binds to the pro-osteogenic α2β1 integrin, and (2) recombinant human bone morphogenetic protein 2 (rhBMP-2). We synthesized PEG hydrogels incorporating GFOGER or the commonly used non-integrin selective adhesive peptide, RGD, in equimolar densities and studied hMSC differentiation responses to each of these surfaces. We then examined the effects of treating murine radial segmental defects with either GFOGER functionalized PEG-MAL hydrogels or GFOGER gels which also incorporated a low dose of rhBMP-2. Our data indicated that GFOGER hydrogels enhanced bone healing compared to empty defects and that incorporating low dose rhBMP-2 in GFOGER gels further improved bone formation. We evaluated the roles of the GFOGER ligand and the MMP-sensitive crosslinker, GCRDVPMSMRGGDRCG (VPM), in this response by comparing bone formation in defects treated with non-degradable hydrogels, degradable hydrogels lacking the GFOGER ligand, and in defects treated with degradable GFOGER hydrogels. Minimal bone formation occurred in response to PEG hydrogels which were not functionalized with any adhesive ligand and there was no bone formation in non-degradable PEG hydrogels, indicating that adhesive function and degradability are essential to bone regeneration in response to GFOGER hydrogels. Our examination of rhBMP-2 dose response within GFOGER hydrogels suggested that low 0.02mg/ml (0.03 μg) dose was

sufficient for robust healing, but that the medium 0.04 mg/ml (0.06 μg) dose increased bone volume and mineral density within the defect compared to the low dose. The high 0.2 mg/ml (0.3 μg) BMP-2 dose induced less bone formation within the defect than the medium dose and altered the structure of the ulna so that it encircled the radius and fused with the radius. FMT analysis and *in vitro* BMP release assays revealed that GFOGER hydrogels provided sustained release of rhBMP-2. Finally, we evaluated the bone regeneration capacity of low dose rhBMP-2 delivery from GFOGER functionalized PEG hydrogels in comparison with collagen sponges, the clinical standard for BMP-2 delivery. We observed superior bone healing in response to GFOGER hydrogel treatment. In conclusion, our bioengineered integrin-specific hydrogel may be a promising bone graft substitute for the treatment of large bone defects.

CHAPTER 1: SPECIFIC AIMS

INTRODUCTION

Skeletal development and bone healing are complex processes involving multiple microenvironmental cues including extracellular matrix-integrin interactions. Integrins mediate important cell functions such as survival, adhesion, proliferation, migration and differentiation. The β1 integrin sub-family of integrins encompasses 12 out of 24 known integrins and primarily mediate cell adhesion to collagen I, the major ECM component of bone. β1 integrins, especially α2β1 integrins and α5β1 are highly expressed in mesenchymal stem cells and osteoprogenitors and are implicated in *in vitro* osteoblastic differentiation and mineralization[1-10]. Despite significant *in vitro* evidence that β1 integrins play a crucial role in differentiation, *in vivo* perturbations of β1 integrins have yielded contradictory results as some conditional β1 integrin deletions have exhibited no skeletal phenotype[11, 12], and dominant negative mutations have displayed only mild skeletal phenotypes[13]. Additionally, in the orthopedic biomaterials field, most ECM-mimetic or bioadhesive strategies have not targeted the previously mentioned pro-osteogenic integrins, but focused primarily on using the short RGD tripeptide sequence which is a promiscuous integrin binding partner.

Over 1 million bone grafting, bone excision and fracture repair procedures are performed each year in the United States, at cost of approximately $5 billion [14-17]. While autografts are the gold standard treatment for large bone defects, they are limited by availability and donor site pain. Growth factor treatments such as BMP therapy provide a promising alternative but are expensive and present clinical safety concerns, primarily due to delivery of BMPs at supraphysiological doses. Therefore, there remains an unmet clinical need for safer, more effective bone graft substitute biomaterials. Understanding the role of integrins on bone formation and exploiting desirable ECM-integrin interactions may enable modulation of host cells for improved orthopaedic therapies.

The two main objectives of this project are to (1) elucidate the role of β1 integrins on bone formation *in vivo* and (2) engineer a biofunctionalized α2β1 integrin-specific PEG hydrogel to promote bone healing in segmental defects. Our hypothesis is that β1 integrins play an important early role in bone formation *in vivo*. We also hypothesize that degradable PEG hydrogels modified with the α2β1 integrin-specific ligand GFOGER will promote bone healing within a critical-sized defect *in vivo*. These objectives will be accomplished through the completion of the following aims:

SPECIFIC AIM I

Define the role of beta 1 integrins on bone formation by inducing targeted β1 integrin deletions in osteolineage cells at three stages of differentiation: 1) mesodermal lineage cells, 2) osteoprogenitor cells, and 3) mature osteoblasts/ osteocytes.

β1 integrins are believed to play an important role in bone formation as β1 integrins are highly expressed in osteoblasts, osteoprogenitors and bone marrow stromal cells. Furthermore, blocking of multiple β1 integrins such as α2β1[2-6, 10], α5β1[7-9], α1β1 [4, 6] and α3β1 [8] in these cells severely impairs *in vitro* osteogenic differentiation and mineralization. However, *in vivo* deletion or functional perturbation of β1 integrins results in only mild skeletal phenotypes. For example, transgenic mice expressing a dominant negative mutant form of the β1 integrin under the 1.8kb rat osteocalcin promoter display minor changes in skeletal development [13, 18, 19]. These mild phenotypes include transient decreases in parietal thickness caused by increased osteoclast activity and altered canalicular structure in osteocytes[13], decreased cancellous bone mass, decreased tibial curvature, and defective response to hindlimb unloading[18], as well as transient decreases in tibial length, ash weight and dry weight, with no changes to femur mechanics[19]. β1 integrin deletion under the osteoblast-specific Col I 2.3kb promoter [20] yielded no change in the skeletal structure of transgenic mice[11, 12]. Because β1 integrins

are essential for embryonic development, global β1 integrin knockout mice cannot be used for studies of *in vivo* β1 integrin function[21]. In order to evaluate the *in vivo* role of β1 integrins on bone formation, we will ablate β1 integrins in osteolineage cells at early, intermediate and late stages of differentiation by generating three different conditional knockout animals. Specifically, we will breed β1 integrin floxed mice with: 1) Twist 2 Cre mice in order to delete β1 integrins in mesodermal lineage cells (Twist 2 Cre is expressed at E9.5 in brachial arches and somites and at E11.5 in mesenchymal condensations in mice), 2) Osterix Cre mice in order to ablate β1 integrins in osteoprogenitor cell (Osterix Cre mice express cre in committed osteoprogenitors in bones derived from both osteochondral and intramembranous ossification from E14.5 onwards), and 3) Osteocalcin Cre mice to induce β1 integrin deletion in mature osteoblasts/ osteocytes. We *hypothesize* that β1 integrins play an important early role in skeletal development.

SPECIFIC AIM II

Evaluate the bone healing induced by GFOGER-modified PEG hydrogels incorporating low dose rhBMP-2 within segmental bone defects.

Although BMP therapies have shown promise as bone graft substitutes, due to limitations in release mechanisms of currently used biomaterial carriers, they are delivered at doses which far exceed physiological concentrations, resulting in high costs and potential complications[22-24]. Tissue engineering strategies for bone regeneration have largely focused on functionalizing materials with the promiscuous RGD peptide, which lacks of modulatory domains or other features found in native ECM ligands as well as specificity to pro-osteogenic integrins. Our group has previously engineered a collagen-derived ligand, GFOGER, which mimics the triple helical structure of collagen to which cells adhere by specific binding of the α2β1 [25] integrin, which is implicated in osteoblastic differentiation and mineralization. In this study, we engineered fully

synthetic, protease degradable PEG-maleimide hydrogels which incorporate the pro-osteogenic GFOGER ligand and low-dose rhBMP-2. We hypothesized that by targeting the α2β1 integrin using the GFOGER adhesive ligand and by also providing sustained, 'on-demand' release of low-dose rhBMP-2 we could promote osteoblastic differentiation of host cells and promote bone regeneration *in vivo*.

.

SIGNIFICANCE

This work is significant and innovative because understanding β1 integrin effects on bone may have implications in regenerative medicine, and may further elucidate the mechanism of bone diseases which involve altered ECM interactions. Furthermore, the study of β1 integrins utilizes novel transgenic models to ablate β1 integrins in osteolineage cells at multiple different stages, whereas previous works have focused on conditional β1 integrin deletions in mature osteoblasts. The study of GFOGER/rhBMP-2 hydrogels is innovative and significant because it will develop a completely synthetic, highly tunable biomaterial which focuses on engineering pro-osteogenic α2β1 integrin-specificity in combination with controlled release of rhBMP-2 in order to induce robust bone regeneration. We expect that the development of GFOGER/low dose rhBMP-2 hydrogels will represent a promising and clinically-relevant strategy for the treatment of large bone defects by promoting bone healing while also providing a potentially safe and low-cost therapy by decreasing the dose of rhBMP-2 required in order to bridge those defects.

CHAPTER 2: LITERATURE REVIEW*

INTEGRINS

Integrins are a family of receptors which primarily mediate adhesion of cells to the extracellular matrix proteins such as collagen and fibronectin [26]. Integrins are heterodimeric transmembrane proteins, each of which consists of α and β subunits. Currently, 8 β and 18 α integrin subunits are known, and these subunits associate non-covalently to form 24 distinct αβ integrin combinations, each with unique binding characteristics (Figure. 2.1). X-ray crystallography analysis of integrin structure demonstrates a globular head connected to rod-like tails, and includes a flexible "knee" region which is involved in the activation state of the integrin. Integrins are capable of transducing signals in both directions across the cell membrane. For example, "outside-in" signaling occurs when ECM ligation to integrins trigger intracellular signaling. Conversely, "inside-out" signaling takes place when intracellular signals modulate integrin activation state and thus change its affinity for its extracellular ECM ligand [27]. Upon ECM binding to their extracellular domains, integrins cluster and their cytoplasmic domains associate with both cytoskeletal and intracellular signal transduction molecules. The association of integrins with the cellular signaling network initiates downstream signaling cascades such as the FAK, protein kinase C, Rac, Rho and MAPK pathways.

---

* Adapted from Shekaran, A., Garcia, A.J., Extracellular matrix-mimetic adhesive biomaterials for bone repair. J Biomed Mater Res A. 2011 96(1): 261-72

The coordinated clustering of ECM ligands, integrins and cytoskeletal components forms macromolecular aggregates known as focal adhesions on the inside and outside of the cell membrane [28]. Because of the central roles of integrin-mediated adhesion to important cellular responses such as survival, growth, migration and differentiation [27, 29, 30], materials strategies which harness ECM-integrin interactions may play a key role in eliciting desired cellular responses *in vivo*.

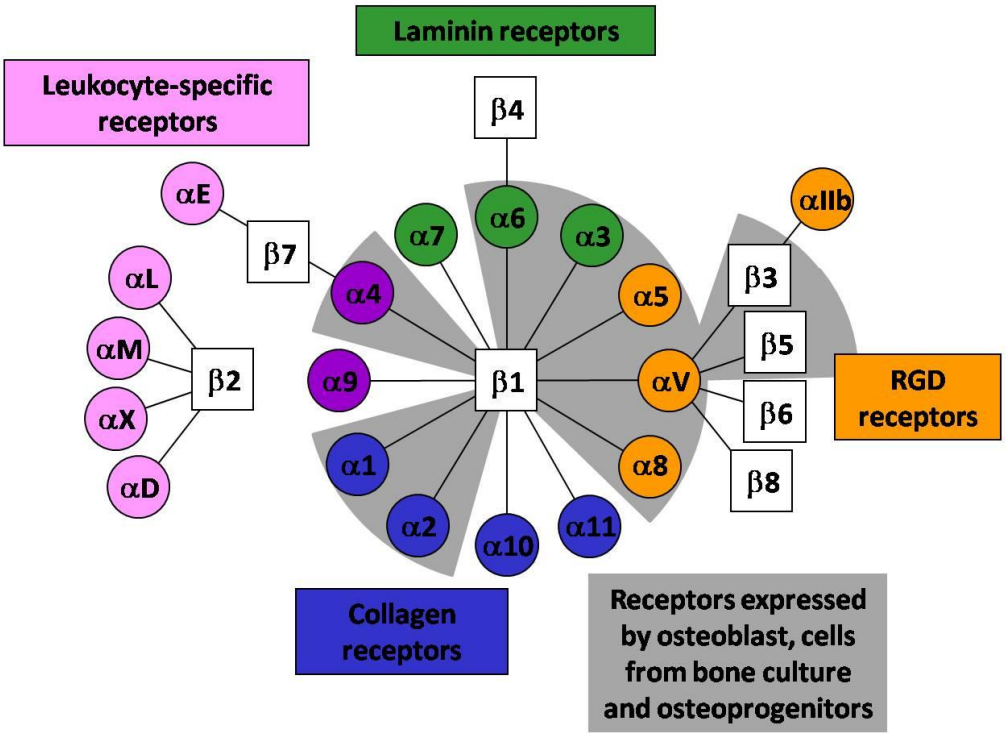

Figure 2.1. Integrin alpha and beta subunit combinations, binding specificity and expression in bone cells. Adapted from Hynes[26].

INTEGRINS IMPLICATED IN BONE FORMATION

The β1 sub-family integrins are the mostly highly expressed integrins in osteoblasts and the predominant mediators of cell adhesion in these cells[31], although

osteoblasts may express the β3 and β5 subunits as well[32, 33]. α subunit expression data has been more inconsistent, with different combinations of α1, α2, α3, α4, α5 and αv subunits having been detected by immunohistochemistry in human and rat bone[32-36]. The expression of the previously mentioned alpha subunits has also variously been determined by flow cytometry, immunoprecipitation, immunocytochemistry and Northern blot analysis on primary bone cultures[31-33, 37-40]. Although reports of α subunit and integrin heterodimer expression in osteoblasts have sometimes been contradictory, multiple studies have identified the α1β1, α2β1, α3β1, α5β1, αvβ3 integrins and their subunits in osteoblasts and bone cultures[31, 35, 39, 40]. A few isolated studies have also found osteoblast expression of α6β1[40], α8β1[8], αvβ1[37] and αvβ5[31]. Integrin expression studies on osteoprogenitor cells have shown similar profiles as osteoblasts, as Gronthos et al. reported the detection of α1β1, α2β1, α5β1, α6β1, αvβ3 and αvβ5 on STRO-1 expressing human bone marrow stromal cells[6] (Table 2.1, Figure. 2.1).

Table 2.1. Composition of Bone Matrix. Composition of bone ECM. Itg – Integrins, Col – Collagen, HAP – Hydroxyapatite, Ca – Calcium, TSP – Thrombospondin.

		Molecular Weight	Function/regulates	Binds To
Organic	Collagens			
	Type I	-	Scaffolding, most abundant	Many
	Type X	-	Present in hypertropic cartilage	-
	Type III	-	Col fibril diameter	-
	Type V	-	Col fibril diameter	-
	Adhesion proteins			
	Fibronectin	~ 400kD	Adhesion	Itg, Col, heparin,
	Thrombospondin	~ 450 kD	Adhesion, bone formation	Ca, HAP, OSN
	Vitronectin	~ 70kD	Adhesion	Itg, Col, heparin,
	Osteopontin	~44-75kD	Adhesion, proliferation, resorption	Itg
	Osteonectin	~35-45kD	HAP deposition, bone formation	Ca, HAP, Col, TSP
	Osteocalcin	~5kD	Osteoclast activity	Ca
	Bone Sialoprotein	~46-75kD	Adhesion, mineralization	Itg
	Alkaline Phosphatase	~80kD	Mineralization	-
	Proteoglycans			
	Biglycan	~270kD	Col fibril diameter	Col
	Decorin	~150kD	Col fibril diameter	Col, TGF-β
Inorganic	Hydroxyapatite	-	Mechanical strength of bone	-

Beta 1 Integrins

Alpha 2 Beta 1

The α2β1 integrin is implicated in pro-osteogenic pathways as it is highly expressed by osteoblast-like cells and is a primary adhesion receptor used by osteoblast-like cells to adhere to collagen[31], the main organic component of bone. Several studies indicate that the interaction of α2β1 integrin with collagen I is a crucial signal for osteoblastic differentiation and matrix mineralization[3, 4, 41-44]. For example, α2β1-mediated adhesion of MC3T3-E1 pre-osteoblasts to collagen I activates Runx2/Cbfa1, a transcription factor that activates osteoblastic differentiation and matrix mineralization[3, 44]. α2β1 ligation to collagen I also induces the phosphorylation of focal adhesion kinase (FAK) and activation of extracellular signal-related kinase (ERK), which has been implicated in the regulation of osteoblast-specific gene expression and matrix mineralization[43-46]. Silencing of the α2 integrin subunit also blocked human osteoblast-like cell osteocalcin expression in response to micron-scale structure of titanium substrates[10]. Furthermore, the collagen–α2β1 integrin interaction promotes an osteoblastic phenotype in rat multipotent bone marrow cells[41, 42]. Schneider et al also showed that perturbation of the α2β1 integrin resulted in a 95% reduction mineralization in an osteosarcoma cell line[47].

Alpha 5 Beta 1

The α5β1 integrin plays an important role in osteogenic differentiation as it is expressed by osteoblasts and osteoprogenitors, and promotes cell survival and matrix mineralization. α5β1 is stably expressed by osteoblasts during varying stages of osteogenesis[8] and is also expressed by bone marrow stromal cells[48]. In addition, α5β1 also mediates cell attachment to fibronectin as well as fibronectin assembly[48]. In mature cells, α5β1 binding is necessary for cell survival and a decrease in α5β1-fibronectin

interaction leads to osteoblast apoptosis[49] through a caspase-dependent mechanism[50]. α5β1 may also be involved in mechanical sensing by osteoblasts *in vitro*[51]. Blockade of the α5β1 integrin inhibits bone-specific gene expression and mineralization in rat calvarial cultures[7, 8] and a rat osteosarcoma cell line[47]. In human mesenchymal stromal cells (hMSC), priming the α5 subunit with an agonist or overexpression of the α5 subunit increases osteogenic capacity[9], while α5β1 blockade decreases the alkaline phosphatase activity of cells cultured on fibronectin[52].

Beta 3 Integrins

Alpha v Beta 3

While engagement of the αvβ3 integrin may support cell adhesion, it has a negative effect on the proliferation and differentiation of osteoprogenitors. Blocking of αvβ3 has been shown to enhance human MSC proliferation on fibronectin and fibronectin fragments[52]. αvβ3 may also inhibit osteoblast differentiation and bone healing *in vivo*. A murine osteoblastic cell line made to overexpress human αvβ3 showed an increase in proliferation rate but a decrease in matrix mineralization[53]. Furthermore, early fracture healing was accelerated in the tibiae of β3-null mice and twenty-three genes related to osteogenesis were upregulated at least two-fold in the β3-null mice[54]. αvβ3 also mediates osteoclast attachment to bone matrix and plays a central role in bone resorption[55, 56].

GLOBAL BETA 1 INTEGRIN KNOCKOUTS

Global β1 integrin knockout results in post-implantation embryonic lethality. Mouse embryos with homozygous β1 integrin deletion had collapsed blastocoels at E4.5 and displayed severe degeneration at E5.5 due to inner cell mass (ICM) failure [21]. A separate study also confirmed that mice with homozygous null β1 integrin mutations

underwent normal development to the blastocyst stage and implanted into the uterine wall, but failed shortly thereafter [57]. In contrast, mice which were heterozygous for the null β1 integrin gene were indistinguishable from wild-type littermates despite having low (50%) expression levels of β1 integrins in the liver, kidney and brain, when compared to wild-type mice. In chimeric embryos established using β1 integrin-null, lacZ positive embryonic stem (ES) cells, the β1 integrin-deficient cells failed to colonize the liver and spleen, but were found to be present at varying levels ranging from 2-25% in all other tissues such as the brain, lung, heart and skeletal muscle [57]. However, it should be noted that in this study, the presence or distribution of β1 integrin null cells was not analyzed in bone tissue. Taken together, these studies demonstrate that β1 integrins are not required for pre-implantation development, but β1 integrin gene mutation results in a recessive lethal defect in mouse embryonic development from E5.5 onwards.

CRE-LOX SYSTEM FOR CONDITIONAL GENE DELETIONS

Cre-lox recombination is a sophisticated technology for genetic manipulation which allows for site-specific recombinase activity and may be used to generate global knockouts, conditional (tissue specific) knockouts or reporters[58]. The Cre-lox system requires two components: 1) Cre recombinase, an enzyme which catalyzes recombination between two loxP sites, and 2) loxP (locus of crossing [x-ing] over in P1) sites, specific 34 base pair (bp) sequences consisting of a core 8bp sequence, where recombination takes place, flanked by two palindromic 13bp sequences (Figure. 2.2 A). When transgenic methods are used to insert loxP sites in the same orientation flanking a target gene, the outcome of Cre-induced loxP site-specific recombination is excision of DNA between the loxP sites, and therefore, deletion of the target gene [59] (Figure. 2.2 B). Transgenic animals with genomes in which target genes are flanked by loxP sites are termed as 'floxed' for the target gene [60, 61]. If mice which are floxed also also express Cre-recombinase under a tissue-specific promoter, gene deletions in those animals will be

restricted to tissues which express that marker (Figure. 2.2 C). Conditional knockout animals may be useful in studying genes for which the global knockout results in prenatal lethality.

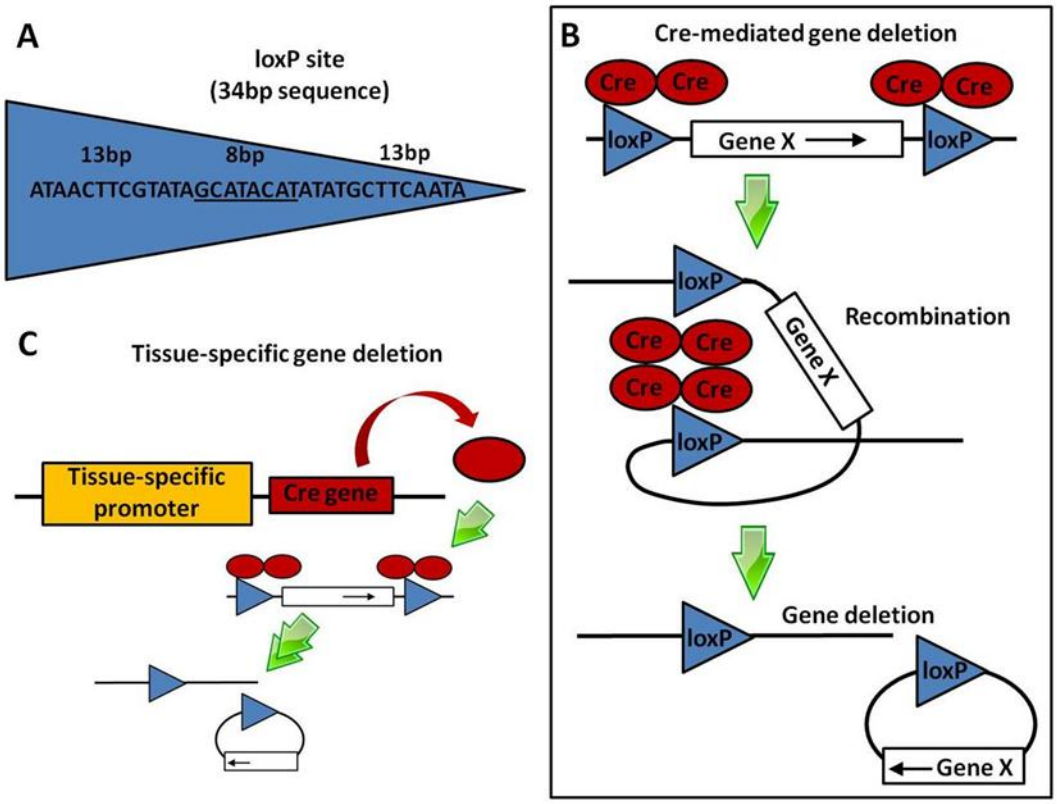

Figure 2.2. Cre-Lox recombination technology. (A) loxP, or locus of crossing [x-ing] at P1 sites are specific 34 base pair sequences. (B) The enzyme cre-recombinase will excise any DNA sequence flanked by loxP sites with the same orientation, and this method can be used for gene deletions. (C) Cre expression under a tissue-specific promoter combined with the presence of a floxed gene in the same transgenic animal can be used to create conditional, tissue-specific gene deletions.

BONE STRUCTURE AND FUNCTION

Bone cells

Bone formation is regulated by osteoblasts, osteoclasts and osteocytes. Osteoblasts are mononucleate bone-forming cells which secrete osteoid, the non-mineralized component of bone extracellular matrix and then mineralize the matrix[62]. Osteoblasts are derived from mesenchymal cells found in the periosteum or bone marrow. Osteoblasts express markers such as osterix, alkaline phosphatase, bone sialoprotein, osteocalcin, osteopontin and osteonetcin. After depositing and mineralizing osteoid, osteoblasts become embedded in the matrix and differentiate into osteocytes. Osteoblasts may also undergo apoptosis or differentiate into bone lining cells[62].

Osteoclasts are multinucleate cells which form when cells of the macrophage/monocyte lineage fuse together. Osteoclasts are polarized cells which resorb bone by secreting H+ ions through the ruffled border into the underlying matrix[62].

Osteocytes are derived from matrix embedded osteoblast. Osteocytes occupy lacunae and extend filapodia through canaliculi in the matrix. Osteocytes have a limited capacity to synthesize or resorb matrix[62].

Bone Extracellular Matrix

In bone, the ECM consists of mainly of an organic phase known as osteoid which constitutes approximately 20% of bone mass, and a mineral phase (Table 1). The organic fraction of bone consists of over 90% type I collagen[63], other minor collagens such as types III and V, and 5% non-collagenous proteins. The non-collagenous proteins in bone include osteocalcin, osteonectin, osteopontin, adhesion proteins such as fibronectin and vitronectin and proteoglycans such as versican, decorin and hyaluronan[64]. The mineral phase of bone is composed of hydroxyapatite, a calcium phosphate compound. The bone

matrix also sequesters growth factors, acting as a reservoir for soluble inductive signals such as bone morphogetenic proteins (BMPs).

Bone ECM serves both structural and biological functions, as the mineralized matrix accounts for the tissue's mechanical properties while it also provides chemical cues which regulate bone cells and acts as a reservoir for ions. Collagen fibrils provide tensile strength to bone and are composed of collagen helices which assemble parallel to each other in a regular quarter-staggered pattern, creating 68 nm gaps between adjacent collagen molecules. Hydroxyapatite crystals, which make up 70% of bone, fill these gaps and are responsible for the compressive strength of bone[62]. Bone ECM also regulates bone cells by providing ECM-integrin bonds which enable the formation of adhesive structures and activate signaling pathways which regulate cell spreading, survival and differentiation.

CRE TRANSGENIC LINES USED FOR BONE-RELATED STUDIES

Twist 2/ Dermo 1-Cre

Twist 2/ Dermo 1 is a basic helix-loop-helix (BHLH) protein [65] and a member of the Twist family of proteins which regulate the development of mesenchymal lineage cells and contribute to skeletal patterning. Like Twist 1, Twist 2 is believed to function as an inhibitor of myogenic or osteoblastic[66] differentiation in mesenchymal stem cells (MSCs) and maintains MSCs in an undifferentiated state. Cre expression in Twist 2-Cre mice is observed at E9.5 in somites and brachial arches. At E11.5, cre expression occurs within mesenchymal condensations during endochondral ossification[67]. At E16.5, Twist 2-Cre expression is detected in chondrocytes within the femoral growth plate as well as in osteoblasts within the perichondrium, periosteum and endosteum[68].

Osterix-Cre

Osterix is a zinc finger protein that is expressed in committed osteoprogenitors in bones formed by both osteochondral and intramembranous ossification. In osterix-cre transgenic mice, cre expression is detected from E14.5 onwards in embryos[67]. In 10 day old mice, cre expression in Osterix-cre mice is observed in the perichondrium, periosteum, primary spongiosa, and in some hypertrophic chondrocytes as well. In osterix-cre mice, the cre recombinase protein is fused with GFP.

Osteocalcin-Cre

Cre expression under the 3.5kb human Osteocalcin promoter has been observed in osteoblasts and osteocytes in mouse calvaria from E17 onwards[69]. Cre-mediated gene deletion under the Osteocalcin promoter is observed in the calvaria, femur and vertebrae in Osteocalcin-Cre mice at the postnatal stage[70].

BONE DEVELOPMENT

Skeletogenesis takes place in two stages. In the first stage, known as skeletal patterning, aggregates of mesenchymal cells called mesenchymal condensations form at the sites of future skeletal formation[62]. BMP signaling may occur earlier than this stage and is required for mesenchymal condensation. In mice, by day E10.5, most of the mesenchymal condensations have formed[71]. During the second phase, these mesenchymal condensations differentiate to form chondrocytes, osteoblasts and osteoclasts in a finely controlled process. Bones are formed either by endochondral ossification or intramembranous ossification. Long bones form through endochondral ossification, in which bone formation proceeds through the development of a cartilage template which is undergoes vascular invasion of bone cells and is remodeled and replaced with bone. In contrast, intramembranous ossification takes place in the

development of flat bones such as the calvarium and part of the clavicle by direct differentiation of cells in the mesenchymal condensations to bone[71].

During endochondral ossification, cells in mesenchymal condensations differentiate into chondrocytes and begin to secrete type II Collagen. However, cells at the periphery of mesenchymal condensations form the perichondrium. At approximately E13.5 non-proliferating elongated pre-hypertrophic chondrocytes form in the middle of the mesenchymal condensations. When pre-hypertrophic chondrocytes begin to express type X Collagen, they become hypertrophic chondrocytes. At this time, cells in the perichondrium begin to express Runx2, the master regulator of osteoblastic differentiation[72], forming the bone collar, which is the precursor to cortical bone. While hypertrophic chondrocytes undergo apoptosis, vascular invasion occurs through the bone collar, carrying osteoblast lineage cells into the center of the cartilage mold, which is now known as the primary spongiosa. These osteoblast lineage cells will subsequently form osteoblasts and deposit bone matrix in what will become trabecular bone. At the ends of each long bone, proliferating and hypertrophic chondrocytes align into columns to form the growth plate, which is responsible for lengthening of the bone[73].

Non-hypertrophic chondrocytes are regulated by FGFs (FGFR3 is an inhibitor of chondrocyte proliferation) [74], Wnt signaling[75], as well as Ihh[76]. The Sox9 and Runx2 transcription factors are important regulators of hypertrophic chondrocytes. Sox9 is necessary for differentiation of mesenchymal cells into proliferating non-hypertrophic chondrocytes[77]. Runx2 inhibits chondrocyte proliferation and hypertrophy[78].

Osteoblast differentiation is regulated by several proteins including Runx2, Twist 1 and 2, as well as Osterix. Runx-2 is required for osteoblast differentiation, and Runx2 knockouts never develop mineralized skeletons, and die of respiratory distress as newborns[79]. Osterix is expressed downstream of Runx2 and is also required for osteoblastic differentiation [80]. Twist 1 and Twist 2 are also implicated in skeletogenesis. Twist 1 haploinsufficiency causes a form of craniosynostosis[81]. Twist 1 and 2 inhibit

osteoblastic differentiation of Runx2 expressing cells between E10.5 and E14.5 in the cranium and appendicular skeleton respectively[66]. Surprisingly, conditional deletion of BMP-2 under the Prx-1 promoter (an osteochondroprogenitor marker) does not inhibit bone development, demonstrating that BMP-2 signaling is not required for bone development[82].

BONE FRACTURE HEALING

Bone fracture healing occurs through a complex interplay of multiple cell types and cellular processes which recapitulates bone development and results in scar-free bone regeneration. Fracture healing may proceed through a combination of endochondral ossification and intramembranous ossification and occurs in multiple stages: (1) initial injury/inflammation, (2) endochondral formation/ periosteal response, (3) primary bone formation/ cartilage resorption, (4) secondary bone formation/ coupled remodeling.

The initial injury/inflammation stage takes place from approximately 0 to 7 days post fracture and is marked by hematoma formation, inflammation and mesenchymal stem cell recruitment. Inflammation takes place during the first 24 hours, following which osteoprogenitor cells are recruited to the fracture site from the periosteum, bone marrow and surrounding tissues[83]. Proteases such as MMP-2 and MMP-14[84] and multiple pro-inflammatory cytokines are upregulated during the first 7 days including MCSF, ILa, IL1b, IL6, IL11, RANKL, OPG, TNFα, and TNFβ. Morphogens which are highly expressed during this stage are BMP-2, TGFβ1 and GDF8. BMP-2 is expressed in a two-phase profile, peaking once at day 1 and decreasing to a minimum at day 7 before increasing steadily again, peaking more strongly at 21 days and then decreasing again from 21-28 days post-fracture [85, 86]. It is noteworthy that BMP-2 is the only BMP which is highly expressed during this early stage. Although BMP-2 is not required for bone development, it is required for fracture healing as conditional BMP-2 knockout mice with mid-diaphyseal femur fractures do not form a callus even after 20 days[82]. Mice lacking

BMP-2 do not have any periosteal activation at day 3 post-fracture, which suggests that BMP-2 is a crucial mediator of the early fracture healing response.

The endochondral formation/ periosteal response takes place from approximately 7 to 14 days post fracture. During this stage, cartilage formation, vascular ingrowth and intramembranous bone formation take place. Cartilage-related ECMs such as Col2a1, Col10a1 and aggrecan are highly expressed. Morphogens such as TGFβ2, TGFβ3, as well as BMP-4, BMP-5 and BMP-6, GDF5, GDF10 and Indian hedgehog (Ihh) begin to be expressed. In addition, MMP-2, and MMP-14, ADAMTS-4 and ADAMTS-15 expression continue to increase while MMP-9, MMP-13 begin to be highly expressed during the endochondral formation stage[84].

During the primary bone formation stage, at approximately 14-28 days post fracture, chondrocytes undergo apoptosis, bone cells are recruited to the fracture callus, neovascularization occurs and osteoclasts are recruited to resorb calcified cartilage. Bone-related ECM proteins such as bone sialoprotein (BSP), osteopontin (OPN), and all BMPs are upregulated during this stage.

Finally, during the secondary bone formation stage, which occurs 3 weeks after fracture, bone marrow is established, the calcified cartilage is resorbed by osteoclasts, and bone remodeling takes place in order to replace woven bone with lamellar bone.

BONE GRAFTS AND CLINICAL NEED

Although bone is unique in its capacity for scar-free regeneration in adults, large bone defects that occur due to traumatic injury, bone deformities or tumor resection are clinically challenging, and may result in non-unions or delayed unions [87]. These non-healing bone defects will require treatment with bone grafts, which are also commonly used in spinal fusions, foot and ankle fusions as well as for reconstructions during revision surgeries for joint replacements. Over 1 million bone grafting, bone excision and

fracture repair surgeries are performed annually in the US, at cost of approximately $5 billion [14-17]. The worldwide bone graft substitute market was valued at $1.9 billion in 2010 and is predicted to reach over $3.3 billion in 2017. Currently used bone graft products as well as their limitations are described below.

Autografts and Allografts

Autografts are currently the gold standard of treatment for non-healing bone defects, followed closely in number of procedures performed by allografts [22]. Together, autograft and allograft tissue account for approximately 90% of bone graft treatments [88]. Autografts are usually harvested from the patients iliac crest, distal femur or proximal tibia, but these treatments suffer from limited supply as well as chronic pain or inflammation at the donor site [22]. Although donor and cadaveric allografts are more readily available than autografts, they carry the risk of immune rejection or transferring viral or bacterial infection. While the risk of infection and immunogenicity may be minimized by tissue processing methods such as allograft freezing, freeze-drying, and ethylene oxide or gamma irradiation sterilization, these processes also decrease allograft osteogenicity due to the absence of viable cells and limit the ability of allografts to remodel [22, 89-91].

Demineralized Bone Matrix

Demineralized bone matrix (DBM) is produced by acid extraction of allografts and is clinically available in a range of forms such as injectable paste, granules, gel, putty, or strips. DBM preparations are osteoconductive due to the ECM left behind but may exhibit non-uniform osteoinductivity due to donor-to-donor variations as well as differences in storage, sterilization and processing methods used[16]. Although DBM has demonstrated osteoinductive properties in animal studies, there have been no randomized, controlled human studies involving the use of DBM alone [22]. It should be noted that DBM products with no added components are regulated as minimally modified human

tissue and therefore received clearance from the FDA without requiring evidence of comparable efficacy to autografts. Products which combine DBM with additives intended to improve ease of handling of the DBM product (e.g. DBM-based putty or pastes) are now regulated by the FDA as medical devices which require 510(k) clearance. DBM is widely used clinically as a 'bone graft extender' meaning that it is used in conjunction with an autograft, rather than as a replacement for autografts.

Ceramics

Ceramics used as bone grafts include calcium phosphates (BioOss, Osteograf, Vitoss, ProOsteon, SRS, Biobon), calcium sulfates and bioglass (Biogran, PerioGlas). These materials generally provide some mechanical support and are osteoconductive, but not osteoinductive. Ceramics are therefore commonly used as carriers for other osteoinductive or bioactive agents such as collagen (Collagraft, Healos), BMPs or cells in composite constructs or as bone graft extenders [16, 88].

Bone Morphogenetic Protein-Based Products

Although bone morphogenetic protein (BMP)-based bone grafts have emerged as promising alternatives to auto and allografts due to their potent bone induction effects, they are limited by high costs and serious safety concerns. Since 2002, bone graft substitutes using BMP-2 (Medtronic's InFUSE) and BMP-7 (Stryker's OP1) have been FDA approved for clinical use in the United States [24, 92, 93]. Medtronic's BMP-2 product, InFUSE, was approved by the FDA for use in lumbar spinal fusions in conjunction with a titanium tapered spinal fusion cage (LT-CAGE Lumber Tapered Fusion Device) using the anterior lumber inter fusion (ALIF) surgical technique, which employs an abdominal approach. InFUSE was also approved in 2004 for use in open tibial fractures and in 2007 for sinus augmentations. Stryker Biotech's BMP-7 product, OP-1 is approved for use in recalcitrant long bone non-unions and certain posterolateral lumbar spinal fusions under a

Humanitarian Device Exemption. Since Medtronic's InFUSE became commercially available, Medtronic quickly become the market leader for bone graft substitutes, particularly for spinal fusions. The Journal of the American Medical Association (JAMA) reported that nationwide use of BMP-based bone grafts for spinal fusions rose from 0.69% of all fusions in 2002 to 24.89% of all spinal fusions in 2006[94]. Medtronic now controls 44% of the global bone graft market, which is worth $2.5 billion. Medtronic also dominates the BMP bone graft market, accounting for 90% of sales. Medtronic's BMP product, the InFUSE bone graft consists of lyophilized recombinant human BMP-2 (rhBMP-2) which is reconstituted in sterile water at a 1.5 mg/ml concentration and applied to a scaffold manufactured from bovine type I Collagen (referred to as an absorbable collagen sponge, or ACS) prior to implantation. Despite the rapid increase in use of BMP products such as InFUSE as bone grafts since 2002, these products have important limitations. First, BMP therapy is extremely expensive; the cost of a single treatment kit for InFUSE may range from $2,500 to $,5000 [95]. Secondly, BMPs need to be administered at supraphysiological concentrations to stimulate bone growth in humans, raising concerns regarding excess bone growth outside the defect site as well as inflammatory and carcinogenic effects [22-24]. Some of these safety concerns may be justified; Medtronic and the InFUSE bone graft have faced greater scrutiny in recent years with an editorial in a 2011 issue of the Spine Journal alleging that that spinal fusion surgeries using the InFUSE bone graft had severe and potentially life-threatening side effects which were not reported in the original Medtronic-sponsored clinical studies, and that many of the authors of these studies had more than $1 million in financial associations with Medtronic[96]. These side effects included ectopic bone formation in the spinal canal, radiculopathy, nerve injuries, retrograde ejaculation in males or other urogenital adverse events, and potentially lethal swelling of the neck and throat tissue following cervical spinal fusions[96]. While the Spine Journal review only addressed safety concerns on InFUSE use in spinal fusions, their findings highlight the general risks of

introducing extremely high doses of BMPs into patients using carriers without controlled release mechanisms. Therefore, there remains an unmet clinical need for cost-effective, safe and efficacious bone graft substitutes.

ECM-MIMETIC BIOMATERIALS FOR ORTHOPAEDIC APPLICATIONS

Full Length Natural ECM Polymers

Due to the important regulatory role that ECM molecules play on cellular responses *in vivo*, full-length ECM proteins have been studied as potential adhesive scaffolds for bone defect healing and implant integration. These ECM polymers include collagen[97-103], fibrin[104-107], hyaluronic acid[108-111], decellularized matrix[112, 113] as well as bone sialoprotein[114] (Table 3). Methods used to functionalize titanium implants with ECM polymers include protein adsorption from solution[100, 110], injection of protein solution into a porous implant[99], dip-coating and covalent tethering[98] and plasma spraying[111]. For the treatment of bone defects, ECM implants have been used in the form of crosslinked membranes[102], sponges[103], gels[105], demineralized bone particles[112] or cut pieces of small intestinal submucosa[113]. Although naturally derived ECM molecules have demonstrated some degree of success in selected studies,[97, 98, 113] the widespread use of natural ECM macromolecules in orthopaedic applications has been hindered by several factors. First, full-length ECM polymers have low solubility, are costly to extract and purify in large quantities, suffer from batch-to-batch variation and potentially suffer from immunogenicity. Furthermore, it is challenging to modify, characterize and control the presentation of natural ECM biomaterials.

ECM-Derived Adhesive Peptides/ Proteins

The above-mentioned limitations of full-length ECM molecules have spurred the use of ECM-derived peptides or recombinant fragments which incorporate the minimal functional sequence of their parent protein [115] in order to convey bioactivity to implant

materials. In contrast to ECM polymers, these peptides and protein fragments may be synthesized in larger quantities, immobilized on non-fouling surfaces at high densities, and may be tailored in composition for specific applications. While natural ECM proteins such as collagens and fibronectin are large macromolecules consisting of thousands of amino acids, only a few short peptide sequences within these polymers serve as integrin recognition and binding sequences which trigger downstream processes such as adhesion, signaling and spreading. For example, in collagens I, II and III, cells bind to the GFOGER[116, 117] peptide sequence, while in fibronectin, the RGD[118], PHSRN[119], REDV[120], and LDV[121] sequences are responsible for cell binding. As a result, short peptide sequences such as these, as well as ECM-derived protein fragment such as FNIII7-10, are used to biofunctionalize titanium surfaces and bone tissue engineering scaffolds[122]. Common peptide/protein fragment functionalization methods for titanium implants include simple adsorption or covalent immobilization onto titanium surfaces. Peptides may be presented on a non-fouling background by covalently tethering them to protein resistant polymer coatings such as polyethylene glycol[122, 123]. Peptide modification strategies for bone regeneration within defects include adsorption to polymer scaffolds[124] or bone matrix[125].

Collagen-mimetic Peptides

GFOGER: The hexapeptide sequence Gly-Phe-Hyp-Gly-Glu-Arg (GFOGER) is found on residues 502–507 of the α1(I) chain of type I collagen and serves as the major recognition site for α2β1 integrin binding[117, 126, 127]. Our group engineered a Col I-mimetic GFOGER containing peptide, GGYGGGPC$(GPP)_5$GFOGER$(GPP)_5$GPC, which recapitulates the triple helical tertiary structure of native collagen as an adhesive ligand for biomaterials. Surfaces presenting adsorbed or covalently immobilized GFOGER peptide support equivalent levels of α2β1 integrin-mediated adhesion of HT1080 fibrosarcoma and MC3T3-E1 osteoblast-like cells as native collagen I[128] and also

promote osteoblastic differentiation of MC3T3-E1 and primary bone marrow stromal cells *in vitro*[25, 129]. Furthermore, GFOGER enhances bone repair *in vivo* within rigorous critical-sized rat femur defect models without the delivery of cells or growth factors[130]. GFOGER-functionalized titanium implants also enhance implant integration in a rat cortical model by improving peri-implant bone formation and implant fixation to bone[25, 129]. Surprisingly, an *in vitro* study by Hennessy et al. found that adsorption of a different triple-helical GFOGER sequence-containing peptide, $GPC(GPP)_5GFOGER(GPP)_5GPC$, did not improve human mesenchymal stem cell adhesion on hydroxyapatite disks[131], although cells cultured on GFOGER-treated tissue culture plastic showed levels of adhesion and spreading equivalent to full-length collagen I. This result contradicts other studies by our group and others which indicate that triple-helical peptides containing the GFOGER sequence support robust cell adhesion[117, 127] and differentiation[129] and may possibly be due to low GFOGER adsorption to the hydroxyapatite disks or variations in the primary sequence of the GFOGER peptides used in these studies.

DGEA: The DGEA sequence has been suggested as the $\alpha2\beta1$ recognition sequence in type I collagen[132], although a different study failed to demonstrate $\alpha2\beta1$ mediated cell responses to DGEA[133]. Soluble DGEA peptide inhibits the osteoblastic phenotype of rat bone marrow stromal cells cultured on type I collagen. DGEA coated hydroxyapatite disks have promoted cell adhesion and upregulated osteoblast marker expression in mesenchymal stem cells *in vitro*[131]. However, surfaces modified with a CCGDGEAG peptide failed to support the adhesion of rat calvarial osteoblasts[134].

P15: P15 is a synthetic 15-amino acid peptide derived from the (766)GTPGPQGIAGQRGVV(780) sequence found in the $\alpha1$(I) chain of type I collagen [135]. Several studies have demonstrated that P15 enhances cell adhesion, osteoblastic gene expression and mineralization on anorganic bone matrix (ABM) *in vitro*[136, 137] and accelerates early bone formation in porcine[125] and rat[138] cranial defects. In a head-to-head comparison of DGEA and P15 coated hydroxyapatite disks implanted into rat tibiae, both

peptides improved new bone formation, but P15 failed to enhance bone implant contact[131]. P15 peptide-coated ABM has also been used in human periodontal osseous defects[139, 140] resulting in better clinical outcomes than open flap debridement alone, and has also been used in a pilot clinical study for long-bone defects[141]. However, P15-coated ABM has not been compared with ABM alone in these human dental applications to determine the role of P-15 alone on the positive effects observed.

RGD

RGD is an adhesive peptide sequence found in many ECM molecules including fibronectin, vitronectin, bone sialoprotein and osteopontin[142]. RGD can bind to multiple integrins such αvβ3, αvβ1, α8β1, αvβ8, αvβ6, αvβ5 and αIIbβ3. However, for certain integrins, binding to RGD is modulated by another sequence, such as the PHSRN synergy site for α5β1[119, 143]. Because RGD serves as a promiscuous binding sequence, many biomaterials have incorporated RGD as an adhesive ligand.

The application of linear RGD peptides onto implant surfaces has generally failed to enhance functional osseointegration as determined by bone-implant contact and mechanical fixation in several independent studies[122, 123, 144, 145]. In addition, Bellis and coworkers demonstrated a negative effect for RGD peptides in bone formation and osseointegration responses to hydroxyapatite implants[146]. In contrast to these studies, Søballe and colleagues did report enhancements in osseointegration for implants presenting cyclic RGD peptides[147, 148]. However, other studies using cyclic RGD have also failed to show improvements in implant fixation in rat tibiae [100] and canine mandibles[149]. Direct comparison among these contradictory studies is confounded by differences in the presence of a non-fouling polymer coating to prevent non-specific adsorption of plasma proteins, the animal model used, as well as implant surface finish (i.e., roughness). It is worth noting that two studies in which RGD was presented on titanium implants in a controlled fashion from non-fouling background coating

demonstrated no improvements in osseointegration[123, 150], suggesting that RGD-functionalization is not effective at enhancing implant integration. Fewer RGD modified materials have been tested as bone grafts within defects, but in those studies, as with titanium implants as well, RGD does not appear to promote bone formation and repair *in vivo*[151].

Fibronectin-mimetic Peptides/Protein Fragments

Fibronectin contains both the RGD adhesion site as well as a PHSRN synergy site. α5β1 binds to RGD in the presence of PHSRN in fibronectin with a forty-fold increase in affinity compared to RGD alone[119] . Each of these domains independently contributes little to binding, but, in combination, they synergistically bind to α5β1 to provide stable adhesion[143, 152]. In contrast, other integrins are unaffected by the synergy site and bind only to the RGD site within fibronectin with a lower affinity than α5β1[153]. Many fibronectin-derived peptides or fragments designed for biomaterial applications therefore recapitulate this interaction between α5β1 and the RGD and PHSRN sites.

FNIII7-10: Our group has engineered a recombinant fragment of fibronectin, FNIII7-10, which encompasses the 7-10th repeats of native fibronectin and binds specifically to the α5β1 integrin. FNIII7-10 enhances both osteoblast adhesion strength and differentiation *in vitro* [150], as well as implant osseointegration in a rat cortical model when compared to titanium implants modified with RGD at an equivalent molar surface density [122]. Furthermore, a simple adsorbed coating this fragment exhibits improved bone apposition and mechanical fixation to bone when compared to full-length fibronectin as fibronectin domains with antagonistic effects are excluded from the fragment [154].

FNIII9*-10: Martino et al. investigated the osteogenic potential of human MSCs on surfaces and hydrogels functionalized with full-length fibronectin (FN), fibronectin fragments (FNIII9-10 and FNIII10) and a more α5β1-specific mutated fibronectin fragment (FNIII9*-10) and demonstrated that FNIII9*-10 and FNIII9-10 supported

higher MSC differentiation than FN. Interestingly, the level of osteoblastic differentiation for each fragment was correlated with its degree of binding specificity for the α5β1 integrin (FNIII9*-10 > FNIII9-10 > FNIII10), which supports other studies suggesting that α5β1 engagement may enhance osteogenesis [122, 150, 154].

RGD-PHSRN: Synthetic peptides designed to co-present the RGD site and PHSRN synergy sites on the same molecule separated by polyglycine linkers result in increased adhesion and metabolic activity of primary rat calvarial osteoblasts [155] and human osteoblast-like cells [156] *in vitro* when compared to surfaces presenting RGD alone.

Other ECM-derived Peptides

Other ECM-derived peptides which have been found to enhance osteoblast adhesion and differentiation *in vitro* include FHRRIKA which is derived from the heparin binding site of bone sialoprotein [157-161], KRSR, which is a heparin binding sequence found on multiple ECM proteins [161-166], the bone sialoprotein derived BSP(278-293) [167], the human vitronectin peptide HVP (351-359) [168-171], an osteopontin derived peptide [172], and a heparin binding peptide, HBP12 [173].

CHAPTER 3: THE ROLE OF BETA 1 INTEGRINS IN BONE FORMATION DURING DEVELOPMENT

ABSTRACT

Bone development, homeostatis, adaptation, and healing are regulated by multiple microenvironmental cues, including integrin signaling. β1 integrins are the most common integrins and represent the main integrin binding partners of collagen I, the major ECM component of bone. While a large body of *in vitro* research clearly demonstrates the importance of β1 integrins on mineralization, *in vivo* bone-specific perturbations of β1 integrins in have demonstrated only mild bone phenotypes thus far. In our study, we conditionally deleted β1 integrins in osteolineage cells at three different stages of differentiation: (1) mesodermal cells under a Twist 2/Dermo 1 promoter, (2) pre-osteoblasts under the Osterix promoter and (3) mature osteoblasts/osteocytes under the Osteocalcin promoter. We found that β1 integrin deletion in mesodermal cells severely impairs prenatal skeletal mineralization and is embryonically lethal. In contrast, β1 integrin deletion in pre-osteoblasts resulted in viable but runted mice with decreased cranial mineralization, tooth defects and increased perinatal mortality. Finally, mice with β1 integrin null osteoblasts and osteocytes displayed very mild bone phenotypes and no change in femur biomechanics. Taken together, our data suggest that β1 integrins play an important role in early bone formation by regulating osteoprogenitor function but are not essential for the function of mature osteoblasts and osteocytes.

INTRODUCTION

Bone development, remodeling and bone healing are complex, dynamic processes which are regulated by the interaction of osteoblasts and osteoclasts with a variety of growth factors and extracellular matrix (ECM) molecules in their environment. Adhesion to ECM is primarily mediated by a family of receptors known as integrins, which also regulate crucial cell functions such as survival, migration and differentiation[174]. Integrins are a family of 24 different αβ heterodimeric receptors [26]. β1 integrins are the largest sub-family of integrins, as β1 integrins associate with 12 different α subunits [26].

β1 integrins are believed to play an important role in bone formation as β1 integrins are highly expressed in osteoblasts, osteoprogenitors and bone marrow stromal cells. Furthermore, blocking of multiple β1 integrins such as α2β1 [2-6], α5β1[7-9], α1β1 [4, 6] and α3β1 [8] in these cells severely impairs *in vitro* osteogenic differentiation and mineralization. In addition, β1 integrins may also regulate survival, as disruption of fibronectin- α5β1 interaction induces apoptosis in differentiated osteoblasts[49]. Although these *in vitro* data strongly suggests that β1 integrins play a crucial role in bone formation, *in vivo* deletion or functional perturbation of β1 integrins result in only mild skeletal phenoypes. For example, transgenic mice expressing a dominant negative mutant form of the β1 integrin under an osteocalcin promoter display normal bone development and only slightly altered responses to the mechanical loading environment[13, 18, 19]. Similarly, ablation of β1 integrin under the osteoblast-specific Col I 2.3kb promoter [20] yielded no change in the skeletal structure of transgenic mice[11, 12]. It should be noted that β1 integrins are essential for embryonic development and therefore, global β1 integrin knockout mice cannot be used for studies of *in vivo* β1 integrin function[21].

We considered the possibility that the apparent contradiction between the *in vitro* and *in vivo* studies may be due to the timing of integrin deletion. We therefore hypothesized that β1 integrins play a crucial role in early bone development processes but

are not required for mineralization by fully differentiated osteoblasts. In order to separately address the roles of β1 integrins in early osteogenic differentiation and mature osteoblast function, we generated conditional knockout mice with β1 integrin deletion targeted to osteolineage cells at three different stages: (1) mesodermal cells by expressing cre recombinase under the Twist 2 (also known as Dermo 1) promoter (TW2-Cre) [68] which is expressed at E9.5 in somites and branchial arches, (2) osteoprogenitor cells by expressing cre recombinase under the Osterix (Sp7) promoter (OSX-Cre) which is first expressed at E14.5 (3) mature osteoblasts and osteocytes by expressing cre recombinase under the Osteocalcin promoter (OCN-Cre) which is expressed from E17.5 onwards [69] (Figure 3.1).

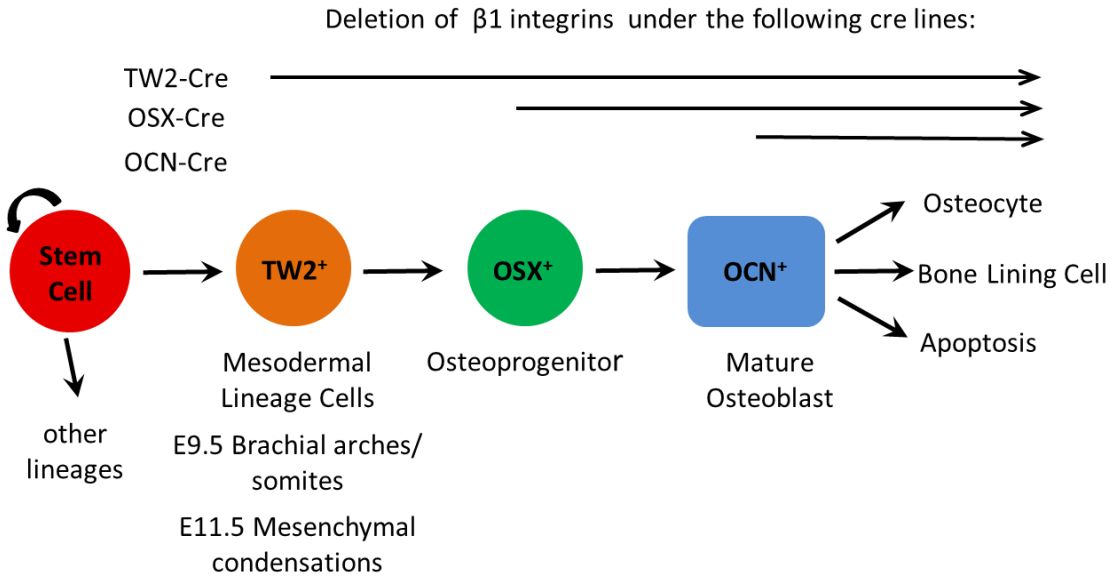

Figure 3.1. Cre-mediated deletions of floxed genes are targeted to mesodermal lineage cells, osteoprogenitor cells and mature osteoblasts respectively inTW2-Cre, OSX-Cre and OCN-Cre transgenic mice.

METHODS

Mouse crosses and genotyping

Homozygous β1 integrin floxed (itgβ1$^{fl/fl}$) mice, B6;129-*Itgb1*^{tm1Efu}/J, as well as TW2-Cre mice, B6.129X1-*Twist2*$^{tm1.1(cre)Dor}$/J, and OSX-Cre mice, B6.Cg-Tg(Sp7-tTA,tetO-EGFP/cre)1Amc/J were purchased from Jackson Laboratories, and OCN-Cre mice were kindly provided by Thomas Clemens. Itgβ1$^{fl/fl}$ mice were mated with Tw2-Cre, Osx-Cre or OCN-Cre mice to generate mice with β1 integrin deletions under the respective promoters: itgβ1$^{fl/fl}$-TW2-Cre, itgβ1$^{fl/fl}$-OSX-Cre and itgβ1$^{fl/fl}$-OCN-Cre. In all *in vivo* studies, these conditional knockout mice were compared with littermates with a wild-type phenotype (itgβ1$^{fl/fl}$ or itgβ1$^{fl/+}$) or with heterozygous conditional knockout genotype. Mice were tail clipped after weaning and genotyped by PCR analysis of genomic DNA extracted using the Qiagen DNeasy Kit. All protocols were approved by the Institutional Animal Care and Use Committee in adherence to federal guidelines for animal care.

Timed mating and embryo harvest

Timed matings were performed by placing breeders together in evening prior to the onset of the 12-hour dark cycle. Females were checked the following morning for plugs. Plugged females were single housed and euthanized at E11.5, E13.5 or E19.5 to harvest embryos. Mouse embryos were harvested by removing the uterine horn, separating implantation sites and peeling away the decidua and amniotic sac. Embryos were tailed clipped for genotyping and fixed in neutral buffered formalin before transfer to 70% ethanol for μCT analysis and further processing for histological analysis.

μCT analysis on E19.5 embryos

E19.5 embryos were imaged using a μCT40^{175} using an X-ray intensity of 145 μA, energy of 55 kVp, integration time of 200 ms, and resolution of 12 μm. The data was

evaluated by applying a Gaussian filter (sigma=1, support =1) using a threshold value of 300 mg HA/ccm.

μCT analysis on adult mouse calvaria and teeth

Mouse were anesthetized in an induction chamber filled with 4% isoflurane, maintained at 1.5% isoflurane and non-invasively imaged using a VivaCT (Scanco Medical) to determine calvarial and tooth structure. Scans were performed using an X-ray intensity of 145 μA, energy of 55 kVp, integration time of 200 ms, and resolution of 30 μm. The data was evaluated by applying a Gaussian filter (sigma=1, support =1) using a threshold value of 540 mg HA/ccm.

μCT analysis and biomechanical testing on intact femurs

To test the effect of β1 integrin deletion on bone development, femurs were harvested from littermates and stored at -80 °C until ready for testing. The frozen femur specimens were thawed under running tap water and imaged in PBS using a μCT 40 (Scanco Medical) to determine femur structure. The mid diaphysis and distal femur were imaged with an X-ray intensity of 145 μA, energy of 55 kVp, integration time of 200 ms, and resolution of 12 μm. The μCT data for the mid diaphysis was evaluated by applying a Gaussian filter (sigma = 0.8, support = 1) and a threshold value of 580mg HA/ccm. An auto-contour algorithm[176] was applied to the μCT scans of the distal femur and the epiphysis and metaphysic were separately evaluated using threshold values of 530 and 615 mg HA/ccm respectively. The μCT data was used to determine the moment of inertia of the femur mid-diaphysis, which was combined with biomechanical testing data to calculate bone material property values. For biomechanical analysis by 3 point bending testing, the femurs were loaded onto bending fixtures with lower span lengths of 6.2 mm. The femora were loaded to failure at a rate of 0.5 mm/s at the mid diaphysis using the 858 Mini Bionix II testing system (MTS).

Femur fracture healing model

A unilateral femur fracture model was used to study fracture healing in 10-13 week old wild type and Itgβ1$^{fl/fl\ cKO\ (OCN)}$ littermate mice. Mice were anesthetized under isoflurane, all hair was removed from the left hindlimb, and the skin was swabbed with alcohol and cycloheximide. A medial incision was then made along the femur and the underlying muscle was blunt dissected to expose the femur. The patella was dislocated to expose the condyles. To stabilize the fracture, a hole was made in the exposed condyles using a 25G needle, and a pre-cut 25G needle shaft was inserted into the intramedullary canal. A custom-made 3-point bending device was used to create a transverse fracture in the femur mid diaphysis. The patella was then repositioned over the condyles, the muscle was sutured and the skin incision was closed with wound clips[177].

Radiography, μCT analysis and biomechanical testing of fracture calluses

At 2 and 5 weeks post-bone fracture, mice were radiographically imaged using the MX-20 Radiography System (Faxitron Imaging) using an X-ray beam energy setting of 23kV and scan time of 15 seconds. Fractured femurs were harvested post-euthanasia from mice at 2 and 5 week time points. After harvest, the intramedullary pins were carefully removed from the fractured femurs and the fracture calluses were wrapped in PBS-soaked gauze and stored at -20 °C. The fracture calluses were thawed under running water and μCT imaged using a μCT (Scanco Medical) with an X-ray intensity of 145 μA, energy of 55 kVp, integration time of 200 ms, and resolution of 12 μm. The 3D reconstructions were evaluated by applying a Gaussian filter (sigma = 0.8, support = 1) and a threshold value set at half the value used to evaluate intact bone.

Histology

Bone samples were fixed in 10% neutral buffered formalin overnight, decalcified in 10% EDTA solution and transferred to 70% ethanol for storage at 4 °C. Fracture callus samples were processed for embedding in Immunobed resin and sectioned to 2 μm

thickness. Other bone samples were embedded in paraffin and sectioned at 5 µm thickness. Sections were deplasticized and stained with Safranin O/Fast Green to visualize cartilage or with Picrosirius Red to visualize collagen fibers.

RESULTS

Embryonic lethality in Itgβ1$^{cKO\ (TW2)}$ mice

Eighty six mice produced from mating itgβ1$^{fl/+}$-TW2-cre mice with itgβ1$^{fl/fl}$ mice were genotyped and analyzed. The intercrosses generated 35 itgβ1$^{fl/+}$ (40.7%), 25 itgβ1$^{fl/+}$ -Tw2-cre (29.1%), 26 itgβ1$^{fl/fl}$ (30.2%), and 0 itgβ1$^{fl/fl}$-Tw2-cre (0%) mice, while the expected Mendelian ratios were 25% for each genotype (Figure 3.2A). The chi-squared value for this genotype distribution was 31.48 with 3 degrees of freedom, and a p-value of < 0.0001 (Figure 3.2A), demonstrating that the itgβ1$^{cKO\ (TW2)}$ genotype was not viable. Among the viable offspring, itgβ1$^{fl/+}$ (WT), itgβ1$^{fl/fl}$ (WT) and itgβ1$^{fl/+}$ -Tw2-cre (het itgβ1$^{cKO\ (TW2)}$) were indistinguishable from each other in terms of gross appearance, size or skeletal structure (Figure 3.2B).

A

	Number of live mice	Expected number of mice
itgβ1$^{fl/+}$/Tw2cre$^{-/-}$	35	21.5
itgβ1$^{fl/+}$/Tw2cre$^{+/-}$	25	21.5
itgβ1$^{fl/fl}$/Tw2cre$^{-/-}$	26	21.5
itgβ1$^{fl/fl}$/Tw2cre$^{+/-}$	0	21.5
Total	86	86
Chi-squared value	31.488	
Degrees of freedom	3	
P-value	< 0.0001	

B

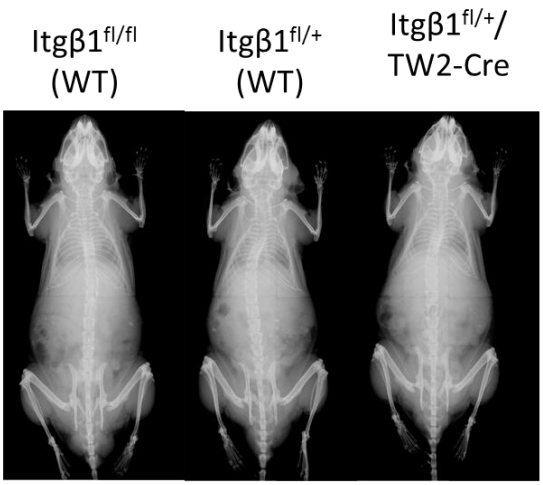

Figure 3.2. itgβ1$^{cko\ (TW2)}$ mice are not viable. (A) Live offspring numbers from intercross of itgβ1$^{fl/+}$-TW2-cre mice with itgβ1$^{fl/fl}$ mice and chi-square test demonstrate that the observed distribution is significantly different from the Mendelian ratio. (B) Radiographs indicate no gross skeletal differences between 10 week old female wild type (Itgβ1$^{fl/fl}$ and Itgβ1$^{fl/+}$) and heterozygous itgβ1$^{fl/+}$-TW2-cre (heterozygous itgβ1cko) littermates.

Severe mineralization defects in E19.5 Itgβ1$^{cKO\ (TW2)}$ embryos

In order to study the effects of β1 deletion in the mesoderm on bone formation, we harvested embryos generated from timed matings between itgβ1$^{fl/+}$-TW2-cre and itgβ1$^{fl/fl}$ mice. At E11.5 and E13.5, itgβ1$^{cKO\ (TW2)}$ embryos were indistinguishable from WT and het itgβ1$^{cKO\ (TW2)}$ littermates (data not shown). However, at E19.5, itgβ1$^{cko\ (TW2)}$ embryos were much smaller (<70% length) than WT littermates (Figure 3.3A), and displayed large abdominal growths where the umbilical cord point of attachment would be expected (Figure 3.3A, cKO 1 and cKO2) as well as cranial hemorrhaging (Figure 3.3A cKO3). µCT analysis of E19.5 embryos revealed considerable skeletal

mineralization in WT and het itgβ1$^{cKO\ (TW2)}$ embryos, but severely reduced mineralization in the skulls and vertebrae (Figure 3.3B and C, cKO1 and cKO3), or a complete lack of skeletal mineralization (cKO2), in itgβ1$^{cKO\ (TW2)}$ embryos. However, in two itgβ1$^{cko\ (TW2)}$ embryos (Figure 3.3B and C, cKO1 and cKO3) mineralization in the long bones and ribs, and appeared normal, suggesting that β1 integrins may have a more crucial role in mineralization of bones formed by intramembranous ossification than those formed by osteochondral ossification. The scapula, however, appeared to be mineralized in itgβ1$^{cko\ (TW2)}$ embryos. It is noteworthy that all the itgβ1$^{cKO\ (TW2)}$ embryos appeared to have umbilical cord or vascular defects. The umbilical cords of WT embryos were clearly filled with blood (Figure 3.4A (i)), but itgβ1$^{cKO\ (TW2)}$ embryos appeared to have blood in their amniotic sac (Figure 3.4A (ii), cKO1) or displayed an attached umbilical cord devoid of blood (Figure 3.4A (iii), cKO2). It is likely that the embryonic lethality in itgβ1$^{cKO\ (TW2)}$ embryos is related to these observed umbilical cord abnormalities, but further analyses are required to fully establish the cause of embryonic lethality. In one of the uterine horns harvested at E19.5, 2 out of 5 implantation sites were considerably smaller than the implantation sites of the WT and itgβ1^{cKO} embryos, suggesting that implanted embryos had already degenerated extensively by E19.5 (Figure 3.4A (iv)). We attempted to harvest the degenerated remains of the embryos from these implantation sites and the putative degenerated embryo is shown in Figure 3.4A (v). Safranin O/Fast Green staining of sections from cKO embryo 1 revealed a lack of hypertrophic chondrocytes in some skeletal elements, suggesting that a lack of mineralization in some skeletal elements of itgβ1$^{cKO\ (TW2)}$ embryos may be due to a defect in chondrocyte differentiation (Figure 3.4B).

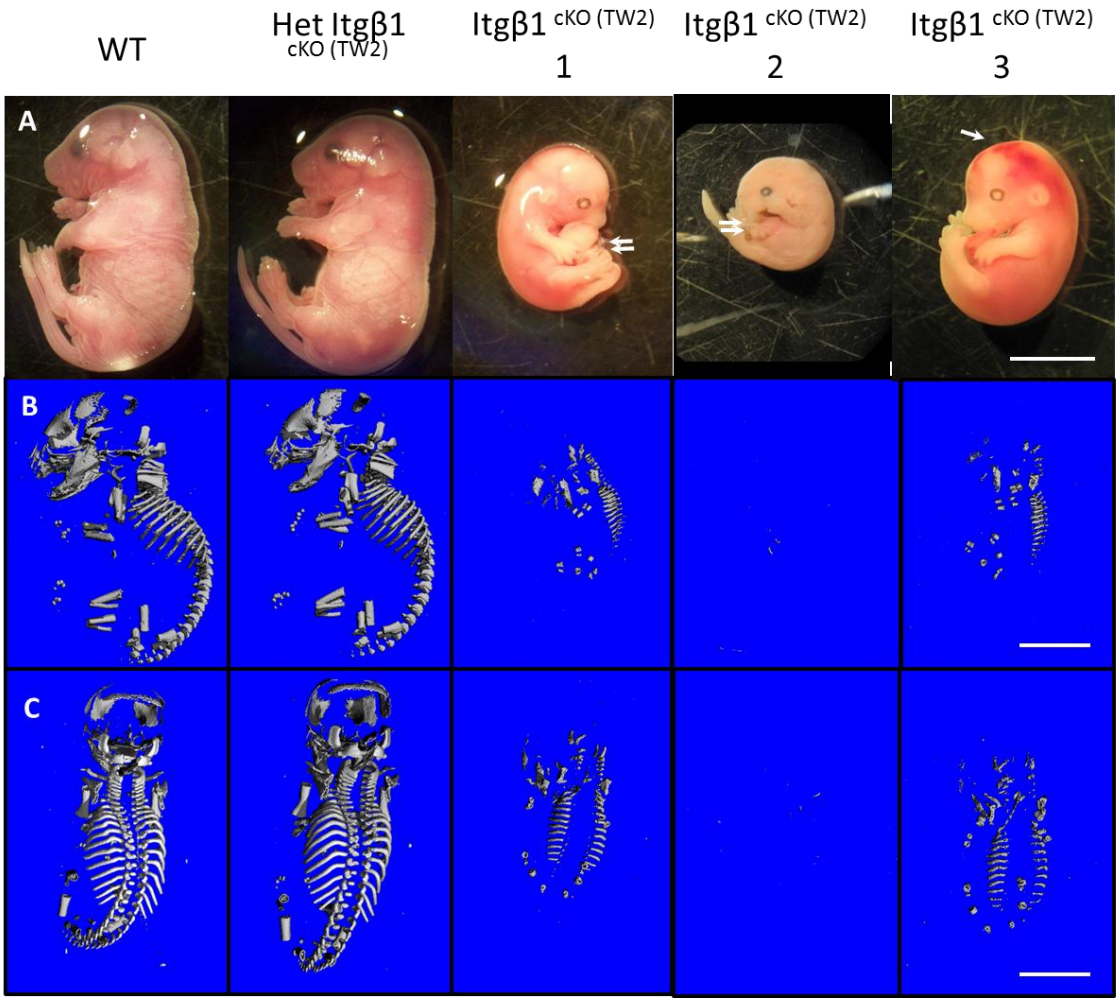

Figure 3.3. β1 integrin deficiency in mesoderm results in severe skeletal mineralization defects in E19.5 embryos. Stereoscopic images of E19.5 embryos. Double white arrows indicate an abnormal large tissue mass in the abdominal region of itgβ1$^{tw2\ cKO}$ embryos1 and 2, single white arrow indicates cranial hemorrhaging in itgβ1$^{tw2\ cKO}$ embryo 3. Itgβ1$^{tw2\ cKO}$ embryos are also smaller than littermates. (B) and (C) MicroCT images of E19.5 embryos indicate reduced mineralization of itgβ1$^{tw2\ cKO}$ embryo skeleton. Scale bars indicate (A) 0.5 cm, (B) and (C) 0.4 cm.

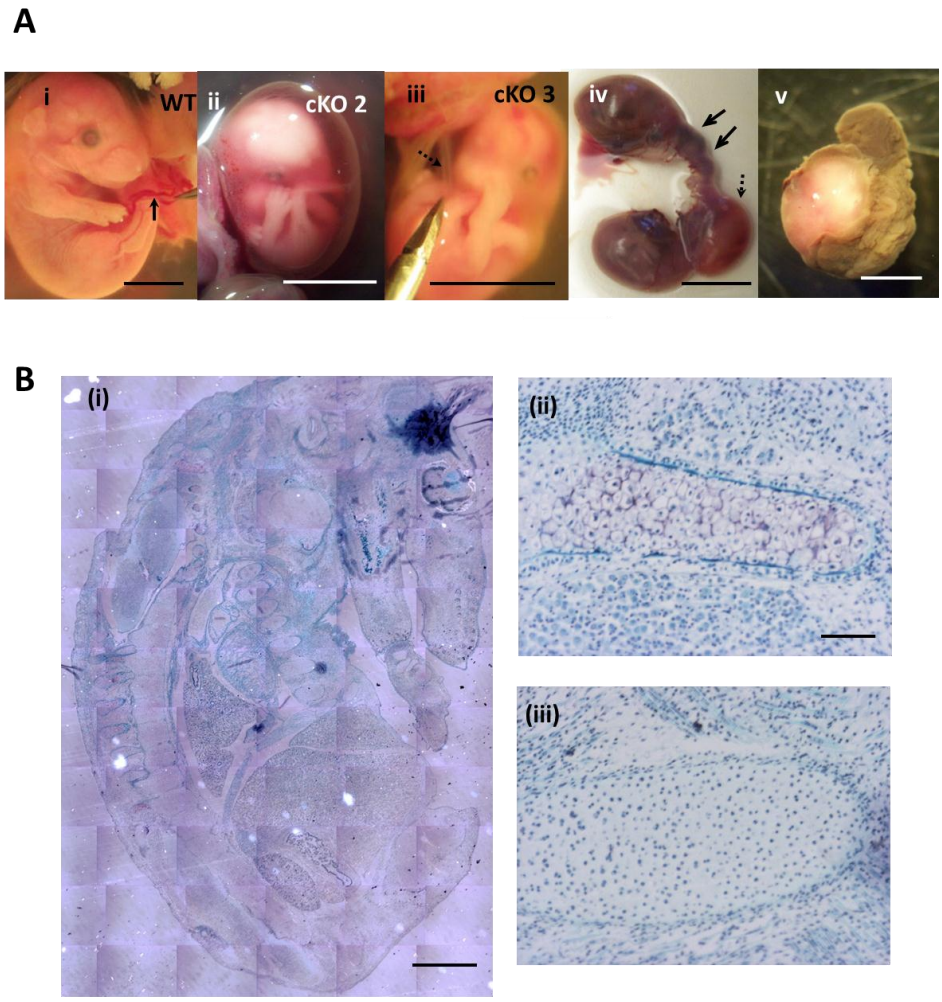

Figure 3.4. Gross deformities of E19.5 embryos and histological evaluation. (A) Stereoscopic images indicates a (i) normal blood-filled umbilical cord attached to a WT embryo (black arrow), (ii) blood within the amniotic sac of itgβ1$^{tw2\ cKO}$ embryo 1, (iii) and a lack of blood in the attached umbilical cord of itgβ1$^{tw2\ cKO}$ embryo 3 (black dashed arrow). (iv) Image of the uterine horn of pregnant dam at E19.5 displaying 5 implantation sites. One of the sites (dashed arrow) was smaller than the two largest sites and was occupied by itgβ1$^{tw2\ cKO}$ embryo 1. Two other sites (solid arrows) were extremely small and appeared severely degenerated. (v) Image of a presumptive resorbed embryo from one of the degenerated implantation sites. (B) Safranin O/Fast Green stained sections of Itgβ1$^{cKO\ (OSX)}$ embryo 1 reveal a lack of hypertrophic chondrocytes within some skeletal

elements. (i) Image constructed by stitching 4x micrographs of section. (ii) Micrographs of skeletal elements. Scale bars indicate (A) (i) , (ii), (iii) 0.5 cm, (iv) 1 cm and (v) 0.1 cm, (B) (i) 0.1 cm, (ii and iii) 100μm.

Itgβ1$^{cKO\ (OSX)}$ mice are runted and exhibit some perinatal mortality

In order to study the effect bone phenotype in the absence of β1 integrins in osteoprogenitor cells, we bred itgβ1$^{cKO\ (OSX)}$ mice. Itgβ1$^{fl/+}$-OSX-cre mice were mated to itgβ1$^{fl/fl}$ mice to generate itgβ1$^{fl/fl}$-OSX-cre (itgβ1$^{cKO\ (OSX)}$) offspring. This intercrossing gave rise to offspring in numbers which were approximately equal to the expected Mendelian ratios. Of 88 offspring genotyped, 22 (25%) itgβ1$^{fl/+}$ (WT), 18 (20.4%) itgβ1$^{fl/fl}$ (WT), 27 (30.6%) itgβ1$^{fl/fl}$-OSX-cre (het itgβ1$^{cKO\ (OSX)}$) and 21 (23.8%) itgβ1$^{fl/fl}$-OSX-cre (itgβ1$^{cKO\ (OSX)}$) mice were born, while the expected distribution was 25% for each genotype. The chi-squared value for this distribution is 1.909 with 3 degrees of freedom, and the two-tailed p value is 0.59. Although newborn pups appeared indistinguishable from each other, at the 21 day old weaning age, some animals in each litter were noticeably smaller than their littermates. After genotyping, we found that both male and female itgβ1$^{cKO\ (OSX)}$ mice were smaller and weighed approximately 25-35% less than their littermates and this weight reduction was maintained at 9 weeks (Figure 3.5A). The weights of both male and female itgβ1$^{cKO\ (OSX)}$ were significantly lower than all other littermates beginning at 27 days old. Female itgβ1$^{cKO\ (OSX)}$ mouse weights were lower than WT littermates at 24 days but not lower than that of het itgβ1$^{cKO\ (OSX)}$ mice. Radiographic analysis of itgβ1$^{cKO\ (OSX)}$ mice did not revealed any gross skeletal deformities, and confirmed that itgβ1$^{cKO\ (OSX)}$ were proportionally smaller than their littermates (Figure 3.5B). It has been reported that young (<6 week old) OSX-Cre transgenic mice have reduced body weights compared to wild-type controls and that this

growth delay is resolved at 12 weeks of age[178]. However, the reduced body weight which we observed in itgβ1$^{fl/fl}$-OSX-cre (itgβ1$^{cKO\ (OSX)}$) was not observed in itgβ1$^{fl/+}$-OSX-cre (het itgβ1$^{cKO\ (OSX)}$) littermates (Figure 3.5A), demonstrating that the growth defect observed is a result of β1 deficiency and not a side effect of the OSX-cre expression system. We also observed instances of perinatal mortality in itgβ1$^{cKO\ (OSX)}$ mice. Two out of 21 itgβ1$^{cKO\ (OSX)}$ mice died between 3 and 5 weeks old (9.5% mortality) compared with no deaths of young mice observed among littermates of other genotypes. However, the mice which died were extremely small, and weighed an average of 4.1g at 4 weeks old, and therefore weighed approximately 30% less than other age-matched itgβ1$^{cKO\ (OSX)}$ mice.

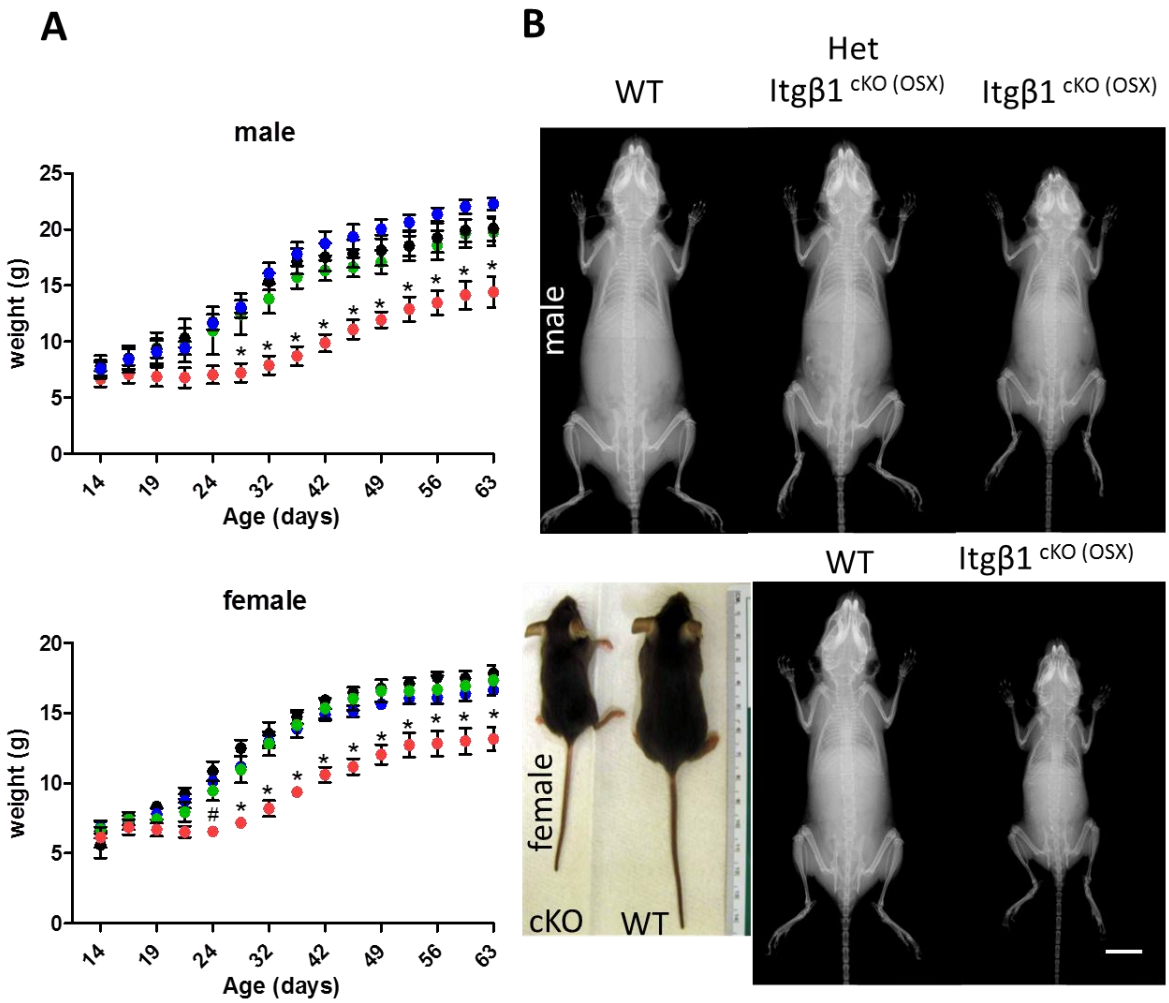

Figure 3.5. Itgβ1$^{cKO\ (OSX)}$ mice are runted. (A) Weights of itgβ1$^{cKO\ (OSX)}$ diverge significantly from their littermates between 24-27 days and reduced weight in itgβ1$^{cKO\ (OSX)}$ mice continue into adulthood. Blue circles, itgβ1$^{fl/fl}$ (WT), black circles, itgβ1$^{fl/+}$ (WT), green circles, het itgβ1$^{cKO\ (OSX)}$, red circles, itgβ1$^{cKO\ (OSX)}$. (B) Radiographs of 5 week old male (top) and female (bottom) littermates indicate that mice are proportionally smaller than their littermates and do not display any gross skeletal deformities. Inset, dorsal view of itgβ1$^{cKO\ (OSX)}$ and WT female littermates. Scale bar 1 cm. * $p<0.05$ compared to WT and het itgβ1$^{cKO\ (OSX)}$, # $p<0.05$ compared to WT only.

Itgβ1$^{cKO\ (OSX)}$ mice display severe tooth defects

We considered the possibility that the reduced weight observed in itgβ1$^{cKO\ (OSX)}$ mice could be due to a tooth defect (Figure 3.6A). Visual examination of the incisors of itgβ1$^{cKO\ (OSX)}$ mice indicated gross tooth abnormalities. Both the mandibular and maxillary incisors of itgβ1$^{cKO\ (OSX)}$ mice were significantly shorter at both 3 and 5 weeks. At 3 weeks, the maxillary and mandibular incisors were barely visible above the gum line of itgβ1$^{cKO\ (OSX)}$ mice. In addition, itgβ1$^{cKO\ (OSX)}$ incisors were misaligned. μCT analysis confirmed that both the maxillary and mandibular incisors in itgβ1$^{cKO\ (OSX)}$ mice were reduced in length at 3, 5 and 8 weeks (Figure 3.6B). The itgβ1$^{cKO\ (OSX)}$ maxillary incisors displayed increased curvature from the lateral view and the tip of one maxillary incisor often overlapped the other at 5 and 8 weeks of age. Itgβ1$^{cKO\ (OSX)}$ mandibular incisors were spaced apart from each other and the tips were curved away from each other at 3, 5 and 8 weeks. The extremely short incisors observed in itgβ1$^{cKO\ (OSX)}$ mice at 3 weeks were accompanied by significantly reduced mineralization of both the mandible and maxilla. In contrast to the observed incisor abnormalities, no gross defects were observed in itgβ1$^{cKO\ (OSX)}$ molars. Incisor defects were not observed at 3, 5 or 8 weeks in het itgβ1$^{cKO\ (OSX)}$ mice. In order to determine if the reduced weight in itgβ1$^{cKO\ (OSX)}$ mice (Figure 3.5) was due to a nutritional deficiency caused by incisor defects and difficulty for the mice to chew hard food pellets, we fed some litters of mice soft food. Even within litters that were provided with a soft diet, itgβ1$^{cKO\ (OSX)}$ mice exhibited decreased weight compared to their littermates (data not shown). This indicates that the reduced weight caused by Osterix-specific β1 integrin deletion is not entirely due to nutritional deficiencies caused by abnormal tooth development in itgβ1$^{cKO\ (OSX)}$ mice.

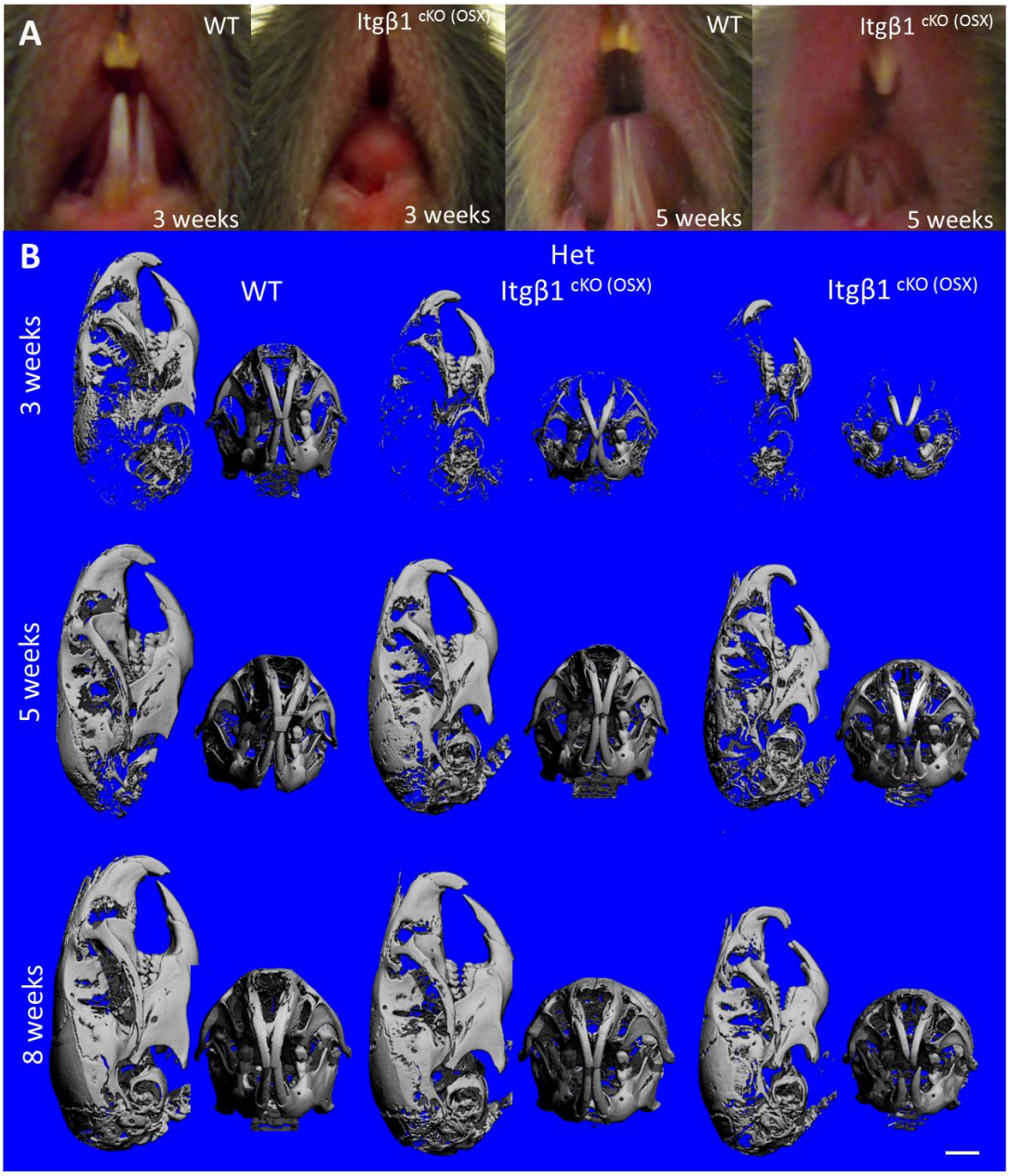

Figure 3.6. β1 integrin deficiency in osteoprogenitor cells results in incisor defects. (A) Ventral view of 3 and 5 week old littermates revealed gross tooth deformities in itgβ1$^{cKO\ (OSX)}$ mice.(B) 3D μCT reconstruction displaying lateral and frontal views of littermate skulls and incisors indicate that itgβ1$^{cKO\ (OSX)}$ mice have short and misaligned incisors. (B) Scale bar 2 mm.

Itgβ1$^{cKO\ (OSX)}$ mouse calvaria are under-mineralized

μCT analysis of mouse skulls revealed severely reduced mineralization in itgβ1$^{cKO\ (OSX)}$ calvaria compared to WT littermates (Figure 3.7). This phenotype was observed in frontal, parietal, interparietal and occipital bones, and was most prominent at 3 weeks, but persisted at 5 and 8 weeks. Mineralization levels in het itgβ1$^{cKO\ (OSX)}$ mice appeared to be intermediate between WT and itgβ1$^{cKO\ (OSX)}$ mice.

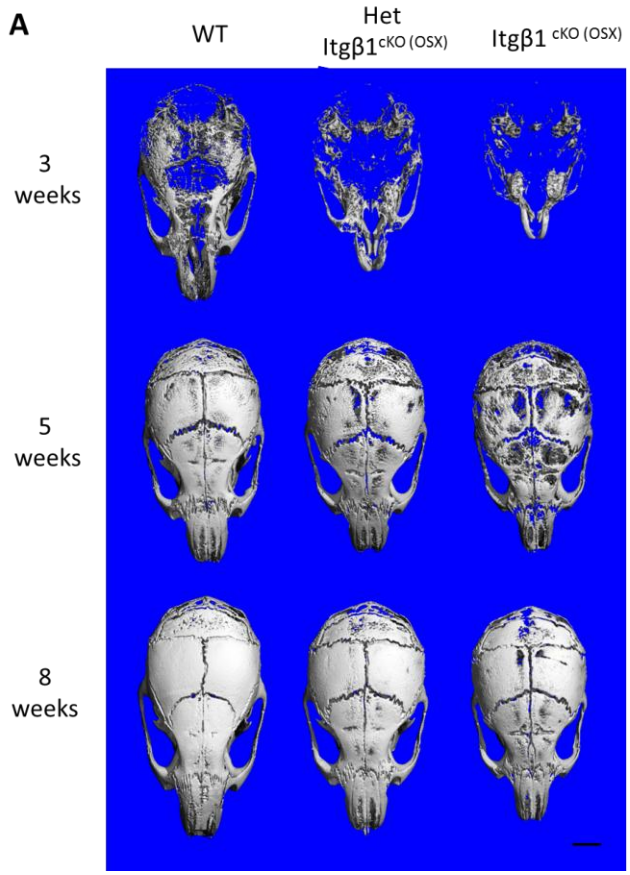

Figure 3.7. Itgβ1$^{cKO\ (OSX)}$ mice have impaired calvarial mineralization. 3D μCT reconstructions displaying the dorsal view of calvaria and underlying skull base in WT, het itgβ1$^{cKO\ (OSX)}$ and itgβ1$^{cKO\ (OSX)}$ littermates at 3, 5 and 8 weeks old indicate significantly reduced calvarial mineralization in itgβ1$^{cKO\ (OSX)}$ mice and an intermediate phenotype in het itgβ1$^{cKO\ (OSX)}$ mice. Scale bar 2 mm.

Itgβ1$^{cKO\ (OSX)}$ mouse femurs have altered structure but heal fractures normally

12-week old itgβ1$^{cKO\ (OSX)}$ femurs analyzed by μCT had abnormal cortical structure from a tranverse view (Figure 3.8A (i)). Mid-diaphyseal cortices of itgβ1$^{cKO\ (OSX)}$ mice appeared more triangular in cross-section than the cortices of their littermates. While itgβ1$^{cKO\ (OSX)}$ epiphyses appeared normal (Figure 3.8A (iii)), metaphyses displayed increased trabecular spacing (Figure 3.8A (ii)). WT and itgβ1$^{cKO\ (OSX)}$ fractured femurs both developed calluses at 2 weeks post fracture and the callus volume decreased by 5 weeks post fracture, demonstrating that β1 integrins are not required in osteoprogenitors for fracture healing (Figure 3.8C).

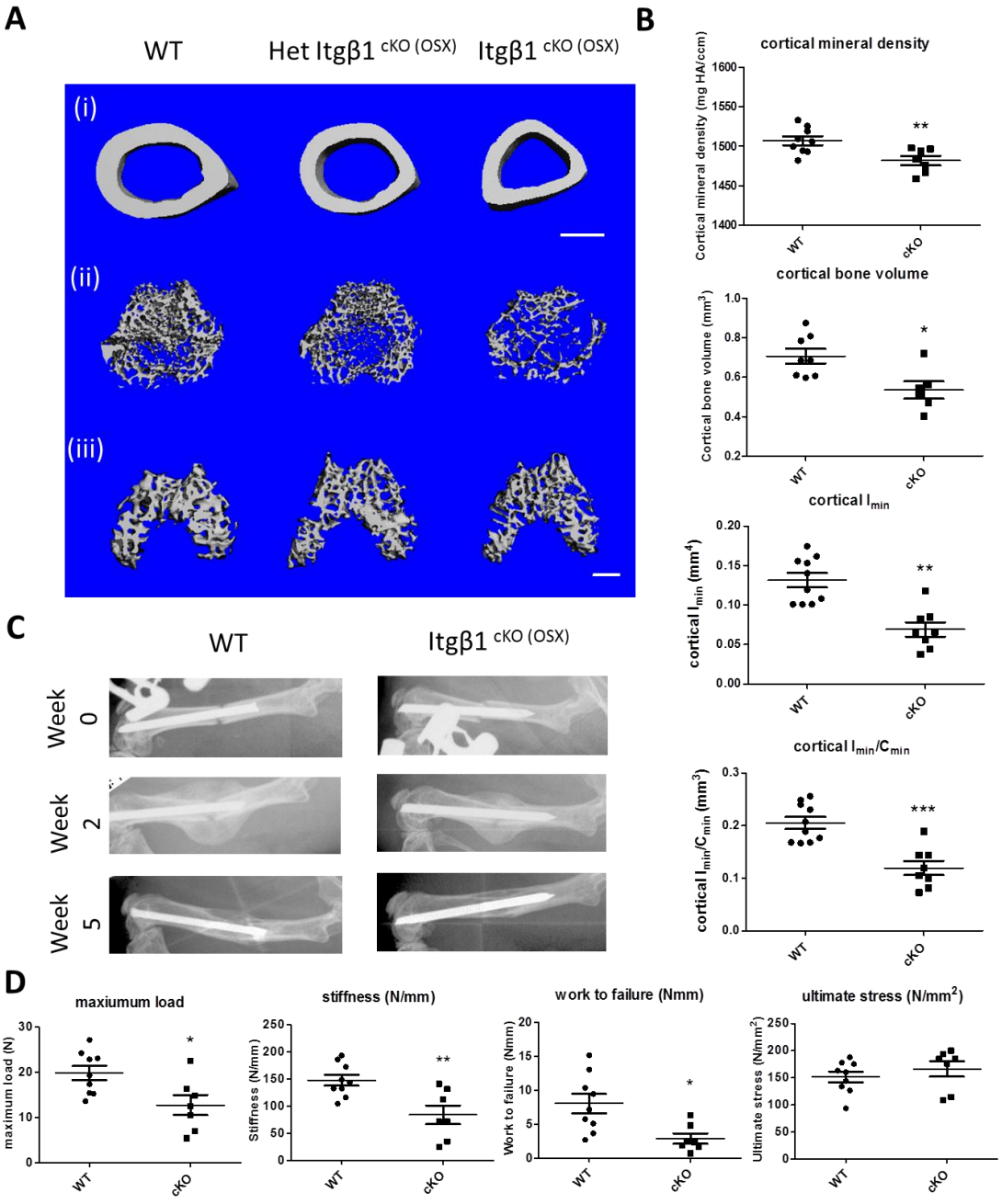

Figure 3.8. β1 integrin deletion in osteoprogenitors results in abnormal femur development, does not inhibit fracture healing in 3 month old mice. (A) 3D μCT reconstructions and (B) μCT histomorphometry measures of the mid diaphyseal cortex. (C) Radiographs of fractured femurs at 0, 2 and 5 weeks post-fracture. (D)

Biomechanical analysis by 3-point bending testing on the mid-diaphysis of intact femurs. Two-tailed t-test, * $p<0.05$, ** $p<0.01$, *** $p<0.001$. Scale bar 0.5 mm.

Itgβ1 $^{cKO\ (OCN)}$ mice are viable and do not exhibit gross abnormalities

Itgβ1 $^{cKO\ (OCN)}$ mice were born viable in the expected Mendelian frequencies and did not exhibit any gross phenotype in terms of size, weight or skeletal structure (data not shown).

OCN-Cre expression is specific to bone

X-gal staining of the femurs and tibiae from mice with the Lacz reporter gene for Cre-mediated recombination showed that cre recombination due to expression of the OCN-Cre transgene was restricted to bone tissue, specifically in the osteocytes in the cortical bone of the femur and tibia, in the periosteum and in the growth plate (Figure 3.9A). As expected, we observed no X-gal staining in the heart, lung, muscle or liver tissue (Figure 3.9B).

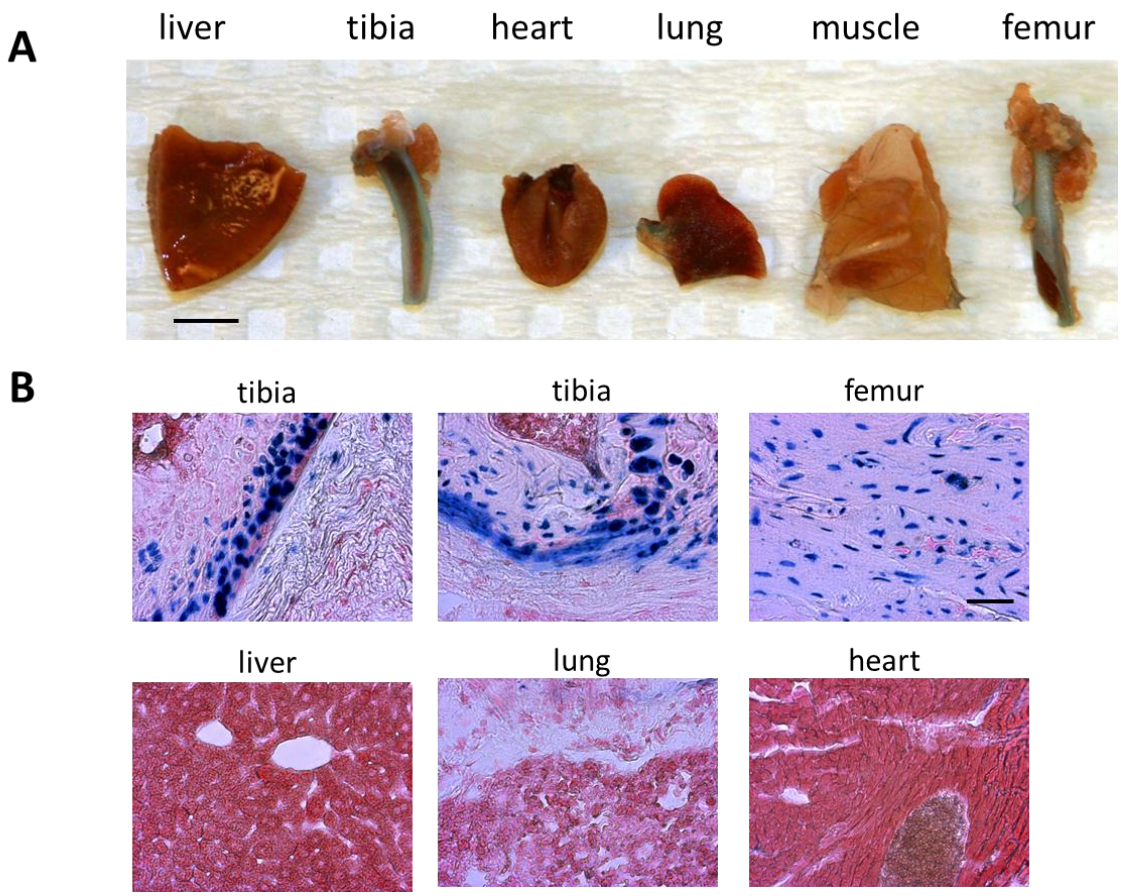

Figure 3.9. Cre-mediated excision of DNA under the OCN-Cre promoter is osteoblast and osteocyte- specific. (A) Whole-mount x-gal stained (blue) of Lacz reporter/OCN-Cre mouse shows that cre expression is specific to bone. (B) Cryosections after whole mount X-gal staining, nuclei counterstained with nuclear fast red (red). Scale bar (A) 0.5 cm, (B) 50 μm.

Femur structure is altered in the absence of β1 integrins in osteocytes/osteoblasts but there are no differences in bone mechanical properties

To assess the effect of β1 integrin deletion osteoblasts and osteocytes on bone development and healing, we analyzed the structure of intact femurs in male 10-week old

$\beta1^{fl/fl}$ (WT) and $\beta1^{fl/fl}$/OCN-Cre (itg$\beta1^{cKO\ (OCN)}$) littermates by μCT analysis. itg$\beta1^{cKO\ (OCN)}$ femurs had thicker cortices with higher bone volumes (Figure 3.10 A and B (i), $p<0.05$) and moments of inertia. In addition, itg$\beta1^{cKO\ (OCN)}$ epiphyses displayed increased connectivity density, trabecular thickness (Figure 3.10 A and B (ii), $p<0.01$) and trabecular number. In contrast, there was reduced connectivity density and higher trabecular thickness in the metaphyses of animals with bone-specific β1 integrin deletion (Figure 3.10 A (iii), $p<0.01$ and 0.05 respectively). Despite this observed difference in bone structure, there were no differences in the biomechanical properties of itg$\beta1^{cKO\ (OCN)}$ as measured by three point bending (Figure 3.10D). Ultimate stress, elastic modulus, maximum load and work to failure values were not significantly different between WT and itg$\beta1^{cKO\ (OCN)}$ femurs.

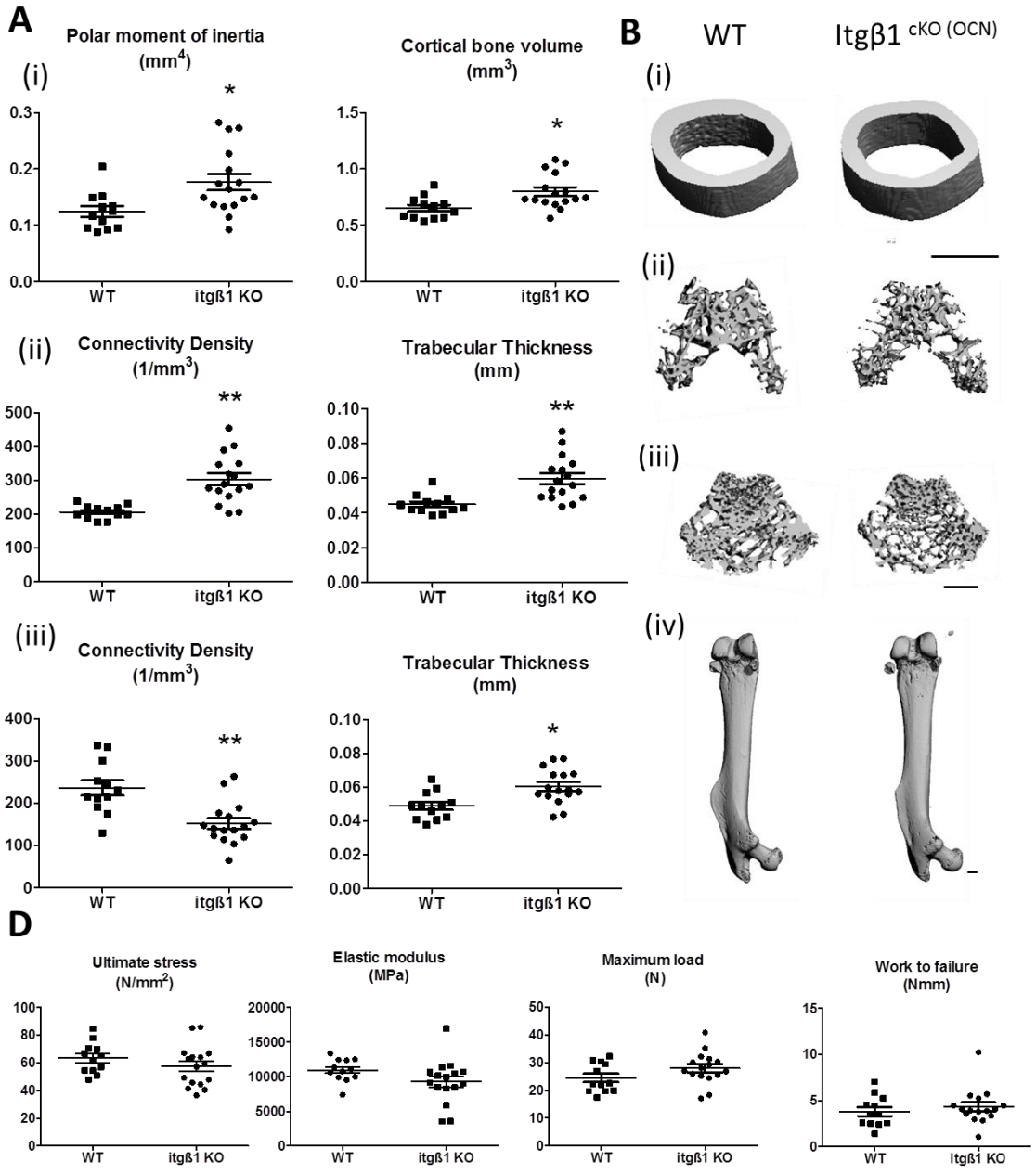

Figure 3.10. Itgβ1 $^{cKO\ (OCN)}$ mice have altered femur structure, but unaltered biomechanical properties. (A) μCT measures and (B) 3D μCT reconstructions for the (i) cortex, (ii) epiphysis, (iii) metaphysis and (iv) entire femur. One-way ANOVA with genotype as fixed effect, parents as random effects, * $p<0.05$, ** $p<0.01$. Scale bar: (C) 500μm .

Loss of β1 integrins in osteocytes/osteoblasts did not change fracture healing capacity

In order to examine the effect of β1 integrin deletion on fracture healing potential, we created mid-diaphyseal femur fractures in WT and itgβ1 $^{cKO\ (OCN)}$ mice and evaluated their healing over 5 weeks. At 2 weeks post-fracture, both WT and itgβ1 $^{cKO\ (OCN)}$ mice displayed callus formation (Figure 3.11A and B). Five weeks after fracture, the calluses for both genotypes of mice remodeled, and no gross structural differences could be observed in radiographs or 3D μCT reconstructions (Figure 3.11A and B). μCT measures such as callus bone volume at 2 weeks and 5 weeks, as well as the moment of inertia at 5 weeks, were not different between groups (Figure 3.11C). In addition, 3-point bending biomechanical testing on the fracture calluses at 5 weeks post-surgery also showed no differences in ultimate stress, elastic modulus, maximum load or work to failure (Figure 3.12A), showing that β1 integrin deficiency in osteoblasts and osteocytes did not impair fracture healing. One representative sample from each group was taken down for histological analysis at 2 and 5 weeks post-fracture. Safranin O staining revealed considerable cartilage presence in both WT and itgβ1 $^{cKO\ (OCN)}$ calluses after 2 weeks (Figure 3.12B). By 5 weeks post-fracture, there was no longer any cartilage present in both WT and itgβ1 $^{cKO\ (OCN)}$ calluses. Qualitatively, there appeared to be a greater amount of cartilage in the WT callus at 2 weeks. There was no difference in the mineral densities of either intact bone or 5 week fracture calluses of WT and itgβ1 $^{cKO\ (OCN)}$ mice (Figure 3.12C). In agreement with this observation, bone marrow stromal cells s harvested from WT and itgβ1 $^{cKO\ (OCN)}$ mice exhibited no differences in alkaline phosphatase activity at 14 days after culture in osteogenic media or in mineralization at 21 days after osteogenic induction (Figure 3.12D). These results demonstrate that β1 integrin deficiency in osteoblasts and osteocytes does not impair fracture healing potential or mineralization.

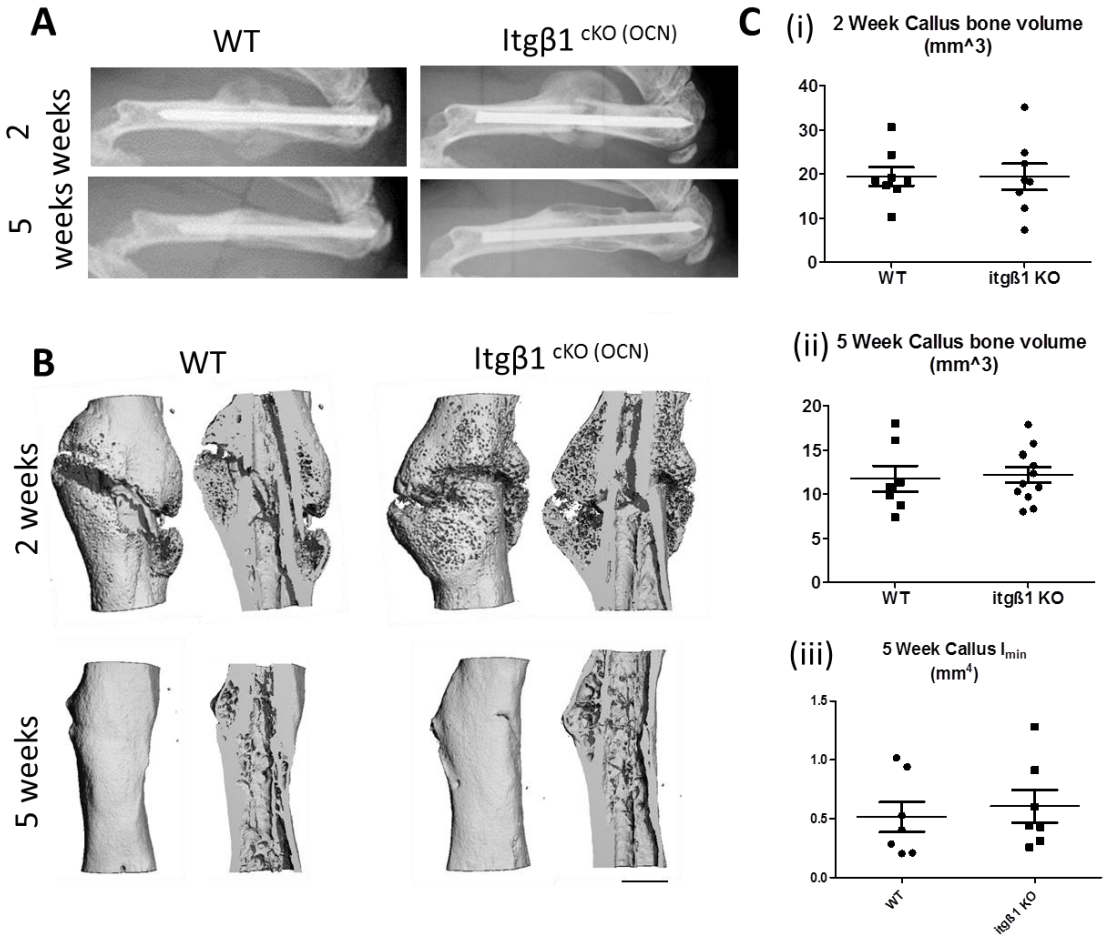

Figure 3.11. Femur fracture healing is not impaired in itgβ1 $^{cKO\ (OCN)}$ mice. (A) Radiographic images, (B) 3D μCT reconstructions and (C) μCT measures of fractured femurs from WT, n=8 and itgβ1 $^{cKO\ (OCN)}$ n=8 littermates at (i) 2 and (ii) 5 weeks post-surgery indicate no differences in fracture healing as a result of β1 integrin deletion under an osteocalcin promoter. Bars indicate standard deviation. One-way ANOVA with genotype as fixed effect, parents, sex and age as random effects , * $p<0.05$, ** $p<0.01$. Scale bar: 1mm.

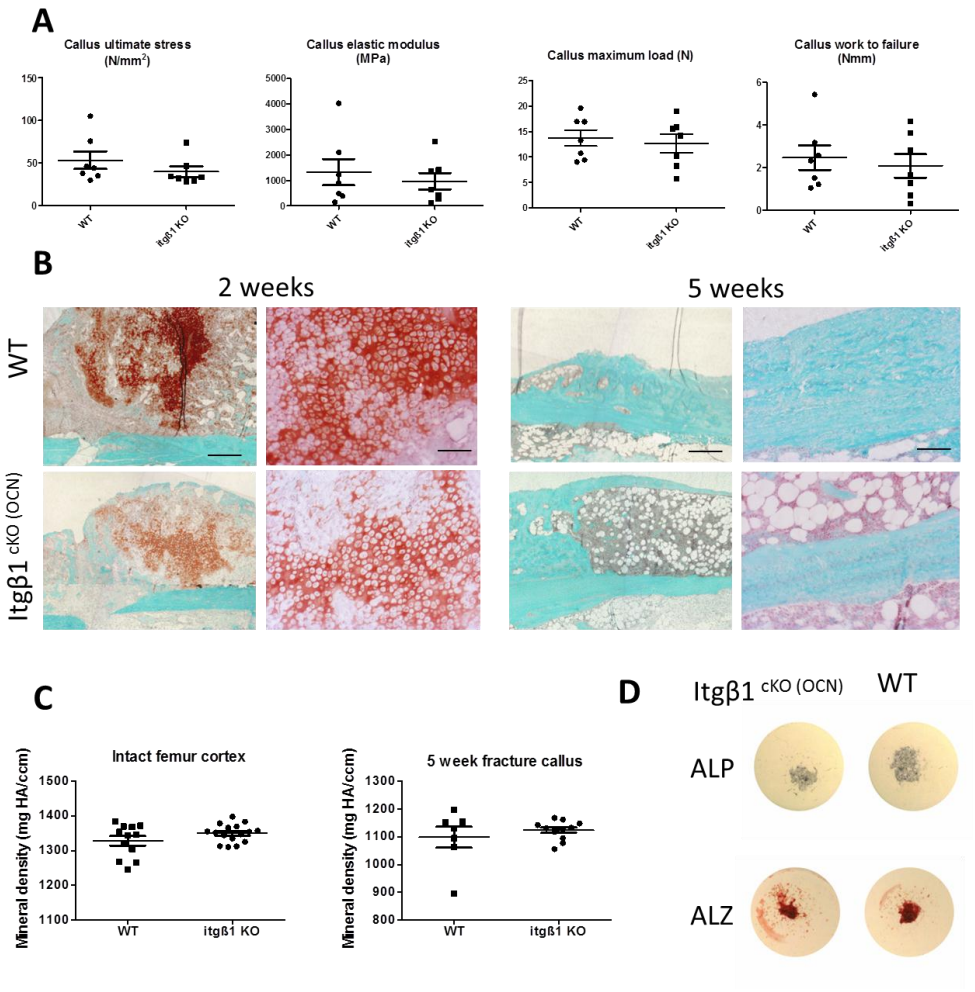

Figure 3.12. Itgβ1 $^{cKO\ (OCN)}$ callus mechanics, histomorphometry, mineral density and BMSC mineralization are unchanged. (A) 5-week biomechanical analysis by 3-point bending and (B) histological evaluation of fractured femurs at 2 and 5 weeks from WT and itg β1 $^{cKO\ OCN}$ littermates by (i) safranin-o /fast green and (ii) picrosirius red staining. (C) μCT evaluation of mineral density in intact femurs and fracture calluses. (D) *In vitro* ALP expression and mineralization (Alizarin red staining, ALZ) of BMSCs after 14 and 21 days of osteogenic induction respectively. Bars indicate standard deviation. One-way ANOVA with genotype as fixed effect, parents and age as random effects, * $p<0.05$, ** $p<0.01$. Scale bar: (B) 300 μm (left), 100 μm (right).

DISCUSSION

β1 integrins are highly expressed in osteoblasts, osteoprogenitors, and perturbation of β1 integrins *in vitro*[1-10] results in reduced differentiation and mineralization, and survival[49]. However, *in vivo* studies have failed to demonstrate a crucial role for β1 integrins in bone formation. For example, transgenic mice expressing a dominant negative mutant form of the β1 integrin under an osteocalcin promoter[13, 18, 19] as well as mice with conditional β1 integrin deletion under the osteoblast-specific Col I 2.3kb promoter [20] have displayed only mild skeletal phenotypes[11, 12]. We hypothesized that this contradictory result may be due to the timing of β1 integrin deletion *in vivo*. In order to address this hypothesis, we generated transgenic mice with β1 integrin loss in osteolineage cells at three different stages by mating β1 integrin-floxed mice with the following transgenic cre-expressing mice: integrin deletion was achieved in (1) mesodermal cells such as somites and mesencymal condensations using Twist2-Cre mice (TW2-Cre)[68], (2) osteoprogenitor cells using Osterix-Cre mice (OSX-Cre), and (3) mature osteoblasts and osteocytes with Osteocalcin-Cre mice (OCN-Cre) [69].

We found that β1integrn loss under the Twist-2 promoter resulted in embryonic lethality, while the distributions of WT and het itgβ1$^{cKO\ (TW2)}$ embryos appeared normal. While itgβ1$^{cKO\ (TW2)}$ embryos appeared indistinguishable from littermates at E11.5 and E 13.5, isolated E19.5 itgβ1$^{cKO\ (TW2)}$ embryos were significantly smaller than WT litter mates and appeared to have gross structural and functional defects of the umbilical cord as well as cranial hemorrhaging. Skeletal mineralization in itgβ1$^{cKO\ (TW2)}$ embryos was markedly reduced, with no mineralization observed at all in one itgβ1$^{cKO\ (TW2)}$ embryo and failure of calvarial and vertebral mineralization displayed in two other itgβ1$^{cKO\ (TW2)}$ embryos. Some implantations sites on harvested uterine horns were extremely small, indicating degeneration of implanted embryos, and suggesting that lethality may have occurred at an early stage in some proportion of the embryos. In contrast, itgβ1$^{cKO\ (OSX)}$ mice were viable and born in the expected Mendelian frequency, but demonstrated

reduced growth compared to WT littermate controls. Itgβ1$^{cKO\ (OSX)}$ mice weighed less than their control littermates at 27 days and exhibited reduced weight until adulthood. Radiographic analysis indicated that itgβ1$^{cKO\ (OSX)}$ mice suffered from proportional and not short-limbed dwarfism. In addition, itgβ1$^{cKO\ (OSX)}$ displayed severe tooth defects. Both maxillary and mandibular incisors were reduced in length and misoriented in itgβ1$^{cKO\ (OSX)}$ mice, while molars appeared grossly normal. igβ1$^{cKO\ (OSX)}$ calvaria also demonstrated impaired mineralization. In addition, itgβ1$^{cKO\ (OSX)}$ femurs displayed decreased mineral density, bone volume and moment of inertia (I_{min}). However, itgβ1$^{cKO\ (OSX)}$ femurs retained their fracture healing capacity. In contrast, itgβ1$^{cKO\ (OCN)}$ mice displayed only mild skeletal phenotypes. Itgβ1$^{cKO\ (OCN)}$ animals were viable and born in the expected Mendelian ratios. Surprisingly, itgβ1$^{cKO\ (OCN)}$ femurs showed increased cortical thickness, as well as higher trabecular thickness in the epihphysis and metaphysis. However, femur biomechanics, as well as the itgβ1$^{cKO\ (OCN)}$ fracture healing response was unchanged.

Previous studies of conditional β1 integrin deletions in mice have shown growth plate abnormalities, short-limbed dwarfism and perinatal lethality with chondrocyte-specific integrin deficiencies[179], but mild phenotypes with osteoblast/osteocyte-specific deletions [13, 18, 19] [11, 12]. Given that β1 integrin deletion under the osteochondroprogenitor marker Prx-1 produced viable mice with short-limbed dwarfism and joint defects due to deficiencies in growth plate and articular cartilage[180], we were surprised that itgβ1$^{cKO\ (TW2)}$ mice did not survive embryonic development, since Twist 2 is also expressed in osteochondroprogenitor cells. However, there are some differences in cre expression under Prx-1 and Twist 2 which may provide an explanation for this observation. While the first cre expression in both Prx-1-cre and Twist 2-cre occurs at E9.5, in Prx-1-cre embryos, expression is seen in mouse limb buds, while in Twist 2-cre embryos, cre expression is seen in somites and branchial arches, but also in skin[67]. Prx-1-cre expression may be more restricted to skeletal regions than Twist 2-cre expression. It is

likely that the cause of embryonic lethality in itgβ1$^{cKO\ (TW2)}$ embryos is not related to skeletal development because embryos lacking mineralized skeletons usually survive embryonic development and die newborn due to respiratory distress, as is seen with Runx2 deficient mice[79]. Studies involving the earliest stage deletion of β1 deletion under osteo or chondro lineage promoters were deletions under Prx-1-cre[180] and Col2a1-cre[179]. Neither of these studies reported defects in mineralization. Therefore, the severe mineralization defects observed in itgβ1$^{cKO\ (TW2)}$ embryos are probably not due to β1 deletion in chondrocytes. The presence of umbilical cord defects and cranial hemorrhaging in itgβ1$^{cKO\ (TW2)}$ embryos may indicate embryonic lethality due to vascular defects. To our knowledge, the skeletal mineralization phenotype we have seen in itgβ1$^{cKO\ (TW2)}$ E19.5 embryos is the most severe mineralization defect observed *in vivo* due to β1 integrin loss in osteochondro lineage cells. Although one itgβ1$^{cKO\ (TW2)}$ E19.5 embryo displayed no skeletal mineralization at all, two other itgβ1$^{cKO\ (TW2)}$ embryos lacked craniofacial and vertebral mineralization but demonstrated mineralized long bones, ribs and scapula. The long bones are part of the appendicular skeleton which is derived from lateral plate mesoderm cells. However, the vertebrae are part of the axial skeleton and derived from sclerotome cells in the somites. In contrast, craniofacial bones are derived from a combination of neural crest and mesoderm-derived cells. The differential effect on β1 integrin deletion on various skeletal elements may be related to their developmental origin.

Itgβ1$^{cKO\ (OSX)}$ mice were viable and displayed reductions in calvarial mineralization as well as incisor defects and growth abnormalities. While itgβ1$^{cKO\ (OSX)}$ calvaria were poorly ossified compared to age-matched littermates at all the time points studied, calvarial mineralization continued to increase with age in the itgβ1$^{cKO\ (OSX)}$ mice, suggesting delayed mineralization in itgβ1$^{cKO\ (OSX)}$ calvaria. Some aspects of the itgβ1$^{cKO\ (OSX)}$ phenotypes reported here have also been observed in mice with global deletions of the collagen-binding α11 or α2 integrins, as well as in α11+ α2 integrin double

knockouts. α11, α2, and α2 +α11 integrin knockout mice exhibit proportional dwarfism attributed to altered IGF-1/GH signaling due diminished GHRH production in the hypothalamus [181]. α11 KO incisors are also shortened[182], although the incisor defect in α11 KO mice do not appear to be as severe as in in itgβ1$^{cKO\ (OSX)}$ mice. It is possible that the proportional dwarfism and incisor defects in itgβ1$^{cKO\ (OSX)}$ mice are partly due to α11β1 and α2β1integrin deletion. The knockout of ICAP-1 (also known as integrin β1 binding protein 1), which binds to[183] and regulates β1 integrin function[184], results in calvarial mineralization defects as well[185], which also supports a role of β1 integrins in calvarial development.

We found that β1 integrin deletion in mature osteoblasts and osteocytes resulted in subtle structural alterations to cortical and trabecular bone in femurs. The cortical thickness as well as trabecular thickness was increased in both the epiphysis and metaphysis of itgβ1$^{cKO\ (OCN)}$ mice. However, the biomechanical properties of femurs were unchanged in itgβ1$^{cKO\ (OCN)}$ mice compared to WT controls. We also found that fracture healing was not impaired in in itgβ1$^{cKO\ (OCN)}$ femurs, as measured by μCT as well as mechanical testing. Our data suggests that β1 integrins are not required for osteoblast function. These results are supported by previous studies involving β1 integrin deletion under an osteocalcin promoter[11, 12], or expression of a dominant-negative form of the β1 integrin under an osteocalcin promoter[13, 18], which have displayed minor phenotypes . While these findings suggest an early important role for β1 integrin in regulating bone development, the mechanism by which this occurs is still unknown. Further studies will be required to elucidate the role of β1 integrins in regulating early skeletal progenitor cells, as well as and how compensation occurs for β1 integrins in osteoblasts, given that the majority of bone ECM proteins are β1 integrin ligands. However, these results must be interpreted with several qualifications. Although Twist 2 is expressed in osteolineage cells, it is not osteolineage specific, and is also expressed in other tissues such as the dermis. Therefore, some aspects of the skeletal phenotype observed in itgβ1$^{cKO\ (TW2)}$

embryos may be modulated by alterations to non-osteolineage cells. We have reported empirical observations on the effects of targeted β1 integrin deletions. However, further studies will be required in order to elucidate the in vitro phenotypes of itgβ1$^{cKO\ (OSX)}$ osteoprogenitors and itgβ1$^{cKO\ (TW2)}$ MSCs, and to determine β1 integrin signaling pathways responsible for our observed phenotype. We also note that although we observed only minor differences between the bone phenotypes of itgβ1$^{cKO\ (OCN)}$ mice and their wild-type littermates, our analyses have focused on the femurs of 10-13 week old mice. Therefore it is possible that transient femur phenotypes in younger mice, or alterations in the development of other bones may occur in itgβ1$^{cKO\ (OCN)}$ mice.

In conclusion, we have demonstrated that β1 integrin deficiency in somites and mesenchymal condensations induce severe defects in skeletal mineralization. This finding highlights that β1 integrins play a crucial role in early skeletal development, especially in the calvaria and vertebrae. We have also shown that β1 integrin deletion in osterix-expressing osteoprogenitors results in a delay in calvarial ossification. In addition, itgβ1$^{cKO\ (OSX)}$ mice display severely shortened maxillary and mandibular incisors, indicating that β1 integrins regulates incisor eruption. However, β1 integrin loss in osteoblasts and osteocytes induces only minor changes to bone phenotype and does not impair fracture healing. Thus we provide the first *in vivo* evidence that β1 integrins are essential for calvarial development and that the regulatory role of β1 integrins is either increasingly diminished or compensated for as skeletal progenitor cells undergo commitment and differentiation.

CHAPTER 4: INTEGRIN-SPECIFIC BIOFUNCTIONALIZED PEG-MAL HYDROGELS ENHANCE BONE REGENERATION IN MURINE SEGMENTAL DEFECTS

INTRODUCTION

Over 1 million bone grafting, bone excision and fracture repair surgeries are performed annually in the US, at cost of approximately $5 billion [14-17]. While autografts, which are usually harvested from the patient's iliac crest, are the gold standard of care, autografts are limited by the available donor graft volume and often cause pain and inflammation at the donor site[22]. Allografts are more readily available than autografts but are processed to prevent the infection and immunogenicity. These processes decrease allograft osteogenicity and structural properties due to the absence of viable cells and limit the ability of allografts to remodel, and result in a high complication rate[22, 89-91]. These limitations of traditional bone grafts have spurred the development of bone graft substitutes such as BMP-containing products which have been widely adopted since 2002, when BMP-2 and BMP-7 products were approved by the FDA for use in humans. While BMP therapy has been successful in stimulating bone formation, the BMP doses used clinically are orders of magnitude higher[186] than physiological concentrations of BMP, resulting in high costs of treatment[95]. Furthermore, delivery of supraphysiological BMP doses without sustained release mechanisms may result in growth factor diffusion away from the defect site and result in complications such as ectopic bone formation, nerve injuries[96], as well as inflammatory and carcinogenic effects [22-24]. Therefore, there remains an unmet clinical need for bone graft substitutes which are safe, cost-effective and efficacious.

Tissue engineering strategies, which deliver materials, bioactive molecules and/or cells *in vivo* to provide microenvironmental cues which stimulate tissue repair, show

great promise in addressing the need for improved bone graft substitutes. Recent efforts have focused on biomimetic strategies focused on engineering synthetic ECM analogues which promote specific integrin-ECM interactions to direct desired host cells responses[25, 187, 188]. Integrins are a family of cell surface receptors which mediate cell-extracellular matrix interactions and regulate crucial cell functions such as survival, growth, migration and differentiation [27, 29, 30]. Specifically, the interaction of α2β1 integrins with collagen I is a crucial signal for osteoblastic differentiation and matrix mineralization [3, 4, 41-44]. The hexapeptide sequence Gly-Phe-Hyp-Gly-Glu-Arg (GFOGER) is found on residues 502–507 of the α1(I) chain of type I collagen and serves as the major recognition site for α2β1 integrin binding [117, 126, 127]. Our group has previously engineered a synthetic collagen I-mimetic GFOGER containing peptide, $GGYGGGPC(GPP)_5GFOGER(GPP)_5GPC$, which recapitulates the triple helical tertiary structure of native collagen and binds specifically to α2β1 integrins. The GFOGER ligand has been shown to recapitulate the bioactivity of collagen I, and is also effective in supporting bone healing and osseointegration *in vivo*. Surfaces presenting adsorbed or covalently immobilized GFOGER peptide support equivalent levels of α2β1 integrin-mediated cell adhesion as native collagen I [128] and also promote osteoblastic differentiation of MC3T3-E1 and primary bone marrow stromal cells *in vitro* [25, 129]. Furthermore, simple adsorption of GFOGER to PCL scaffolds enhances bone repair *in vivo* within rigorous critical-sized rat femur defect models without the delivery of cells or growth factors [130]. GFOGER-functionalized titanium implants also enhance implant integration in a rat cortical model by improving peri-implant bone formation and implant fixation to bone [25, 129].

In this study, we incorporated the adhesive α2β1 integrin-specific GFOGER ligand combined with low dose rhBMP-2 in a protease-degradable PEG-maleimide hydrogel and evaluated the regenerative potential of our biomaterial in a murine radial segmental defect model. We chose to deliver the bioactive ligand and growth factors

within a PEG-maleimide hydrogel because synthetic hydrogels offer advantages such as low inflammatory profiles, tailorable mechanical properties and biofunctionality[189, 190]. We hypothesized that presentation of the integrin-specific GFOGER in combination with sustained, cell-mediated 'on-demand' release of low-dose rhBMP-2 would promote osteoblastic differentiation of host cells and promote bone regeneration *in vivo*.

METHODS

Hydrogel synthesis and collagen sponge implant preparation

GFOGER peptide, $GGYGGGPC(GPP)_5GFOGER(GPP)_5GPC$, (4 kDa peptide, 12kDa as the self-assembled triple helical molecule) was custom synthesized via solid phase synthesis by Activotec (Figure 4.1A). Four- arm, maleimide-end functionalized (>95%) PEG macromer (, PEG-MAL, 20 kDa) was purchased from Laysan Bio (Figure 4.1B). The RGD adhesive peptide GRGDSPC (RGD) and bi-cysteine crosslinker peptide GCRDVPMSMRGGDRCG (VPM)[191, 192] were synthesized by AAPTEC. Carrier-free rhBMP-2 was purchased from R&D Biosystems. PEG-MAL hydrogels were synthesized by reacting PEG-MAL with adhesive ligands (RGD or GFOGER) followed by rhBMP-2 and the VPM crosslinking peptide and incubating at 37C (Figure 4.1C). Thin 2D gel discs were fabricated by coverslipping gel solutions with sterile coverslips which were treated with Sigmacote to increase their hydrophobicity. 1.5 µL of hydrogel was cast within each 4 mm long polyimide sleeve for ease of handling during *in vivo* implantation. 3 mm thick collagen sponges were cut with a 1 mm diameter biopsy sponge and placed within the polyimide sleeves prior to implantation. Polyimide sleeves were laser machined with 200 µm diameter holes to allow for cell invasion and nutrient transport into the defect site.

hMSC cell culture and differentiation assays

hMSCs were obtained from Lonza. hMSCs were cultured in MSCGM (Lonza) and seeded for osteogenic differentiation assays at a density of 10,000 cells/cm^{2}on thin hydrogel surfaces. hMSCs were then cultured for up to 21 days in osteogenic induction media (Lonza). After 3 days of culture in osteogenic media, cells were rinsed in PBS and incubated in 2 μM calcein and 4 μM ethidium homodimer for 30 minutes for Live/Dead staining, and then imaged on a Zeiss microscope At 14 days post-induction, hMSCs were assayed for alkaline phosphatase activity (ALP). Briefly, cells were scraped in PBS, transferred to cold 50 mM Tris-HCl and sonicated to lyse the cells. The total protein content for each lysate sample was determined using a BCA assay kit (Thermo Scientific) according to the manufacturer's instructions. Samples were diluted to the same total protein content before assaying for ALP. Samples and ALP standards were loaded into a 96-well plate, then incubated with MUP substrate at 37 °C for 1 hour and read at 360 nm excitation and 465nm emission. Mineral deposition at 21 days post-induction was assayed by Alizarin Red staining. Cells were fixed in 10% formalin, rinsed twice in water and incubated in 2% Alizarin Red solution for 20 minutes. After 4 washes in water, the stained cells were scraped in 10% acetic acid and heated to 85 °C for 10 minutes. The supernatant was collected after centrifugation, neutralized with 10% ammonium hydroxide and read in a 96-well plate at 405nm.

Thiol quantification assay

We carried out a thiol quantification assay in order to determine the efficiency of GFOGER ligand incorporation to PEG-MAL via Michael addition reaction of the thiol

containing cysteine amino acid residues with maleimide groups. The thiol measure-IT assay kit was purchased from Invitrogen. PEG-MAL was reacted with GFOGER ligand at various molar ratios for 1 hour at 37 °C. A 96-well plate was pre-loaded with the working solution and PEG-GFOGER reaction mixtures as well as GFOGER standards then added to appropriate wells. After 5 minute incubation at room temperature, the plate was read at 494nm excitation and 517nm emission.

Murine radial segmental defect surgery

B6129SF2/J wild-type male mice (8-10 week old) were purchased from Jackson Laboratories. Mice were anesthetized under isoflurane and fur was removed from the right forelimb using a depilatory cream. The forelimb was then swabbed with chlorohexidine and alcohol to sterilize the surgical site and a 1.5 cm incision was made in the skin. Muscle tissue overlying the ulna and radius were blunt dissected, and a 2.5 mm defect was created in the radius using a custom-machined bone cutter, while leaving the ulna intact. Hydrogel or collagen sponge placed within polyimide sleeves were implanted into the defect by fitting the sleeve over the radius at the proximal and distal ends of the defect, so that the hydrogel or collagen sponge filled the defect space. The incision was then closed with vicryl suture and wound clips. Mice were provided with a single dose of slow release buprenorphine for pain relief and were monitored post-surgery for signs of distress, normal eating habits and movement.

Radiography, μCT analysis and biomechanical evaluation

Every two weeks after surgery, radial defects were imaged radiographically with the MX-20 Radiography System (Faxitron Imaging) using an X-ray beam energy setting of 23kV and scan time of 15 seconds. At 4 and 8 weeks post-surgery, radial defects were

non-invasively analyzed by μCT scanning a 3.2 mm length of defect using a VivaCT (Scanco Medical) using the following parameters: intensity of 145 μA, energy of 55 kVp, integration time of 200 ms, and resolution of 15 μm. Evaluation of bone formation within the radial defect was performed by hand contouring 2D slices to include only the radius and exclude ulnar bone. The data was evaluated by applying a Gaussian filter (sigma=1, support =1) using a threshold value of 540mg HA/ccm. 3D μCT reconstructions display the full 3.2 mm length of radius scanned. However, in order to ensure that only new bone formation was measured, quantification of bone volume and mineral density within the defect was performed by evaluating only the middle 2.0 mm of defect. defect. For biomechanical testing, radii were potted win Wood's metal within a custom potting apparatus. After potting, the ulna was cut and the radii were loaded onto a Bose ELF 3200 testing system. Torque was applied to the samples at 3 degress per second until failure.

GFOGER and rhBMP-2 labeling and FMT analysis

Vivotag 800 and Vivotag 680 XL amine reactive NHS ester near infrared (IR) dyes were purchased from Perkin Elmer. GFOGER peptide and rhBMP-2 were labeled with Vivotag 680 and Vivotag 800 respectively. GFOGER peptide was reconstituted in 50 mM sodium carbonate buffer, pH 8.5 and reacted with excess Vivotag 800 dissolved in PBS for 2 hours at room temperature. rhBMP-2, which was lyophilized in acid, was reconstituted in NaOH to obtain an rhBMP-2 solution at neutral pH. rhBMP-2 was reacted with excess Vivotag 800 dissolved in PBS for 1 hour at room temperature. Labeled GFOGER and rhBMP were both desalted using Zeba 7kD MWCO columns to remove unreacted dyes and salts from the solutions, and then snap frozen and lyophilized overnight. GFOGER ligand or rhBMP-2 retention within the defect site was analyzed

using a FMT 4000 instrument (Perkin Elmer). Fur was removed from the right forelimb of mice and placed within a mouse imaging cassette, with their forelimbs resting on a tissue imaging block. Mouse forelimbs were scanned at a source density of 1 mm with a total of 65 total source points per scan on the 680 or 790 laser channels for Vivotag 680 and Vivotag 800 respectively. Vivotag 680 or Vivotag 800 conjugates were selected as the agents in the scan setting scans. The IR dye signal was quantified by placing rectangular prism-shaped 3D regions of interest markers (ROIs) around the right forelimb and thresholding at 0 nM concentration. The total amount of IR dye per animal was reported normalized to the day 0 value. For in vitro release studies, Vivotag 800-labeled rhBMP-2 was encapsulated within 5ul hydrogels consisting of 4% wt/vol PEG-maleimide functionalized with 2mM GFOGER at a final rh-BMP-2 concentration of 0.04 μg/ul. 5ul of 0.04 μg/ul rh-BMP-2 was also pipetted into collagen sponges. The hydrogels and collagen sponges were each placed in 200ul PBS or 0.1 mg/ml collagenase I solution. rhBMP-2 release into from the hydrogel or sponge into solution was measured by taking 5μl aliquots of the solution at various timepoints and reading their fluorescence values using a Xenogen IVIS Lumino II fluorescence imager.

Histology

Animals were euthanized 8 weeks after surgery by excess CO_2 inhalation and their radii and ulna were harvested. Soft tissue was removed carefully without disturbing the defect and the bones fixed in 10% neutral buffered formalin overnight. Samples were then briefly rinsed in tap water and decalcified in formic acid for two days. The samples were then processed for embedding in Immunobed (GMA) resin and sectioned to 2 μm

thickness. GAM sections were deplasticized and stained with Safranin O/Fast Green, Picrosirius Red or H&E.

Statistical analysis

Data was analyzed by one-way ANOVA with post-hoc Tukey in JMP, or with Student's t-test. A p value of less than 0.05 was considered significant.

RESULTS

Functionalizing PEG-MAL with GFOGER

The thiol containing GFOGER ligand was covalently tethered to PEG-MAL by Michael addition reaction (Figure 4.1D) between the thiol groups in the cysteine amino acid residues of GFOGER and the maleimide groups in PEG-MAL. In order to determine the efficiency of GFOGER peptide tethering efficiency to PEG-MAL, we reacted GFOGER peptide with PEG-MAL at varying ratios of maleimide: triple helical GFOGER molecule and measured the concentration of free thiols present in the reaction mixture, with known concentrations of GFOGER as a standard. GFOGER incorporation increased from 0% at a maleimide: GFOGER ratio of 0 to almost 100% at a maleimide: GFOGER ratio of 5.5 (Figure 4.1E). Therefore, at a maleimide: GFOGER molar ratio of 5.5 or higher, all the GFOGER that reacted with PEG-MAL will be incorporated into the final GFOGER-PEG hydrogel.

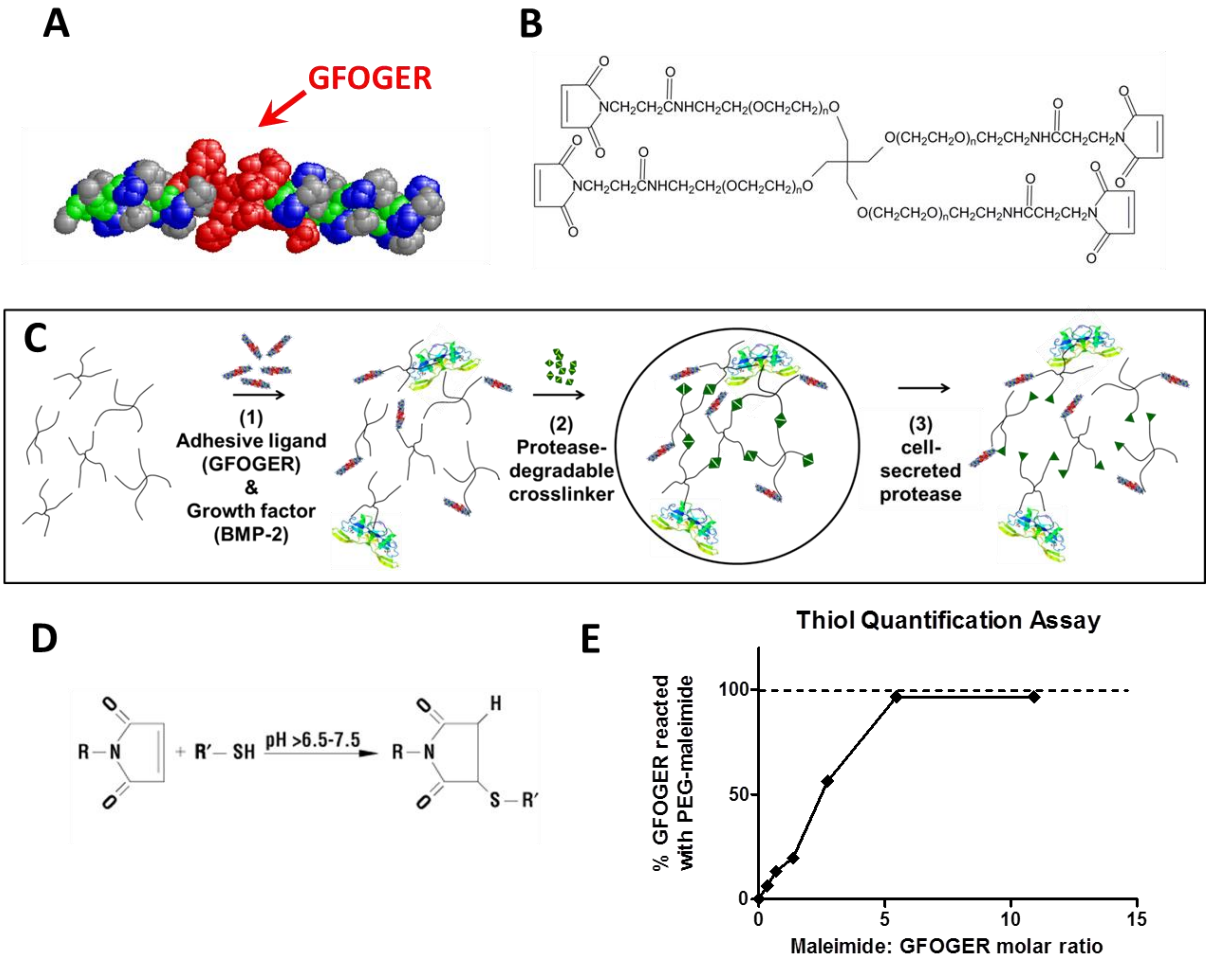

Figure 4.1. The synthetic GFOGER ligand tethered to PEG-MAL at controlled densities and chemically crosslinked to form a protease-degradable hydrogel network. (A) A space-filling model of the GFOGER ligand. (B) Chemical structure of branched 4-armed PEG-maleimide macromer. (C) Protease sensitive PEG hydrogels incorporating GFOGER and BMP-2 are synthesized by reacting PEG-MAL with GFOGER and BMP-2 and adding a protease-degradable bi-cysteine peptide to form a crosslinked hydrogel network. (D) Maleimide groups form covalent bonds with sulhydryl-containing molecules at physiological pH by Michael addition to form a thioester linkage. (E) GFOGER ligand reacts completely with PEG-MAL when the maleimide: GFOGER ratio exceeds 5.5.

hMSC adhesion, viability and differentiation on GFOGER or RGD hydrogels

In order to assess if GFOGER functionalized PEG hydrogels could support cell adhesion, viability and differentiation, we seeded hMSCs atop thin flat PEG-MAL hydrogels functionalized with GFOGER or RGD at equimolar densities. We observed an increase in hMSC adhesion and spreading on both GFOGER and RGD hydrogels with ligand densities ranging from 0.5 mM to 2 mM (Figure 4.2A), while cells on PEG-only (no RGD or GFOGER) and 2 mM non adhesive RDG gels remained rounded and supported extremely low levels of adhesion (Figure 4.2A). This intrinsically low background of PEG allowed us to detect differences in bioactivity of GFOGER or RGD ligands. Live/dead staining of hMSCs after 3 days of culture on hydrogel surfaces demonstrated high cell viability on both 2 mM GFOGER and 2 mM RGD surfaces (Figure 4.2B). While 2mM GFOGER and RGD surfaces supported similar levels of adhesion and viability, alkaline phosphatase activity of hMSCs on GFOGER surfaces was significantly higher than on RGD surfaces, $p<0.05$ (Figure 4.2C). GFOGER hydrogels also enhanced *in vitro* mineralization compared to RGD gels. hMSCs cultured on GFOGER surfaces had Alizarin red staining and extraction values which were 30% higher than hMSCs on RGD gels, $p<0.01$ (Figure 4.2D).

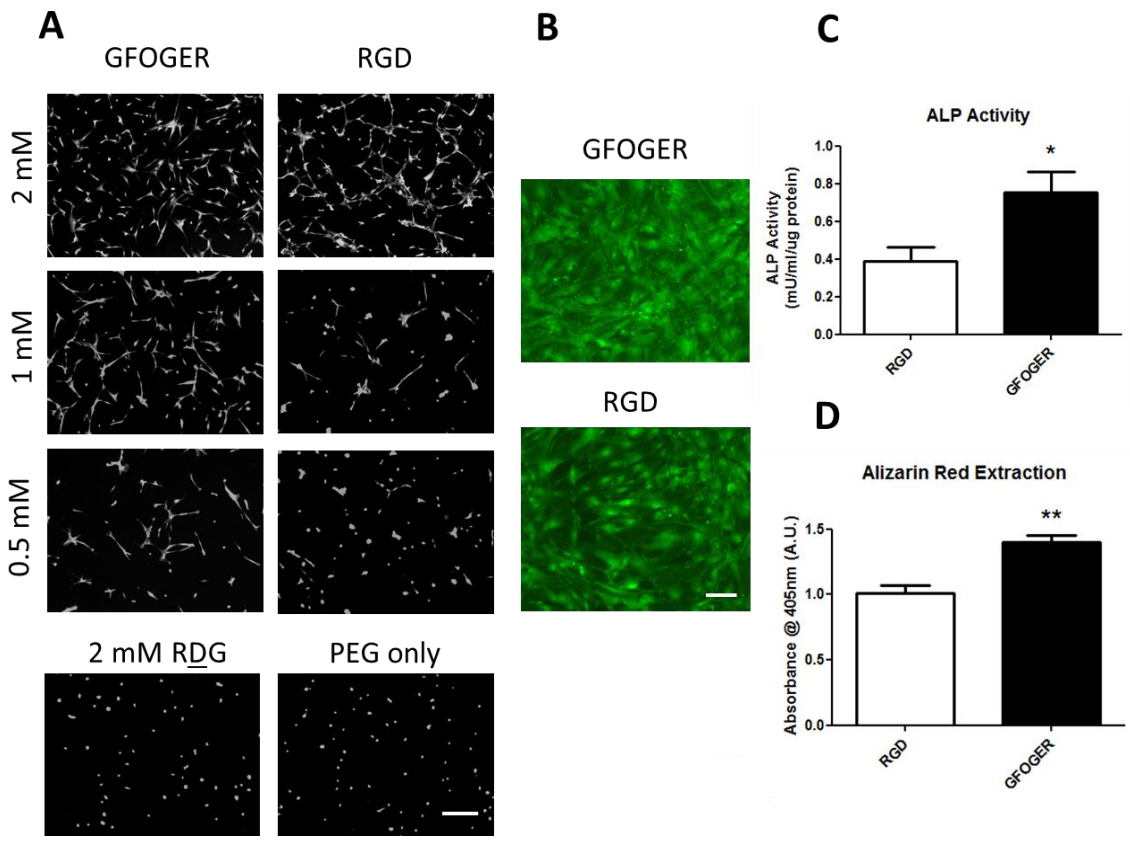

Figure 4.2. hMSC adhesion, viability and differentiation on GFOGER and RGD hydrogel surfaces. (A) Micrographs of calcein-stained hMSCs on GFOGER and RGD gel surfaces at varying bulk densities of ligand 1 day after seeding. (B) Live/Dead stained hMSCs on 2 mM GFOGER and 2 mM RGD hydrogel surfaces 3 days after osteogenic induction. (C) ALP activity at 14 days and (D) Alizarin Red stain for mineralization at 21 days post induction. Scale bar (A) 50 μm and (B) 20 μm.

Bone formation in response to GFOGER and GFOGER/BMP hydrogels

To evaluate the effect of GFOGER and GFOGER/BMP hydrogels on bone formation, we implanted these materials into murine radial critical-sized segmental defects. 2.5 mm long segmental defects (Figure 4.3) were created in the right radii of age-matched male mice, while leaving the ulna intact (Figure 4.4A, week 0). In a pilot study, we established that there were no differences in bone formation within untreated empty

defects and defects which received an empty tube implant. We subsequently used empty tube implants as our negative controls. The conditions tested were defects treated with polyimide tubes with (1) no hydrogel (empty tubes), (2) 4% (wt/v) PEG hydrogels functionalized with 2 mM GFOGER (GFOGER), or (3) 4% (wt/v) PEG hydrogels modified with 2 mM GFOGER and incorporating 0.03 μg of rh-BMP-2 (GFOGER/0.03 μg rhBMP-2). While negligible bone formation occurred at the ends defects treated with empty tubes, GFOGER and GFOGER/0.03 μg rhBMP-2 treated defects showed significantly greater bone regeneration over time (Figure 4.4B and C). Four out of 6 GFOGER-treated defects came close to bridging the defects and 5/7 GFOGER/0.03 μg rhBMP-2-treated defects bridged after 8 weeks (Figure 4.4B). Despite the increased rate of bridging with GFOGER/0.03 μg rhBMP-2 implants compared to GFOGER implants, the bone volume values between these groups was not significantly different at 4 or 8 weeks. In contrast, bone volumes in GFOGER-treated and GFOGER/0.03 μg rhBMP-2-treated defects were higher than in empty tube defects at 8 weeks post-surgery, $p<0.05$ (Figure 4.4C). However, there were no differences in bone mineral density between any of the groups at either time points (Figure 4.4C).

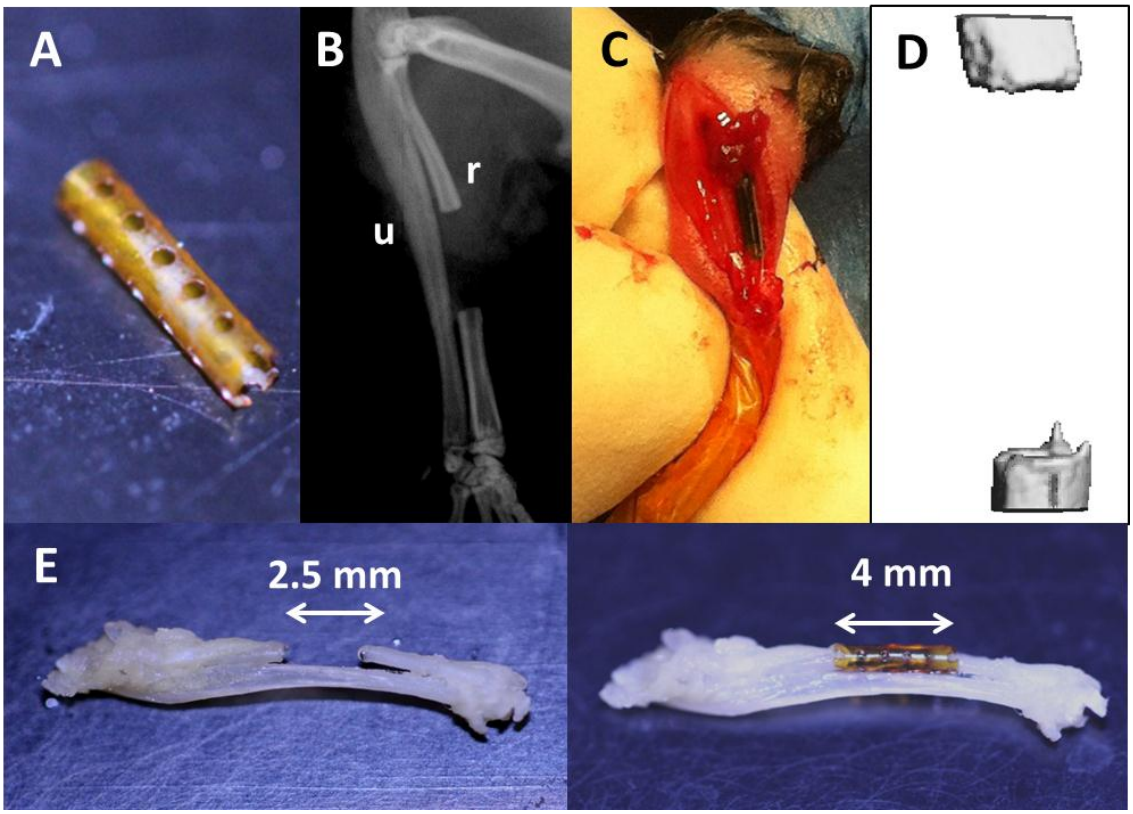

Figure 4.3. Murine radial segmental defect model. (A) Hydrogels are pre-cast in a polyimide sleeve with 200 μm diameter holes along the tube walls. (B) 2.5 mm defects are created in the radius (r) while leaving the ulna (u) intact to stabilize the defect. (C) Radial defect with hydrogel-sleeve implant, hydrogel is blue for better visualization. (D) Sample 3D μCT reconstruction of radial defect 3 days after surgery. (E) Excised radius and ulna with 2.5 mm radial defect (left) and with 4 mm polyimide sleeve fitted over the defect (right).

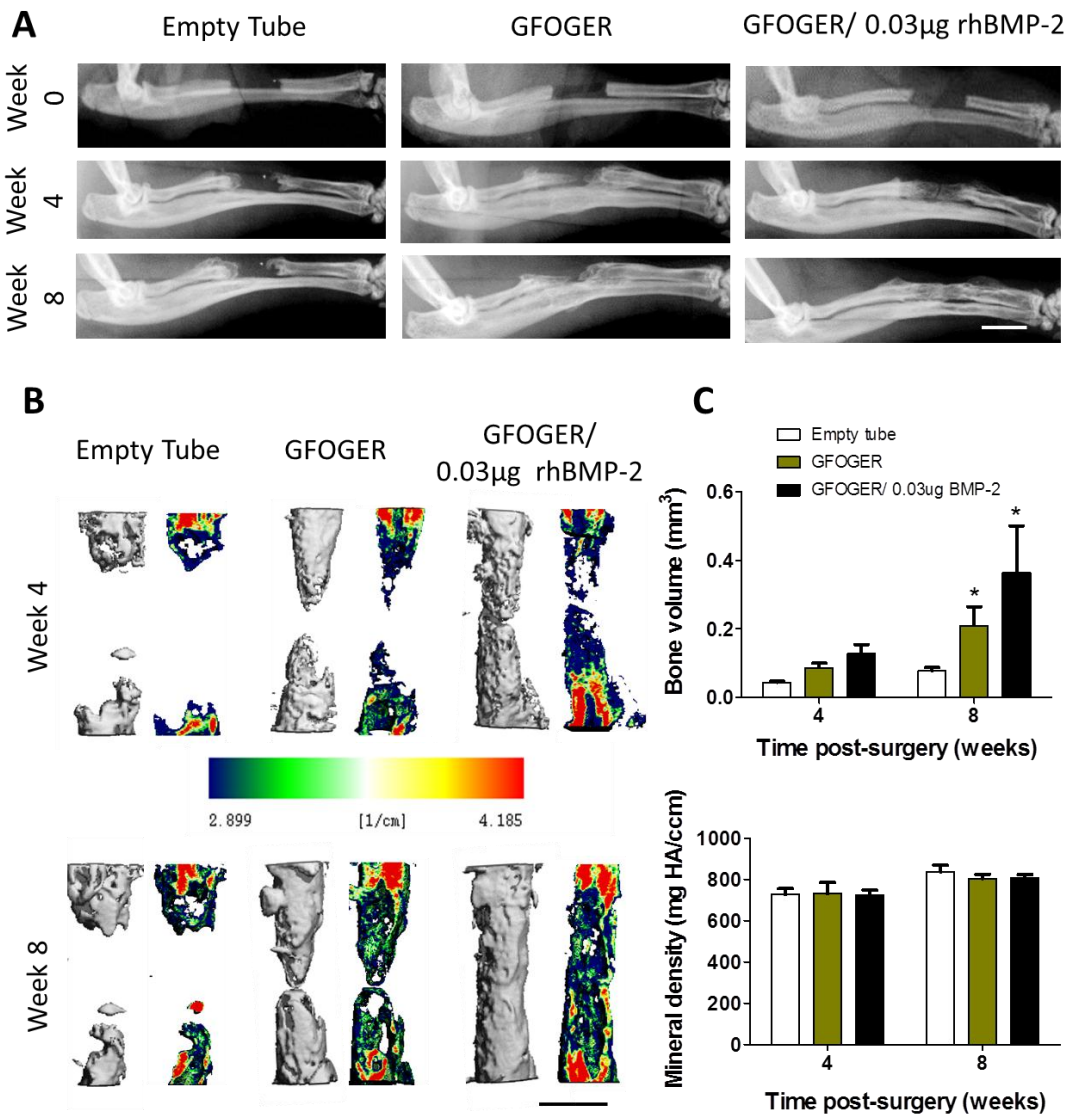

Figure 4.4. Radiographic and µCT evaluation of bone healing in response defects treated with GFOGER hydrogels or GFOGER/0.03µg rhBMP-2. (A) Representative radiographic images, (B) 3D µCT reconstructions (left) and mineral density mappings on saggital sections of the same defects (right) and (C) quantitative µCT measures of radial defects at 4 and 8 weeks post-surgery. Scale bar (A) 2mm, (B) 1mm. * $p<0.05$.

Role of adhesive ligand and protease-degradable crosslinker in bone formation

To determine the role of the adhesive ligand and protease degradable crosslinker GCRDVPMSMRGGDRCG (VPM) in our biomaterial system, we next tested three types of hydrogels within radial segmental defects: (1) 4% PEG-maleimide hydrogels functionalized with 2 mM GFOGER and crosslinked with VPM, the MMP-sensitive crosslinker (GFOGER), (2) 4% PEG-maleimide hydrogels crosslinked with VPM (PEG-only) and (3) PEG-maleimide hydrogels crosslinked with DTT, a small molecule crosslinker that is not sensitive to MMP-mediated degradation (non-degradable PEG). PEG hydrogels crosslinked with the VPM crosslinker peptide has previously been shown to degrade in response to MMP-1 andMMP-2, with k_{cat} values of 5.25 +/- 0.95 s^{-1}, 4.82 +/- 0.79 s^{-1}[1192]. In addition, VPM is also sensitive to plasmin-mediated cleavage[191]. At 4 weeks, GFOGER treated defects showed bone repair (Figure 4.5B and C). However, defects treated with PEG-only hydrogels displayed minimal bone formation. Bone defects treated with non-degradable PEG hydrogels showed signs of bone resorption in radiographs. At 8 weeks, the radial defect size appeared larger in defects treated with non-degradable PEG hydrogels (Figure 4.5B). The bone volume in GFOGER-treated defects was significantly greater than that in both PEG-only and non-degradable PEG hydrogel treated defects at both 4 and 8 weeks, $p<0.05$ (Figure 4.6C).

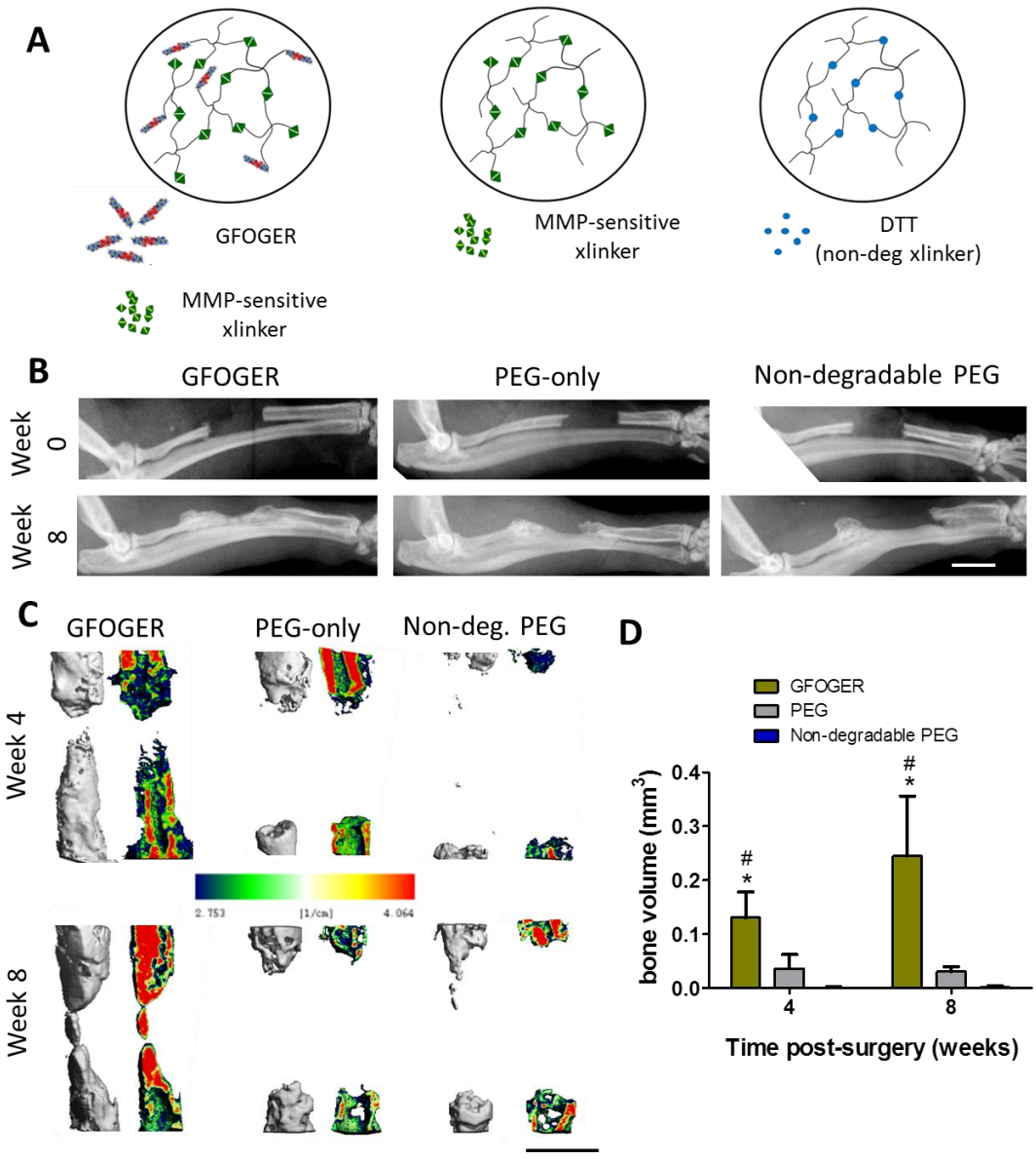

Figure 4.5. Radiographic and μCT evaluation of bone healing in response defects treated with protease-degradable GFOGER-modified or PEG-only hydrogels, and non-degradable PEG hydrogels. (A) Representative radiographic images, (B) 3D μCT reconstructions (left) and mineral density mappings on sagittal sections of the same defects (right), (C) quantitative μCT measures of radial defects at 4 and 8 weeks post-surgery. (D) Diagram of composition of GFOGER, PEG-only and non-degradable hydrogels. Scale bar (A) 2mm, (B) 1mm. * $p<0.05$.

Effect of BMP-2 dose in GFOGER hydrogels on bone healing

Next, we studied the dose response of BMP-2 within our GFOGER hydrogels in radial segmental defects. We tested the effects of 4% GFOGER functionalized PEG hydrogels with 0 μg, 0.03 μg, 0.06 μg, and 0.3 μg rhBMP-2, with empty tubes serving as a negative control. Increasing the BMP dose improved bone formation within the defects (Figure 4.6). As observed previously, there was minimal bone healing in defects treated with empty tubes. However, as seen in the 3D μCT reconstructions, consistent more than 70% bridging was observed by week 8 beginning with the 0.03 μg dose by 8 weeks. Bridging occurred by 4 weeks for the 0.06 μg and 0.3 μg doses. Bone formation was accelerated with the 0.03 μg rhBMP-2 dose, which resulted in increased bone volume at 4 weeks compared to empty tubes (Figure 4.6D). 8 weeks after surgery, defects treated with all BMP-2 doses as well as GFOGER hydrogels with no BMP-2 had higher bone volumes than with empty tubes. In addition, the 0.06 μg BMP-2 dose enhanced bone regeneration over GFOGER hydrogels alone, while surprisingly, the 0.3 μg BMP-2 dose did not. Transverse views of 3D μCT reconstructions reveal that this was because a 0.06 μg BMP-2 primarily induced bone formation within the radial defect space, while causing minimal alterations to the structure of the ulna. In contrast, the high 0.3 μg BMP-2 dose resulted mainly in changes to the ulna, which over time encircled the outside of the radius and fused with it, with little bone formation occurring within the defect space (Figure 4.6C).

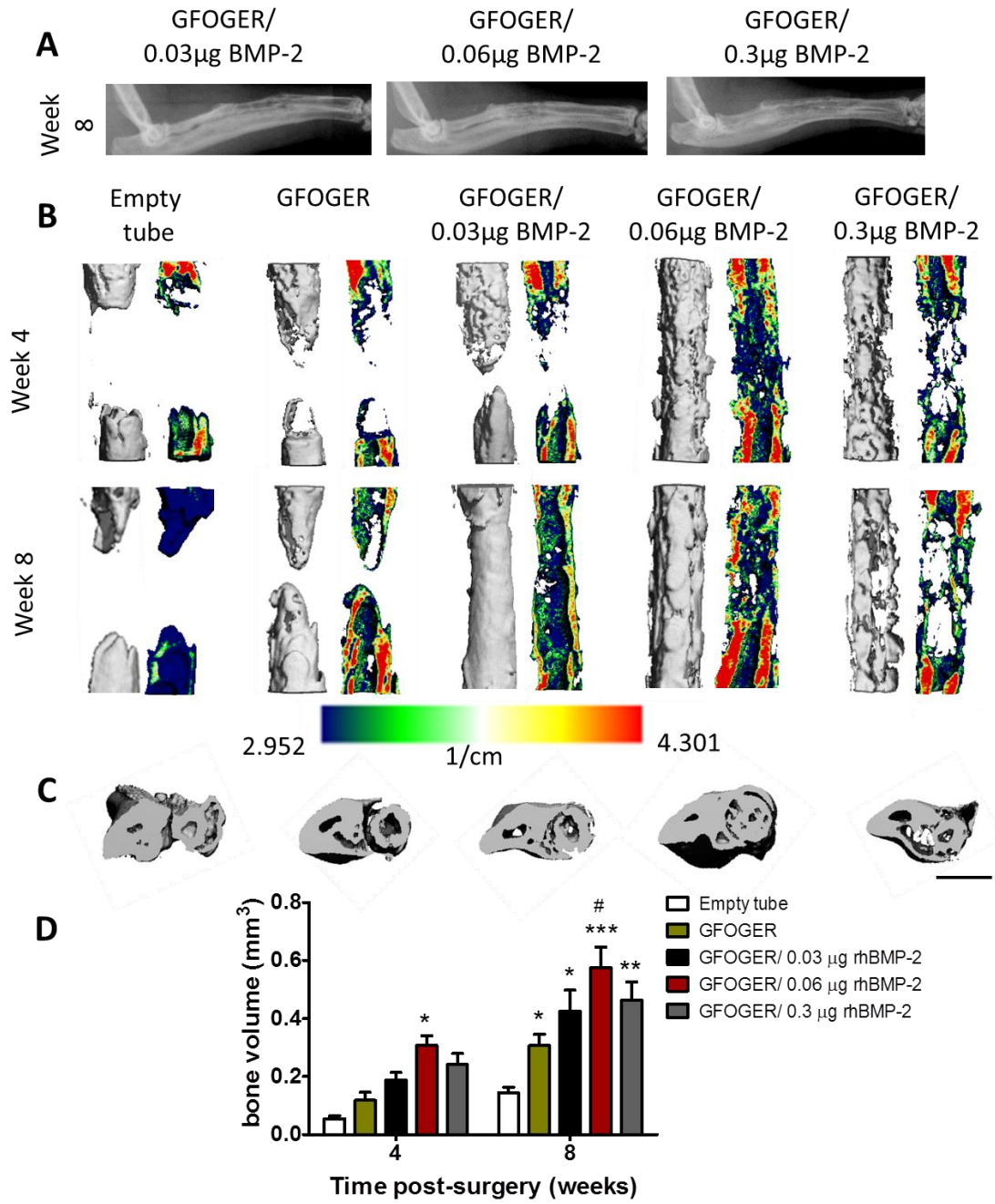

Figure 4.6. Radiographic and µCT evaluation of bone healing in response to rhBMP-2 dose in GFOGER hydrogels. (A) Representative radiographic images, (B) 3D µCT reconstructions (left) and mineral density mappings on sagittal sections of the same defects (right), (C) transverse view of 3D reconstructions and (D) µCT measures of bone formation at 4 and 8 weeks post-surgery. Scale bar (A) 2 mm, (B) 1 mm, (C) 1 mm. * $p<0.05$ compared to empty defect, # $p<0.05$ compared to GFOGER hydrogel.

Hydrogel degradation and BMP-2 release

In order to study the *in vivo* BMP-2 release from our hydrogels as well as the degradation and clearance of the hydrogel from the defect space, we labeled GFOGER and BMP-2 with near IR dyes, Vivotag 680 and 800 respectively. We then synthesized 4% PEG-MAL hydrogels incorporating 2 mM labeled GFOGER and 0.3 μg of labeled BMP-2 and implanted them within radial defects. The defects were non-invasively imaged by FMT to determine the percentage of initially implanted GFOGER and BMP-2 which remained in the defect site over a 14 day period (Figure 4.7A and B). We found that BMP-2 incorporated within GFOGER hydrogels underwent sustained release, with as much as 20% of the dose retained 14 days after surgery. When modeled as a one-phase decay, the half-life of BMP-2 within the defect was 3.9 days. GFOGER was released from the defect site slower than BMP-2. Since the GFOGER ligand is tethered to PEG-MAL, the rate of GFOGER signal loss is also an indicator of the rate of hydrogel degradation. The half-life of labeled GFOGER within the defect is 6.8 days when modeled as one-phase decay. Safranin O/Fast Green stained GMA sections of treated defects did not stain positively for safranin O at 8 weeks post-surgery (Figure 4.8A and B), suggesting either that bone healing within the radial defect does not occur through endochondral ossification, or if it does occur by endochondral ossification, that all chondrocytes have undergone apoptosis by 8 weeks post-surgery. Bone tissue within defect sites in all treatment cases appeared to be non-woven at 8 weeks, and in the empty tube condition, the middle of the defect contained mostly cell infiltrate and little bone tissue (Figure 4.8B). GFOGER hydrogel remnants were not observed in any of the hydrogel-treated defects, indicating that the implanted hydrogel had completely degraded within 8 weeks.

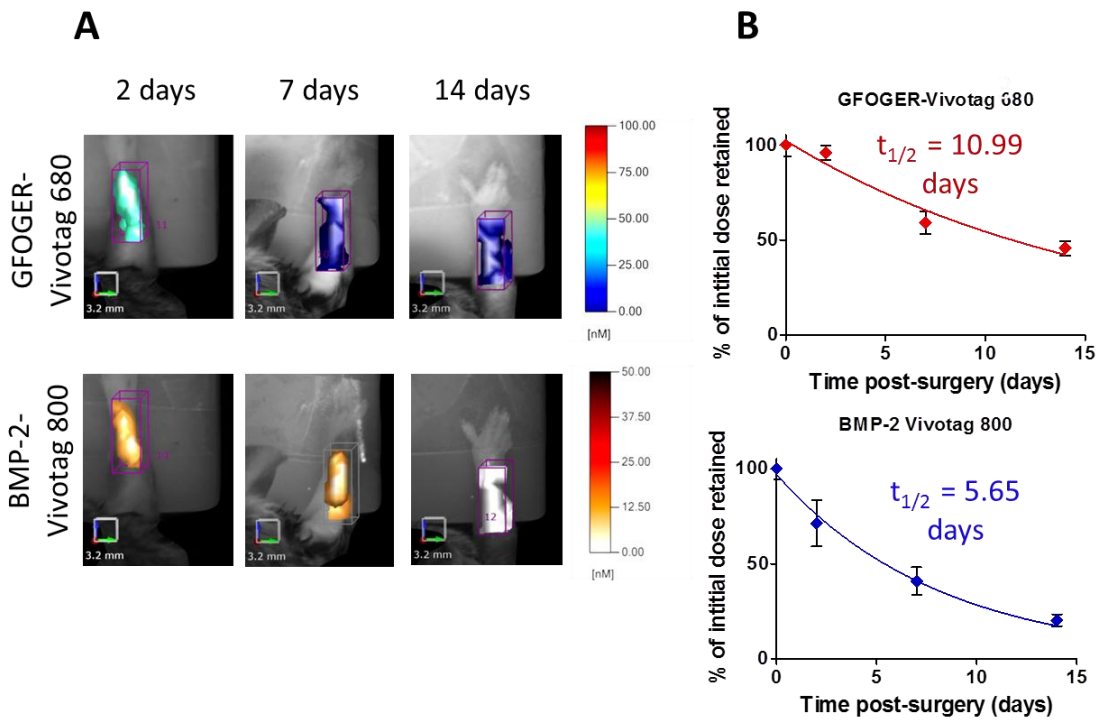

Figure 4.7. Evaluation of hydrogel degradation and BMP release. (A) Representative FMT images and (B) FMT quantification of % implanted dose retained in radial defect space over time *in vivo*. GFOGER peptide was labelled with near-infrared dye Vivotag 680 and rhBMP-2 was labelled with Vivotag 800. (C) *In vitro* release of BMP-2 from GFOGER hydrogels.

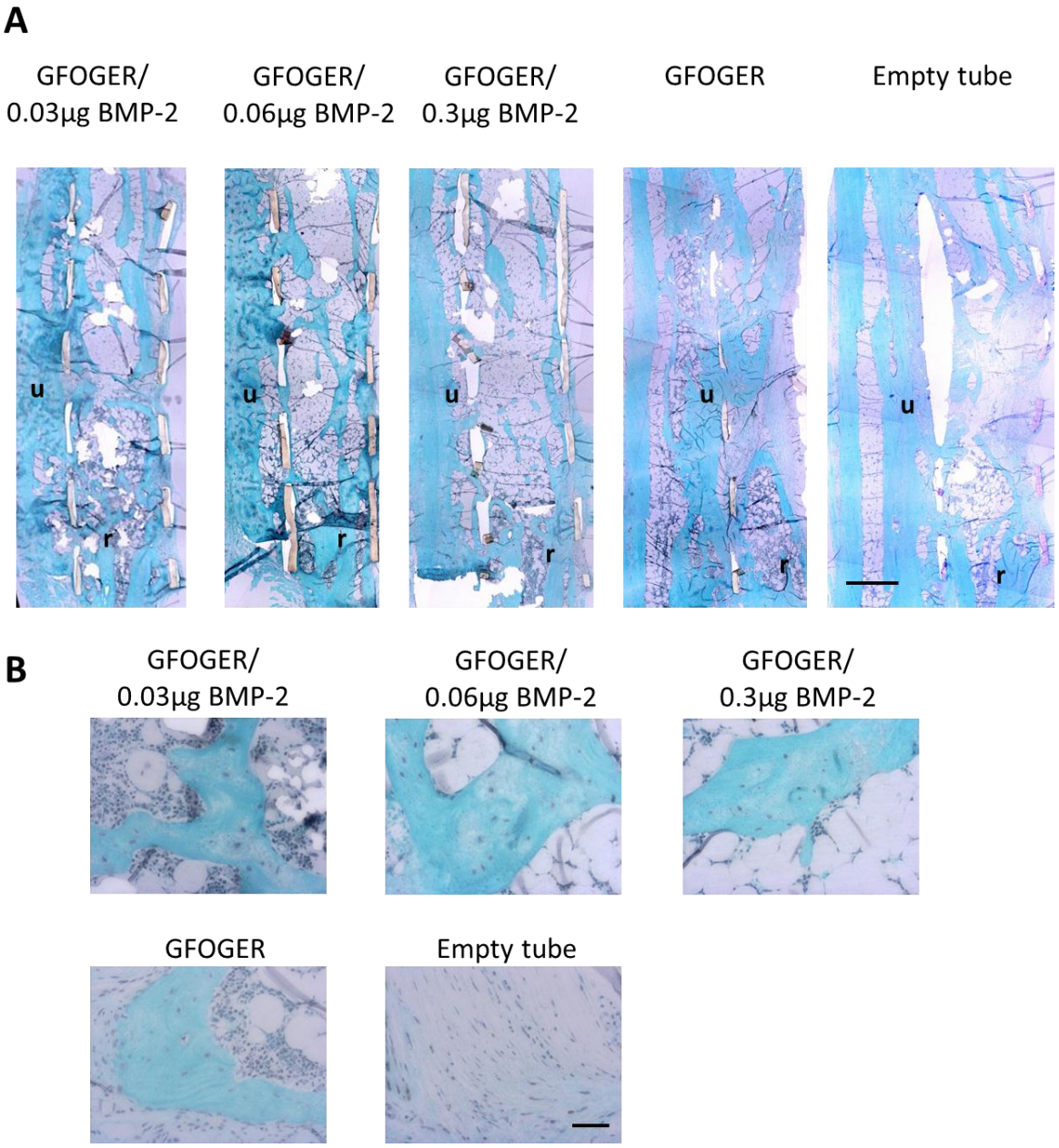

Figure 4.8. Histological evaluation of bone healing in response to rhBMP-2 dose in GFOGER hydrogels at 8 weeks post surgery. GMA sections stained with safranin O/Fast green. u, ulna, r, radius. Scale bar (A) 0.5 mm, (B) 50 µm

Effect of biomaterial scaffold/delivery on bone healing in radial defect

BMP-2 used clinically in delivered within a collagen foam scaffold. Therefore, in order to compare our biomaterial to the clinical standard, we next examined the role of the scaffold or delivery vehicle on bone formation in response to 0.03 μg BMP-2, the lowest dose that we tested in the dose-response study. 0.03 μg BMP-2 was delivered within a 4% PEG-maleimide hydrogel functionalized with 2 mM GFOGER (GFOGER/ 0.03 μg rhBMP-2) or within a collagen foam scaffold (collagen/0.03 μg rhBMP-2). μCT evaluation revealed that GFOGER/BMP-2 hydrogel implants induced bone healing to a much greater extent than collagen sponge/BMP-2 implants. 4 weeks after surgery, the bone volume in GFOGER/0.03 μg rhBMP-2-treated defects was significantly greater than in collagen/0.03 μg rhBMP-2-treated defects, $p<0.05$ (Figure 4.9A and B). The improvement in bone healing induced by GFOGER/0.03 μg rhBMP-2 treatment over collagen/0.03 μg rhBMP-2 treatment was even more pronounced at week 8, when the bone volume was three times as much in GFOGER hydrogels, $p<0.001$ (Figure 4.9A and B). There was no difference in mineral density between the two groups, although the mineral density for each group increased over time. Our analysis of the *in vivo* release of near IR dye-labelled BMP-2 from GFOGER gels and collagen foams indicate that a greater percentage of delivered BMP-2 is retained within the defect site at 1 and 5 days post implantation in GFOGER gels (Figure 4.10A). The half-life of BMP-2 within GFOGER hydrogels *in vivo* is higher than in collagen foams, although it did not reach significance (Figure 4.10A). *In vitro* release assays confirm that GFOGER hydrogels support sustained release of BMP-2 compared to collagen sponges in either PBS (Figure 4.10B) or a collagenase I solution (Figure 4.10C).

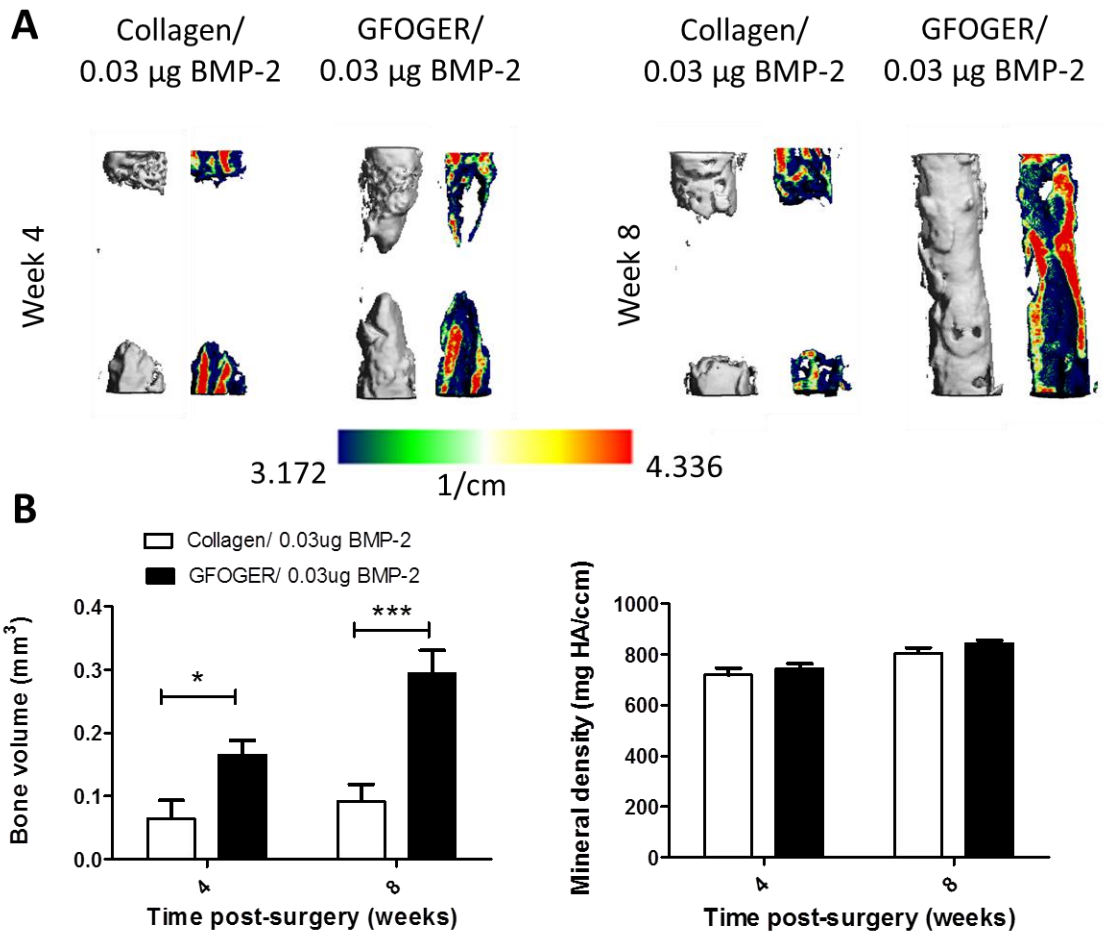

Figure 4.9. µCT evaluation of radial defects treated with GFOGER/ 0.03µg rh-BMP-2 or collagen sponge/ 0.03µg rh-BMP-2. (A) 3D µCT reconstruction images and (B) µCT measures demonstrate improved bone healing in defects treated with GFOGER/ 0.03µg rh-BMP-2 compared to collagen sponge/ 0.03µg rh-BMP-2. *p<0.05, **p<0.01, ***p<0.001.

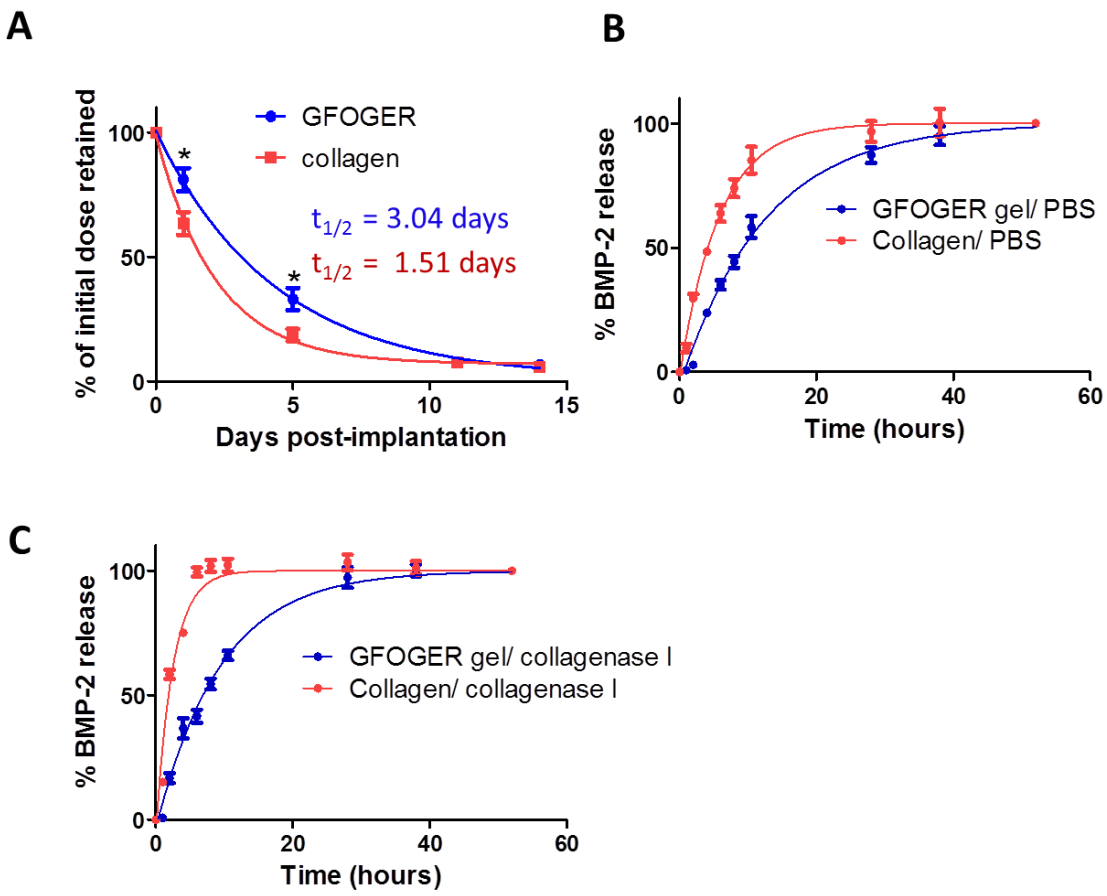

Figure 4.10. In vitro and in vivo evaluation of Vivotag 800-labelled BMP-2 release from GFOGER hydrogels or collagen sponges. (A) FMT quantification of % implanted dose retained in radial defect space over time *in vivo*. *In vitro* release profiles of Vivotag-BMP-2 from GFOGER hydrogels and collagen sponges in (B) PBS and (C) in 0.1mg/ml collagenase I solution.

DISCUSSION

Bone grafts are used for spinal, foot and ankle fusions, revision arthroplasty surgeries, as well as large, non-healing bone defects caused by injury, cancer resection or disease. Because the gold-standard autograft treatments may cause donor pain[22] and processed allografts exhibit limited remodeling[22, 89-91], growth factor treatments such as Infuse (BMP-2 therapy) are becoming more widely used in the clinic. However, BMP treatments present cost-effectiveness limitations[95] and clinical safety concerns[22-24, 96], primarily because BMPs are delivered at supraphysiological doses. Therefore, there is a strong motivation to engineer safe and cost-effective materials which reduce the therapeutic dose of growth factors required to achieve robust healing of critical sized bone defects.

This study evaluated the effect of implanted PEG hydrogels incorporating the α2β1 integrin-specific ligand GFOGER as well as low doses of BMP-2 on osteoblastic differentiation and bone regeneration within a segmental defect. *In vitro*, GFOGER hydrogels supported approximately equal levels of hMSC adhesion and survival as hydrogels functionalized with equimolar densities of the non-integrin selective adhesive ligand, RGD (GRGDSPC). While cell adhesion and survival was unaltered on GFOGER hydrogels, GFOGER hydrogels supported increased differentiation and mineralization of hMSCs compared to RGD. These results indicate that cell adhesion to GFOGER promotes osteoblastic differentiation and mineralization. Our group has previously shown that GFOGER coatings improve mechanical fixation of titanium implants to bone [25, 129], and adsorbed GFOGER coatings on PCL scaffolds enhance bone regeneration in a rat femoral defects [130], and these previous findings further support the pro-osteogenic activity of GFOGER *in vitro*.

In vivo, we found that treatment of murine radial defects with MMP-sensitive GFOGER-functionalized PEG hydrogels increased bone formation but failed to induce

consistent bridging of defects after 8 weeks. However, when we encapsulated low (0.03 μg or 0.02 mg/ml) doses of BMP-2 within GFOGER hydrogels, we observed defect bridging at 8 weeks post-surgery. Since the clinical standard BMP-2 therapy involves BMP-2 delivery at a concentration of 1.5 mg/ml within a collagen sponge, the BMP-2 concentration required for segmental defect healing within GFOGER hydrogels is almost an order of magnitude lower than the clinical standard (assuming proportional scaling across species).

Bone formation in defects treated with PEG-only or non-degradable hydrogels supported minimal healing, suggesting that both the presence of an adhesive ligand as well as protease-sensitive degradation of the hydrogel are necessary to for the enhanced bone healing response stimulated by GFOGER hydrogels. This result is in agreement with published studies[193].

Analysis of the dose response of BMP-2 within our biomaterial system showed that while the low 0.03 μg BMP-2 was sufficient for bridging at 8 weeks, 0.06 μg of BMP-2 accelerated bone healing and increased the volume of bone present within the bridged defect at 8 weeks. Surprisingly, the highest dose tested, 0.3 μg of BMP-2, resulted in decreased levels of bone formation within the defect site compared to the medium 0.06 μg dose. We also observed that in mice treated with the high 0.3 μg BMP-2 dose, there were gross deformations in the structure of the ulna, which expanded, encircled the radius and fused with it. We speculate that the observed low levels of radial healing in combination with expansion and deformation of the ulna in response to treatment with high BMP-2 dose may be due to excessively high growth factor gradients causing differentiation and mineralization of osteoprogenitors before they migrated into the radial defect site. BMP-2 is known to stimulate have both chemotactic migration[194] and osteoblastic differentiation[195] and high BMP-2 concentrations may favor the latter. It is also possible that delivery of hydrogels incorporating the high BMP-2 dose induced osteolysis within the defect site. Osteolysis, end-plate resorption and subsidence are

potential complications of BMP-2 therapy in spinal fusions[196, 197], and have been reported to occur in up to 20-70% of cases[96]. Furthermore, BMP receptors are expressed on osteoclasts[198] and multiple BMPs[199]including BMP-2[198] stimulate osteoclastic bone resorption. Regardless of the mechanism, this unanticipated alteration to the ulnar structure and decreased bone healing in mice receiving high BMP-2 doses highlights the undesired effects of excessive BMP-2 signaling and further underscores the importance of precisely controlling BMP-2 dose, delivery method and release kinetics in order to direct appropriate bone formation. Although the medium medium 0.06 μg BMP-2 dose, supported the greatest volume of bone formation within the radial defect, the structure of the ulna was slightly altered in mice treated with the 0.06 μg BMP-2 dose. In contrast, there was little observable impact of the low BMP-2 dose on the ulna, and the low BMP-2 dose was sufficient to induce defect bridging. We therefore chose to use this low 0.03 μg BMP-2 dose in our subsequent comparison of delivery vehicles.

GFOGER hydrogels provided sustained release of encapsulated growth factor, as BMP-2 was retained within the defect site for over two weeks, with a half-life of 4 days. Over 10% of the initial BMP-2 signal was still detected at the defect after 14 days. The retention time of GFOGER within the defect was even higher than for BMP-2 as the half-life of labeled GFOGER was 7 days. As GFOGER is covalently tethered to the 4-armed PEG-maleimide monomer, the half-life of GFOGER localization at the defect site is an indicator of the degradation and clearance rate of the gel and suggests that over 90% of the implanted hydrogel is degraded in 3 weeks.

The clinical standard for BMP-2 delivery uses an absorbable collagen sponge as the growth factor carrier. When we compared GFOGER hydrogels loaded with low (0.03 μg) doses of BMP-2 to the clinical standard, we found that GFOGER hydrogels induced three times as much bone formation within the radial defects compared to collagen sponges with the same BMP-2 dose ($p<0.001$). In vivo and in vitro BMP-2 release studies indicate that BMP-2 is released more slowly and exhibits prolonged retention

within the defect site with GFOGER hydrogel delivery vehicles when compared to collagen scaffolds. The tightly crosslinked PEG hydrogel system physically entraps BMP-2, and we therefore expected slower BMP-2 release from GFOGER hydrogels than from collagen sponges which have an open porous structure.

It is likely that the enhanced healing response to low dose BMP-2 delivery within GFOGER hydrogel scaffolds in this study are due to a combination of sustained delivery of of BMP-2 from the hydrogels as well as the intrinsic pro-osteogenic bioactivity of the GFOGER ligand compared to collagen foams. Although collagen scaffolds are approved for clinical applications[200] and have demonstrated favorable cell adhesion properties[201], collagen scaffold implants without delivered growth factors do not induce improvements in bone formation[202]. In contrast to collagen sponges, we have observed in this study that GFOGER-functionalized PEG hydrogels without encapsulated growth factors promote bone regeneration in our study. Other studies have confirmed osteogenic GFOGER bioactivity by demonstrating that GFOGER coatings upregulate in vivo osseointegration and skeletal regeneration[25, 129, 130]. In addition, osteoblastic differentiation on GFOGER coated surfaces exceed differentiation on collagen coated surfaces, indicating that the GFOGER peptide has a greater osteogenic effect than its parent molecule, likely due to specific α2β1 integrin specificity achieved by the removal of extraneous collagen domains which do not upregulate osteoblastic signaling[128].

Our biomaterial strategy benefits from several advantages. The GFOGER hydrogel is completely synthetic, well-defined and highly tunable extracellular matrix analog. The modular PEG-MAL hydrogel system also affords great versatility in biomaterial design by allowing precise control of PEG weight percent and ligand density, proteolytic degradation rate, incorporated growth factor dose, as well as possible combinations of ligands or growth factors, suggesting that the results presented here can be further optimized. Furthermore, many components of the hydrogel system such as PEG-MAL, GFOGER adhesive peptide and VPM crosslinker peptide are commercially

available, easy to fabricate and much less expensive than recombinant growth factors. The low BMP-2 dose required to support defect bridging with GFOGER hydrogels increases the cost-effectiveness of this material while also potentially limiting adverse responses currently observed with BMP therapies. In addition, PEG is well tolerated *in vivo*[203, 204] and is clinically approved in multiple products, which suggests that GFOGER hydrogels would be safe for therapeutic use. MMP-sensitive crosslinks within our bioartificial matrices allows for fairly rapid, 'on demand' release of BMP-2 driven by cell-mediated proteolysis. Finally, our PEG-maleimide-based biofunctionalized matrices are highly versatile and tunable, as multiple hydrogel properties such as porosity, stiffness, degradation rate, adhesive functionality, ligand density and incorporated growth factor type and release profile may be tuned by varying the hydrogel composition.

Despite the aforementioned advantages of our bioartificial hydrogel matrices, our biomaterial has certain limitations. First, BMP-2 is encapsulated within the PEG hydrogel and may therefore have reduced residence time within the defect compared to strategies which utilize covalent growth factor immobilization affinity to immobilized groups. Second, because we have chosen a cell-free biomaterial therapeutic strategy, bone formation within our biomaterial relies on endogenous cell invasion. As a result, the biomaterial design requires a balance between facilitating cell invasion, which is favored by loose and rapidly degrading polymer networks, with the sustained of BMP-2 release, which is favored by tight networks and slow biomaterial. Third, we pre-cast hydrogels within an impermeable polyimide sleeve to improve the handling of soft hydrogels for implantation. Although the plastic sleeve was laser machined with holes to improve nutrient transport and cell invasion, the use of an impermeable plastic sleeve is not ideal and may contribute to decreased bone healing. Lastly, because the murine radial segmental defect model as well as the non-porous sleeve for biomaterial delivery are not widely used, it may be challenging to compare our data to other studies of bone healing in mice.

In conclusion, we have developed a synthetic bioartificial PEG-MAL based matrix which is functionalized with the α2β1 integrin-specific ligand GFOGER and provides sustained release of BMP-2. These GFOGER hydrogels lacking BMP-2 promote bone regeneration in radial segmental defects, while GFOGER hydrogels incorporating low-dose BMP-2 induce bridging and improved bone formation compared to clinical standard collagen sponges delivering the same BMP-2 dose. Therefore, GFOGER-functionalized PEG-MAL hydrogels incorporating low dose BMP-2 may have therapeutic potential as biomaterial bone graft substitutes.

CHAPTER 8: FUTURE CONSIDERATIONS

Role of beta 1 integrins in bone formation

We have observed that β1 integrin deletion in osteochondro progenitor cells under the Twist 2 promoter impairs calvarial and vertebral mineralization, while integrin deletion under the Osterix promoter induces growth abnormalities, delayed calvarial ossification, incisor defects and under-mineralized femurs. While these empirical observations suggest that β1 integrins play a crucial role in early bone development by regulating osteoprogenitor cells, further studies are required to establish the mechanism of regulation. We are currently investigating the mechanism by which β1 integrins regulate calvarial development by analyzing the gene expression profiles of calvarial tissue in itgβ1$^{cKO\ (OSX)}$ embryos at E18.5, shortly after the onset of cre recombinase expression in the calvarium. We are also investigating osteoblast and osteoclast numbers, as well as chondrocyte morphology within the calvaria and femurs of in itgβ1$^{cKO\ (OSX)}$ mice in order to determine the cell types responsible for the reduced mineral density, and growth abnormalities.

We have also observed that that β1 integrin deletion in osteochondro progenitor cells under the Twist 2 results in embryonic lethality which occurs after E13.5. By E18.5, surviving in itgβ1$^{cKO\ (TW2)}$ embryos are abnormally small and exhibit impaired skeletal mineralization as well as umbilical cord deformities. However, by E18.5, degenerated implantation sites are visible on the uterine horn, indicating that developmental impairments due to β1 integrin knockout in Twist 2 expressing cells occurs at an earlier stage. Future work may include analyzing embryos at intermediate stages such as E15.5 to determine the stage at which normal embryonic development can no longer occur in the absence of β1 integrins in mesodermal cells. Detailed histological analysis of these embryos will be required to determine the cause of embryonic lethality. This study will elucidate the role of β1 integrins on prenatal development.

We have also found in this study that β1 integrin knockout in mature osteoblasts and osteocytes result in only mild alterations to bone phenotypes. This suggests that osteoblasts do not require β1 integrins to function, which is surprising given that most collagen receptors are β1 integrins. This observation raises the question of how osteoblasts adapt to the loss of β1 integrins and maintain necessary adhesions. It is possible that compensations in integrin expression and ECM may occur in osteoblasts in response to β1 integrin deletions.

The β1 sub-family of integrins includes 12 different integrins. Therefore deletions of β1 integrin partner α subunits individually or in combination will elucidate the roles of specific integrins on bone development as well as redundancies among these integrins in regulating the formation of skeletal elements.

Integrin-specific PEG hydrogels and bone healing

Biomaterials for Enhanced Bone Healing

We have shown that engineered GFOGER functionalized PEG matrices promote bone healing and induce robust bone regeneration within a murine radial segmental defect. Furthermore, these engineered bioartificial matrices bridge segmental defects when combined with low-dose BMP-2 and induce improved bone regeneration compared when compared to collagen sponges incorporating low-dose BMP-2. While these results demonstrate the clinical potential of GFOGER PEG hydrogels, the design flexibility of our biomaterial system allows us to tune multiple properties of the hydrogel in order to optimize its performance as a bone graft substitute. Although delivery of BMP-2 alone has been clinically successful in inducing bone formation within large defects, bone healing in large defects is often limited by insufficient vascularization[205]. Furthermore, combinations of growth factors such as BMP-2 and PDGF have been shown to promote healing within calvarial defects [206]. Therefore, delivery of angiogenic growth factors or

combinations of growth factors within GFOGER hydrogels could be used to promote bone regeneration. We are currently investigating the effect on VEFG delivery from GFOGER PEG hydrogels on bone healing, In this study, we used a relatively low 4% weight by volume concentration of PEG-maleimide as well as the VPM crosslinker which undergoes rapid MMP-mediated cleavage to fabricate our hydrogels. A design variation using higher PEG concentrations and peptide crosslinkers which undergo less rapid cleavage than VPM would provide slower release of encapsulated growth factor, which may yield further enhancements in bone healing. The growth factor release profile may also be tuned by covalently tethering the growth factor to the PEG-maleimide which we have previously demonstrated with VEGF delivery from PEG hydrogels. Because rhBMP-2 lacks free cysteines, it is not amenable to Michael addition-mediated immobilization to the PEG-maleimide monomer. However, a modified sequence of BMP-2 containing free cysteines could be employed to immobilize BMP-2 and further improve its release kinetcs. The BMP-2 release profile may also be modified by covalently immobilizing BMP-2 affinity domains within the hydrogel. While this study has focused on the cell-free delivery of growth factors from GFOGER hydrogels, these hydrogels may also be suitable carriers for the delivery of encapsulated stem cells. Such a strategy may be especially valuable in older patients or patients with defective stem cells.

GFOGER-Modified PEG Hydrogels for Basic Science Studies

Integrin-specific GFOGER functionalized PEG hydrogels present a useful biomaterial system for basic science studies on the role of bioactive ligands on cell behaviors. PEG provides a ‘clean slate’ protein resistant background onto which desired bioactive molecules may be functionalized at controlled densities. In addition, the stiffness of the hydrogels may be independently controlled by varying the PEG concentration. We are currently using PEG maleimide hydrogels to study the interaction of environmental cues

such as substrate stiffness, adhesive ligand and ligand density on cell morphology, osteoblastic differentiation and mineralization.

Transgenic Models to Study Osteoprogenitor Invasion into Defect

Bone healing within large defects may be limited by multiple factors such as vascularization and osteoprogenitor invasion into the defect which are challenging to monitor non-invasively *in vivo* and are also difficult to model *in vitro*. Therefore, a method which enables non-invasive measurement osteoprogenitor invasion would facilitate the rational design of biomaterials for the treatment of large non-healing defects.We have bred transgenic mice in which osteochondro progenitor cells express luciferase (under the Twist 2 promoter), which enables non-invasive imaging and quantification of osteochondro progenitors. Using this transgenic model, we may investigate the temporal profile of osteoprogenitor recruitment in response to different biomaterials and determine the correlation between these profiles and bone healing outcomes.

REFERENCES

1. Park, J.H. et al. The responses to surface wettability gradients induced by chitosan nanofilms on microtextured titanium mediated by specific integrin receptors. *Biomaterials* **33**, 7386-7393 (2012).
2. Takeuchi, Y. & Matsumoto, T. Interaction between Collagen and Alpha-2-Beta-1-Integrin Enhances Tyrosine Phosphorylation of Focal Adhesion Kinase and Osteoblast Differentiation. *Journal of Bone and Mineral Research* **10**, S303-S303 (1995).
3. Xiao, G., Wang, D., Benson, M.D., Karsenty, G. & Franceschi, R.T. Role of the alpha2-integrin in osteoblast-specific gene expression and activation of the Osf2 transcription factor. *J Biol Chem* **273**, 32988-32994 (1998).
4. Jikko, A., Harris, S.E., Chen, D., Mendrick, D.L. & Damsky, C.H. Collagen integrin receptors regulate early osteoblast differentiation induced by BMP-2. *J Bone Miner Res* **14**, 1075-1083 (1999).
5. Mizuno, M., Fujisawa, R. & Kuboki, Y. Type I collagen-induced osteoblastic differentiation of bone-marrow cells mediated by collagen-alpha2beta1 integrin interaction. *J Cell Physiol* **184**, 207-213 (2000).
6. Gronthos, S., Simmons, P.J., Graves, S.E. & Robey, P.G. Integrin-mediated interactions between human bone marrow stromal precursor cells and the extracellular matrix. *Bone* **28**, 174-181 (2001).

7. Moursi, A.M. et al. Fibronectin regulates calvarial osteoblast differentiation. *J Cell Sci* **109 (Pt 6)**, 1369-1380 (1996).

8. Moursi, A.M., Globus, R.K. & Damsky, C.H. Interactions between integrin receptors and fibronectin are required for calvarial osteoblast differentiation in vitro. *J Cell Sci* **110 (Pt 18)**, 2187-2196 (1997).

9. Hamidouche, Z. et al. Priming integrin alpha5 promotes human mesenchymal stromal cell osteoblast differentiation and osteogenesis. *Proc Natl Acad Sci U S A* **106**, 18587-18591 (2009).

10. Olivares-Navarrete, R. et al. Integrin alpha2beta1 plays a critical role in osteoblast response to micron-scale surface structure and surface energy of titanium substrates. *Proc Natl Acad Sci U S A* **105**, 15767-15772 (2008).

11. Phillips, J.A. et al. Role for beta1 integrins in cortical osteocytes during acute musculoskeletal disuse. *Matrix Biol* **27**, 609-618 (2008).

12. Litzenberger, J.B., Kim, J.B., Tummala, P. & Jacobs, C.R. Beta1 integrins mediate mechanosensitive signaling pathways in osteocytes. *Calcif Tissue Int* **86**, 325-332 (2010).

13. Zimmerman, D., Jin, F., Leboy, P., Hardy, S. & Damsky, C. Impaired bone formation in transgenic mice resulting from altered integrin function in osteoblasts. *Developmental biology* **220**, 2-15 (2000).

14. Bucholz, R.W. Nonallograft osteoconductive bone graft substitutes. *Clin Orthop Relat Res*, 44-52 (2002).

15. Finkemeier, C.G. Bone-grafting and bone-graft substitutes. *J Bone Joint Surg Am* **84-A**, 454-464 (2002).

16. Giannoudis, P.V., Dinopoulos, H. & Tsiridis, E. Bone substitutes: an update. *Injury* **36 Suppl 3**, S20-27 (2005).

17. Kretlow, J.D. & Mikos, A.G. Review: mineralization of synthetic polymer scaffolds for bone tissue engineering. *Tissue Eng* **13**, 927-938 (2007).

18. Iwaniec, U.T. et al. Effects of disrupted beta1-integrin function on the skeletal response to short-term hindlimb unloading in mice. *Journal of applied physiology* **98**, 690-696 (2005).

19. Globus, R.K. et al. Skeletal phenotype of growing transgenic mice that express a function-perturbing form of beta1 integrin in osteoblasts. *Calcif Tissue Int* **76**, 39-49 (2005).

20. Dacquin, R., Starbuck, M., Schinke, T. & Karsenty, G. Mouse alpha1(I)-collagen promoter is the best known promoter to drive efficient Cre recombinase expression in osteoblast. *Dev Dyn* **224**, 245-251 (2002).

21. Stephens, L.E. et al. Deletion of beta 1 integrins in mice results in inner cell mass failure and peri-implantation lethality. *Genes Dev* **9**, 1883-1895 (1995).

22. De Long, W.G., Jr. et al. Bone grafts and bone graft substitutes in orthopaedic trauma surgery. A critical analysis. *J Bone Joint Surg Am* **89**, 649-658 (2007).

23. Yoon, S.T. & Boden, S.D. Osteoinductive molecules in orthopaedics: basic science and preclinical studies. *Clin Orthop Relat Res*, 33-43 (2002).

24. Bishop, G.B. & Einhorn, T.A. Current and future clinical applications of bone morphogenetic proteins in orthopaedic trauma surgery. *Int Orthop* **31**, 721-727 (2007).

25. Reyes, C.D., Petrie, T.A., Burns, K.L., Schwartz, Z. & Garcia, A.J. Biomolecular surface coating to enhance orthopaedic tissue healing and integration. *Biomaterials* **28**, 3228-3235 (2007).

26. Hynes, R.O. Integrins: bidirectional, allosteric signaling machines. *Cell* **110**, 673-687 (2002).

27. Giancotti, F.G. & Ruoslahti, E. Integrin signaling. *Science* **285**, 1028-1032 (1999).

28. Petit, V. & Thiery, J.P. Focal adhesions: structure and dynamics. *Biol Cell* **92**, 477-494 (2000).

29. Bourdoulous, S., Orend, G., MacKenna, D.A., Pasqualini, R. & Ruoslahti, E. Fibronectin matrix regulates activation of RHO and CDC42 GTPases and cell cycle progression. *J Cell Biol* **143**, 267-276 (1998).

30. Chen, C.S., Mrksich, M., Huang, S., Whitesides, G.M. & Ingber, D.E. Geometric control of cell life and death. *Science* **276**, 1425-1428 (1997).

31. Gronthos, S., Stewart, K., Graves, S.E., Hay, S. & Simmons, P.J. Integrin expression and function on human osteoblast-like cells. *Journal of Bone and Mineral Research* **12**, 1189-1197 (1997).

32. Bennett, J.H., Carter, D.H., Alavi, A.L., Beresford, J.N. & Walsh, S. Patterns of integrin expression in a human mandibular explant model of osteoblast differentiation. *Arch Oral Biol* **46**, 229-238 (2001).

33. Grzesik, W.J. & Robey, P.G. Bone matrix RGD glycoproteins: immunolocalization and interaction with human primary osteoblastic bone cells in vitro. *J Bone Miner Res* **9**, 487-496 (1994).

34. Clover, J., Dodds, R.A. & Gowen, M. Integrin subunit expression by human osteoblasts and osteoclasts in situ and in culture. *J Cell Sci* **103 (Pt 1)**, 267-271 (1992).

35. Hughes, D.E., Salter, D.M., Dedhar, S. & Simpson, R. Integrin expression in human bone. *J Bone Miner Res* **8**, 527-533 (1993).

36. Ganta, D.R., McCarthy, M.B. & Gronowicz, G.A. Ascorbic acid alters collagen integrins in bone culture. *Endocrinology* **138**, 3606-3612 (1997).

37. Saito, T., Albelda, S.M. & Brighton, C.T. Identification of integrin receptors on cultured human bone cells. *J Orthop Res* **12**, 384-394 (1994).

38. Yu, Y.M., Becvar, R., Yamada, Y. & Reddi, A.H. Changes in the gene expression of collagens, fibronectin, integrin and proteoglycans during matrix-induced bone morphogenesis. *Biochem Biophys Res Commun* **177**, 427-432 (1991).

39. Brighton, C.T. & Albelda, S.M. Identification of integrin cell-substratum adhesion receptors on cultured rat bone cells. *J Orthop Res* **10**, 766-773 (1992).

40. Castoldi, M. et al. Osteoblastic cells from rat long bone. II: Adhesion to substrata and integrin expression in primary and propagated cultures. *Cell Biol Int* **21**, 7-16 (1997).

41. Mizuno, M., Fujisawa, R. & Kuboki, Y. Type I collagen-induced osteoblastic differentiation of bone-marrow cells mediated by collagen-alpha 2 beta 1 integrin interaction. *Journal of Cellular Physiology* **184**, 207-213 (2000).

42. Mizuno, M. & Kuboki, Y. Osteoblast-related gene expression of bone marrow cells during the osteoblastic differentiation induced by type I collagen. *J Biochem* **129**, 133-138 (2001).

43. Suzawa, M. et al. Stimulation of Smad1 transcriptional activity by Ras-extracellular signal-regulated kinase pathway: a possible mechanism for collagen-dependent osteoblastic differentiation. *J Bone Miner Res* **17**, 240-248 (2002).

44. Takeuchi, Y. et al. Differentiation and transforming growth factor-beta receptor down-regulation by collagen-alpha2beta1 integrin interaction is mediated by focal adhesion kinase and its downstream signals in murine osteoblastic cells. *J Biol Chem* **272**, 29309-29316 (1997).

45. Tamura, Y. et al. Focal adhesion kinase activity is required for bone morphogenetic protein--Smad1 signaling and osteoblastic differentiation in murine MC3T3-E1 cells. *J Bone Miner Res* **16**, 1772-1779 (2001).

46. Xiao, G. et al. MAPK pathways activate and phosphorylate the osteoblast-specific transcription factor, Cbfa1. *J Biol Chem* **275**, 4453-4459 (2000).

47. Schneider, G.B., Zaharias, R. & Stanford, C. Osteoblast integrin adhesion and signaling regulate mineralization. *J Dent Res* **80**, 1540-1544 (2001).

48. Van der Velde-Zimmermann, D. et al. Fibronectin distribution in human bone marrow stroma: matrix assembly and tumor cell adhesion via alpha5 beta1 integrin. *Exp Cell Res* **230**, 111-120 (1997).

49. Globus, R.K. et al. Fibronectin is a survival factor for differentiated osteoblasts. *J Cell Sci* **111 (Pt 10)**, 1385-1393 (1998).

50. Kaabeche, K. et al. Cbl-mediated ubiquitination of alpha5 integrin subunit mediates fibronectin-dependent osteoblast detachment and apoptosis induced by FGFR2 activation. *J Cell Sci* **118**, 1223-1232 (2005).

51. Salter, D.M., Robb, J.E. & Wright, M.O. Electrophysiological responses of human bone cells to mechanical stimulation: evidence for specific integrin function in mechanotransduction. *J Bone Miner Res* **12**, 1133-1141 (1997).

52. Martino, M.M. et al. Controlling integrin specificity and stem cell differentiation in 2D and 3D environments through regulation of fibronectin domain stability. *Biomaterials* **30**, 1089-1097 (2009).

53. Cheng, S.L., Lai, C.F., Blystone, S.D. & Avioli, L.V. Bone mineralization and osteoblast differentiation are negatively modulated by integrin alpha(v)beta3. *J Bone Miner Res* **16**, 277-288 (2001).

54. Huang, J. et al. Impact of order and disorder in RGD nanopatterns on cell adhesion. *Nano Lett* **9**, 1111-1116 (2009).

55. Hartman, G.D. & Duggan, M.E. alpha(v)beta(3) Integrin antagonists as inhibitors of bone resorption. *Expert opinion on investigational drugs* **9**, 1281-1291 (2000).

56. Ross, F.P. et al. Interactions between the bone matrix proteins osteopontin and bone sialoprotein and the osteoclast integrin alpha v beta 3 potentiate bone resorption. *J Biol Chem* **268**, 9901-9907 (1993).

57. Fassler, R. & Meyer, M. Consequences of lack of beta 1 integrin gene expression in mice. *Genes Dev* **9**, 1896-1908 (1995).

58. Sauer, B. Inducible gene targeting in mice using the Cre/lox system. *Methods* **14**, 381-392 (1998).

59. Nagy, A. Cre recombinase: the universal reagent for genome tailoring. *Genesis* **26**, 99-109 (2000).

60. Lewandoski, M. Conditional control of gene expression in the mouse. *Nat Rev Genet* **2**, 743-755 (2001).

61. Gossen, M. & Bujard, H. Studying gene function in eukaryotes by conditional gene inactivation. *Annu Rev Genet* **36**, 153-173 (2002).

62. Principles of Bone Biology, Vol. 1, Edn. 2. (2002).

63. Gelse, K., Poschl, E. & Aigner, T. Collagens--structure, function, and biosynthesis. *Adv Drug Deliv Rev* **55**, 1531-1546 (2003).

64. Robey, P.G., John, P.B., Lawrence, G.R. & Gideon, A.R. in Principles of Bone Biology (Second Edition) 225-237 (Academic Press, San Diego; 2002).

65. Li, L., Cserjesi, P. & Olson, E.N. Dermo-1: a novel twist-related bHLH protein expressed in the developing dermis. *Developmental biology* **172**, 280-292 (1995).

66. Bialek, P. et al. A twist code determines the onset of osteoblast differentiation. *Developmental cell* **6**, 423-435 (2004).

67. Elefteriou, F. & Yang, X. Genetic mouse models for bone studies--strengths and limitations. *Bone* **49**, 1242-1254 (2011).

68. Yu, K. et al. Conditional inactivation of FGF receptor 2 reveals an essential role for FGF signaling in the regulation of osteoblast function and bone growth. *Development* **130**, 3063-3074 (2003).

69. Zhang, M. et al. Osteoblast-specific knockout of the insulin-like growth factor (IGF) receptor gene reveals an essential role of IGF signaling in bone matrix mineralization. *J Biol Chem* **277**, 44005-44012 (2002).

70. Tan, X. et al. Smad4 is required for maintaining normal murine postnatal bone homeostasis. *J Cell Sci* **120**, 2162-2170 (2007).

71. Karsenty, G., Kronenberg, H.M. & Settembre, C. Genetic control of bone formation. *Annual review of cell and developmental biology* **25**, 629-648 (2009).

72. Ducy, P., Zhang, R., Geoffroy, V., Ridall, A.L. & Karsenty, G. Osf2/Cbfa1: a transcriptional activator of osteoblast differentiation. *Cell* **89**, 747-754 (1997).

73. Karsenty, G. & Wagner, E.F. Reaching a genetic and molecular understanding of skeletal development. *Developmental cell* **2**, 389-406 (2002).

74. Naski, M.C., Wang, Q., Xu, J. & Ornitz, D.M. Graded activation of fibroblast growth factor receptor 3 by mutations causing achondroplasia and thanatophoric dysplasia. *Nature genetics* **13**, 233-237 (1996).

75. Hartmann, C. Skeletal development--Wnts are in control. *Molecules and cells* **24**, 177-184 (2007).

76. Kobayashi, T. et al. Indian hedgehog stimulates periarticular chondrocyte differentiation to regulate growth plate length independently of PTHrP. *The Journal of clinical investigation* **115**, 1734-1742 (2005).

77. Barna, M. & Niswander, L. Visualization of cartilage formation: insight into cellular properties of skeletal progenitors and chondrodysplasia syndromes. *Developmental cell* **12**, 931-941 (2007).

78. Hinoi, E. et al. Runx2 inhibits chondrocyte proliferation and hypertrophy through its expression in the perichondrium. *Genes Dev* **20**, 2937-2942 (2006).

79. Komori, T. et al. Targeted disruption of Cbfa1 results in a complete lack of bone formation owing to maturational arrest of osteoblasts. *Cell* **89**, 755-764 (1997).

80. Nakashima, K. et al. The novel zinc finger-containing transcription factor osterix is required for osteoblast differentiation and bone formation. *Cell* **108**, 17-29 (2002).

81. Howard, T.D. et al. Mutations in TWIST, a basic helix-loop-helix transcription factor, in Saethre-Chotzen syndrome. *Nature genetics* **15**, 36-41 (1997).

82. Tsuji, K. et al. BMP2 activity, although dispensable for bone formation, is required for the initiation of fracture healing. *Nature genetics* **38**, 1424-1429 (2006).

83. Gerstenfeld, L.C., Cullinane, D.M., Barnes, G.L., Graves, D.T. & Einhorn, T.A. Fracture healing as a post-natal developmental process: molecular, spatial, and temporal aspects of its regulation. *Journal of cellular biochemistry* **88**, 873-884 (2003).

84. Wang, K. et al. Analysis of fracture healing by large-scale transcriptional profile identified temporal relationships between metalloproteinase and ADAMTS mRNA expression. *Matrix Biol* **25**, 271-281 (2006).

85. Niikura, T., Hak, D.J. & Reddi, A.H. Global gene profiling reveals a downregulation of BMP gene expression in experimental atrophic nonunions compared to standard healing fractures. *J Orthop Res* **24**, 1463-1471 (2006).

86. Cho, T.J., Gerstenfeld, L.C. & Einhorn, T.A. Differential temporal expression of members of the transforming growth factor beta superfamily during murine fracture healing. *J Bone Miner Res* **17**, 513-520 (2002).

87. Johnson, E.E., Urist, M.R. & Finerman, G.A. Resistant nonunions and partial or complete segmental defects of long bones. Treatment with implants of a

composite of human bone morphogenetic protein (BMP) and autolyzed, antigen-extracted, allogeneic (AAA) bone. *Clin Orthop Relat Res*, 229-237 (1992).

88. Laurencin, C., Khan, Y. & El-Amin, S.F. Bone graft substitutes. *Expert Rev Med Devices* **3**, 49-57 (2006).

89. Finkemeier, C.G. Bone-grafting and bone-graft substitutes. *J Bone Joint Surg.Am.* **84-A**, 454-464 (2002).

90. Sorger, J.I. et al. Allograft fractures revisited. *Clin Orthop Relat Res*, 66-74 (2001).

91. Mankin, H.J., Hornicek, F.J. & Raskin, K.A. Infection in massive bone allografts. *Clin Orthop Relat Res*, 210-216 (2005).

92. Boden, S.D. The ABCs of BMPs. *Orthop Nurs* **24**, 49-52; quiz 53-44 (2005).

93. Cancedda, R., Giannoni, P. & Mastrogiacomo, M. A tissue engineering approach to bone repair in large animal models and in clinical practice. *Biomaterials* **28**, 4240-4250 (2007).

94. Cahill, K.S., Chi, J.H., Day, A. & Claus, E.B. Prevalence, complications, and hospital charges associated with use of bone-morphogenetic proteins in spinal fusion procedures. *JAMA : the journal of the American Medical Association* **302**, 58-66 (2009).

95. Desai, B.M. Osteobiologics. *Am J Orthop (Belle Mead NJ)* **36**, 8-11 (2007).

96. Carragee, E.J., Hurwitz, E.L. & Weiner, B.K. A critical review of recombinant human bone morphogenetic protein-2 trials in spinal surgery: emerging safety concerns and lessons learned. *The spine journal : official journal of the North American Spine Society* **11**, 471-491 (2011).

97. Morra, M. et al. Surface analysis and effects on interfacial bone microhardness of collagen-coated titanium implants: a rabbit model. *Int J Oral Maxillofac Implants* **20**, 23-30 (2005).

98. Schliephake, H. et al. Effect of immobilized bone morphogenic protein 2 coating of titanium implants on peri-implant bone formation. *Clin Oral Implants Res* **16**, 563-569 (2005).

99. Svehla, M., Morberg, P., Bruce, W. & Walsh, W.R. No effect of a type I collagen gel coating in uncemented implant fixation. *J Biomed Mater Res B Appl Biomater* **74**, 423-428 (2005).

100. Rammelt, S. et al. Coating of titanium implants with collagen, RGD peptide and chondroitin sulfate. *Biomaterials* **27**, 5561-5571 (2006).

101. Liu, X. et al. Repairing goat tibia segmental bone defect using scaffold cultured with mesenchymal stem cells. *J Biomed Mater Res B Appl Biomater*.

102. Caiazza, S. et al. Evaluation of guided bone regeneration in rabbit femur using collagen membranes. *Implant Dent* **9**, 219-225 (2000).

103. d'Aquino, R. et al. Human mandible bone defect repair by the grafting of dental pulp stem/progenitor cells and collagen sponge biocomplexes. *Eur Cell Mater* **18**, 75-83 (2009).

104. Ben-Ari, A. et al. Isolation and implantation of bone marrow-derived mesenchymal stem cells with fibrin micro beads to repair a critical-size bone defect in mice. *Tissue Eng Part A* **15**, 2537-2546 (2009).

105. Kim, S.J., Jang, J.D. & Lee, S.K. Treatment of long tubular bone defect of rabbit using autologous cultured osteoblasts mixed with fibrin. *Cytotechnology* **54**, 115-120 (2007).

106. Karp, J.M., Sarraf, F., Shoichet, M.S. & Davies, J.E. Fibrin-filled scaffolds for bone-tissue engineering: An in vivo study. *J Biomed Mater Res A* **71**, 162-171 (2004).

107. Perka, C. et al. Segmental bone repair by tissue-engineered periosteal cell transplants with bioresorbable fleece and fibrin scaffolds in rabbits. *Biomaterials* **21**, 1145-1153 (2000).

108. Solchaga, L.A., Dennis, J.E., Goldberg, V.M. & Caplan, A.I. Hyaluronic acid-based polymers as cell carriers for tissue-engineered repair of bone and cartilage. *J Orthop Res* **17**, 205-213 (1999).

109. Paderni, S., Terzi, S. & Amendola, L. Major bone defect treatment with an osteoconductive bone substitute. *Chir Organi Mov* **93**, 89-96 (2009).

110. Barros, R.R. et al. Effect of biofunctionalized implant surface on osseointegration: a histomorphometric study in dogs. *Braz Dent J* **20**, 91-98 (2009).

111. Lin, H., Xu, H., Zhang, X. & de Groot, K. Tensile tests of interface between bone and plasma-sprayed HA coating-titanium implant. *J Biomed Mater Res* **43**, 113-122 (1998).

112. Kurkalli, B.G., Gurevitch, O., Sosnik, A., Cohn, D. & Slavin, S. Repair of bone defect using bone marrow cells and demineralized bone matrix supplemented with polymeric materials. *Curr Stem Cell Res Ther* **5**, 49-56.

113. Suckow, M.A., Voytik-Harbin, S.L., Terril, L.A. & Badylak, S.F. Enhanced bone regeneration using porcine small intestinal submucosa. *J Invest Surg* **12**, 277-287 (1999).

114. Graf, H.L., Stoeva, S., Armbruster, F.P., Neuhaus, J. & Hilbig, H. Effect of bone sialoprotein and collagen coating on cell attachment to TICER and pure titanium implant surfaces. *Int J Oral Maxillofac Surg* **37**, 634-640 (2008).

115. Shakesheff, K., Cannizzaro, S. & Langer, R. Creating biomimetic micro-environments with synthetic polymer-peptide hybrid molecules. *J Biomater Sci Polym Ed* **9**, 507-518 (1998).

116. Emsley, J., Knight, C.G., Farndale, R.W. & Barnes, M.J. Structure of the integrin alpha2beta1-binding collagen peptide. *J Mol Biol* **335**, 1019-1028 (2004).

117. Knight, C.G. et al. Identification in collagen type I of an integrin alpha2 beta1-binding site containing an essential GER sequence. *J Biol Chem* **273**, 33287-33294 (1998).

118. Leahy, D.J., Aukhil, I. & Erickson, H.P. 2.0 A crystal structure of a four-domain segment of human fibronectin encompassing the RGD loop and synergy region. *Cell* **84**, 155-164 (1996).

119. Aota, S., Nomizu, M. & Yamada, K.M. The short amino acid sequence Pro-His-Ser-Arg-Asn in human fibronectin enhances cell-adhesive function. *J Biol Chem* **269**, 24756-24761 (1994).

120. Humphries, M.J., Akiyama, S.K., Komoriya, A., Olden, K. & Yamada, K.M. Identification of an alternatively spliced site in human plasma fibronectin that mediates cell type-specific adhesion. *J Cell Biol* **103**, 2637-2647 (1986).

121. Komoriya, A. et al. The minimal essential sequence for a major cell type-specific adhesion site (CS1) within the alternatively spliced type III connecting segment domain of fibronectin is leucine-aspartic acid-valine. *J Biol Chem* **266**, 15075-15079 (1991).

122. Petrie, T.A., Capadona, J.R., Reyes, C.D. & Garcia, A.J. Integrin specificity and enhanced cellular activities associated with surfaces presenting a recombinant fibronectin fragment compared to RGD supports. *Biomaterials* **27**, 5459-5470 (2006).

123. Barber, T.A. et al. Peri-implant bone formation and implant integration strength of peptide-modified p(AAM-co-EG/AAC) interpenetrating polymer network-coated titanium implants. *J Biomed Mater Res A* **80**, 306-320 (2007).

124. Wojtowicz, A.M. et al. Coating of biomaterial scaffolds with the collagen-mimetic peptide GFOGER for bone defect repair. *Biomaterials* **31**, 2574-2582.

125. Thorwarth, M. et al. Bioactivation of an anorganic bone matrix by P-15 peptide for the promotion of early bone formation. *Biomaterials* **26**, 5648-5657 (2005).

126. Morton, L.F. et al. Conformation-dependent platelet adhesion to collagen involving integrin alpha 2 beta 1-mediated and other mechanisms: multiple alpha 2 beta 1-recognition sites in collagen type I. *Biochem J* **299 (Pt 3)**, 791-797 (1994).

127. Knight, C.G. et al. The collagen-binding A-domains of integrins alpha(1)beta(1) and alpha(2)beta(1) recognize the same specific amino acid sequence, GFOGER, in native (triple-helical) collagens. *J Biol Chem* **275**, 35-40 (2000).

128. Reyes, C.D. & Garcia, A.J. Engineering integrin-specific surfaces with a triple-helical collagen-mimetic peptide. *J Biomed Mater Res A* **65**, 511-523 (2003).

129. Reyes, C.D. & Garcia, A.J. Alpha2beta1 integrin-specific collagen-mimetic surfaces supporting osteoblastic differentiation. *J Biomed Mater Res A* **69**, 591-600 (2004).

130. Wojtowicz, A.M. et al. Coating of biomaterial scaffolds with the collagen-mimetic peptide GFOGER for bone defect repair. *Biomaterials* **31**, 2574-2582 (2010).

131. Hennessy, K.M. et al. The effect of collagen I mimetic peptides on mesenchymal stem cell adhesion and differentiation, and on bone formation at hydroxyapatite surfaces. *Biomaterials* **30**, 1898-1909 (2009).

132. Staatz, W.D. et al. Identification of a tetrapeptide recognition sequence for the alpha 2 beta 1 integrin in collagen. *J Biol Chem* **266**, 7363-7367 (1991).

133. McCann, T.J., Mason, W.T., Meikle, M.C. & McDonald, F. A collagen peptide motif activates tyrosine kinase-dependent calcium signalling pathways in human osteoblast-like cells. *Matrix Biol* **16**, 273-283 (1997).

134. Harbers, G.M. & Healy, K.E. The effect of ligand type and density on osteoblast adhesion, proliferation, and matrix mineralization. *J Biomed Mater Res A* **75**, 855-869 (2005).

135. Bhatnagar, R.S., Qian, J.J. & Gough, C.A. The role in cell binding of a beta-bend within the triple helical region in collagen alpha 1 (I) chain: structural and biological evidence for conformational tautomerism on fiber surface. *J Biomol Struct Dyn* **14**, 547-560 (1997).

136. Bhatnagar, R.S. et al. Design of biomimetic habitats for tissue engineering with P-15, a synthetic peptide analogue of collagen. *Tissue Eng* **5**, 53-65 (1999).

137. Nguyen, H., Qian, J.J., Bhatnagar, R.S. & Li, S. Enhanced cell attachment and osteoblastic activity by P-15 peptide-coated matrix in hydrogels. *Biochem Biophys Res Commun* **311**, 179-186 (2003).

138. Artzi, Z. et al. Histomorphometric evaluation of natural mineral combined with a synthetic cell-binding peptide (P-15) in critical-size defects in the rat calvaria. *Int J Oral Maxillofac Implants* **23**, 1063-1070 (2008).

139. Radhakrishnan, S. & Anusuya, C.N. Comparative clinical evaluation of combination anorganic bovine-derived hydroxyapatite matrix (ABM)/cell binding peptide (P-15) and open flap debridement (DEBR) in human periodontal osseous defects: a 6 month pilot study. *J Int Acad Periodontol* **6**, 101-107 (2004).

140. Bhongade, M.L. & Tiwari, I.R. A comparative evaluation of the effectiveness of an anorganic bone matrix/cell binding peptide with an open flap debridement in human infrabony defects: a clinical and radiographic study. *J Contemp Dent Pract* **8**, 25-34 (2007).

141. Gomar, F., Orozco, R., Villar, J.L. & Arrizabalaga, F. P-15 small peptide bone graft substitute in the treatment of non-unions and delayed union. A pilot clinical trial. *Int Orthop* **31**, 93-99 (2007).

142. Pytela, R., Pierschbacher, M.D., Argraves, S., Suzuki, S. & Ruoslahti, E. Arginine-glycine-aspartic acid adhesion receptors. *Methods Enzymol* **144**, 475-489 (1987).

143. Redick, S.D., Settles, D.L., Briscoe, G. & Erickson, H.P. Defining fibronectin's cell adhesion synergy site by site-directed mutagenesis. *J Cell Biol* **149**, 521-527 (2000).

144. Ho, J.E., Barber, T.A., Virdi, A.S., Sumner, D.R. & Healy, K.E. The effect of enzymatically degradable IPN coatings on peri-implant bone formation and implant fixation. *J Biomed Mater Res A* **81**, 720-727 (2007).

145. Ferris, D.M. et al. RGD-coated titanium implants stimulate increased bone formation in vivo. *Biomaterials* **20**, 2323-2331 (1999).

146. Hennessy, K.M. et al. The effect of RGD peptides on osseointegration of hydroxyapatite biomaterials. *Biomaterials* **29**, 3075-3083 (2008).

147. Elmengaard, B., Bechtold, J.E. & Soballe, K. In vivo study of the effect of RGD treatment on bone ongrowth on press-fit titanium alloy implants. *Biomaterials* **26**, 3521-3526 (2005).

148. Elmengaard, B., Bechtold, J.E. & Soballe, K. In vivo effects of RGD-coated titanium implants inserted in two bone-gap models. *J Biomed Mater Res A* **75**, 249-255 (2005).

149. Schliephake, H. et al. Effect of RGD peptide coating of titanium implants on periimplant bone formation in the alveolar crest. An experimental pilot study in dogs. *Clin Oral Implants Res* **13**, 312-319 (2002).

150. Petrie, T.A. et al. The effect of integrin-specific bioactive coatings on tissue healing and implant osseointegration. *Biomaterials* **29**, 2849-2857 (2008).

151. Miljkovic, N.D. et al. Calcium aluminate, RGD-modified calcium aluminate, and beta-tricalcium phosphate implants in a calvarial defect. *J Craniofac Surg* **20**, 1538-1543 (2009).

152. Garcia, A.J., Schwarzbauer, J.E. & Boettiger, D. Distinct activation states of alpha5beta1 integrin show differential binding to RGD and synergy domains of fibronectin. *Biochemistry* **41**, 9063-9069 (2002).

153. Pierschbacher, M.D. & Ruoslahti, E. Cell attachment activity of fibronectin can be duplicated by small synthetic fragments of the molecule. *Nature* **309**, 30-33 (1984).

154. Petrie, T.A., Reyes, C.D., Burns, K.L. & Garcia, A.J. Simple application of fibronectin-mimetic coating enhances osseointegration of titanium implants. *J Cell Mol Med* (2008).

155. Benoit, D.S. & Anseth, K.S. The effect on osteoblast function of colocalized RGD and PHSRN epitopes on PEG surfaces. *Biomaterials* **26**, 5209-5220 (2005).

156. Kim, T.I. et al. Design and biological activity of synthetic oligopeptides with Pro-His-Ser-Arg-Asn (PHSRN) and Arg-Gly-Asp (RGD) motifs for human osteoblast-like cell (MG-63) adhesion. *Biotechnology Letters* **24**, 2029-2033 (2002).

157. Healy, K.E., Rezania, A. & Stile, R.A. Designing biomaterials to direct biological responses. *Ann N Y Acad Sci* **875**, 24-35 (1999).

158. Rezania, A. & Healy, K.E. Integrin subunits responsible for adhesion of human osteoblast-like cells to biomimetic peptide surfaces. *J Orthop Res* **17**, 615-623 (1999).

159. Rezania, A. & Healy, K.E. Biomimetic peptide surfaces that regulate adhesion, spreading, cytoskeletal organization, and mineralization of the matrix deposited by osteoblast-like cells. *Biotechnol Prog* **15**, 19-32 (1999).

160. Stile, R.A. & Healy, K.E. Thermo-responsive peptide-modified hydrogels for tissue regeneration. *Biomacromolecules* **2**, 185-194 (2001).

161. Schuler, M. et al. Comparison of the response of cultured osteoblasts and osteoblasts outgrown from rat calvarial bone chips to nonfouling KRSR and FHRRIKA-peptide modified rough titanium surfaces. *J Biomed Mater Res B Appl Biomater* **91**, 517-527 (2009).

162. Dee, K.C., Andersen, T.T. & Bizios, R. Design and function of novel osteoblast-adhesive peptides for chemical modification of biomaterials. *J Biomed Mater Res* **40**, 371-377 (1998).

163. Dettin, M. et al. Novel osteoblast-adhesive peptides for dental/orthopedic biomaterials. *J Biomed Mater Res* **60**, 466-471 (2002).

164. Hasenbein, M.E., Andersen, T.T. & Bizios, R. Micropatterned surfaces modified with select peptides promote exclusive interactions with osteoblasts. *Biomaterials* **23**, 3937-3942 (2002).

165. Nelson, M., Balasundaram, G. & Webster, T.J. Increased osteoblast adhesion on nanoparticulate crystalline hydroxyapatite functionalized with KRSR. *Int J Nanomedicine* **1**, 339-349 (2006).

166. Balasundaram, G. & Webster, T.J. Increased osteoblast adhesion on nanograined Ti modified with KRSR. *J Biomed Mater Res A* **80**, 602-611 (2007).

167. Rapuano, B.E., Wu, C. & MacDonald, D.E. Osteoblast-like cell adhesion to bone sialoprotein peptides. *J Orthop Res* **22**, 353-361 (2004).

168. Dettin, M. et al. Evaluation of silicon dioxide-based coating enriched with bioactive peptides mapped on human vitronectin and fibronectin: in vitro and in vivo assays. *Tissue Eng* **12**, 3509-3523 (2006).

169. Bagno, A. et al. Human osteoblast-like cell adhesion on titanium substrates covalently functionalized with synthetic peptides. *Bone* **40**, 693-699 (2007).

170. Cacchioli, A., Ravanetti, F., Bagno, A., Dettin, M. & Gabbi, C. Human Vitronectin-Derived Peptide Covalently Grafted onto Titanium Surface Improves Osteogenic Activity: A Pilot In Vivo Study on Rabbits. *Tissue Eng Part A* **15**, 2917-2926 (2009).

171. Dettin, M. et al. Covalent surface modification of titanium oxide with different adhesive peptides: surface characterization and osteoblast-like cell adhesion. *J Biomed Mater Res A* **90**, 35-45 (2009).

172. Shin, H., Zygourakis, K., Farach-Carson, M.C., Yaszemski, M.J. & Mikos, A.G. Attachment, proliferation, and migration of marrow stromal osteoblasts cultured on biomimetic hydrogels modified with an osteopontin-derived peptide. *Biomaterials* **25**, 895-906 (2004).

173. Kim, H.E., Kim, H.W. & Jang, J.H. Identification and characterization of a novel heparin-binding peptide for promoting osteoblast adhesion and proliferation by screening an Escherichia coli cell surface display peptide library. *J Pept Sci* **15**, 43-47 (2009).

174. Aplin, A.E., Hogan, B.P., Tomeu, J. & Juliano, R.L. Cell adhesion differentially regulates the nucleocytoplasmic distribution of active MAP kinases. *J Cell Sci* **115**, 2781-2790 (2002).

175. Guldberg, R.E., Lin, A.S., Coleman, R., Robertson, G. & Duvall, C. Microcomputed tomography imaging of skeletal development and growth. *Birth defects research. Part C, Embryo today : reviews* **72**, 250-259 (2004).

176. Buie, H.R., Campbell, G.M., Klinck, R.J., MacNeil, J.A. & Boyd, S.K. Automatic segmentation of cortical and trabecular compartments based on a dual threshold technique for in vivo micro-CT bone analysis. *Bone* **41**, 505-515 (2007).

177. Duvall, C.L., Taylor, W.R., Weiss, D., Wojtowicz, A.M. & Guldberg, R.E. Impaired angiogenesis, early callus formation, and late stage remodeling in fracture healing of osteopontin-deficient mice. *J Bone Miner Res* **22**, 286-297 (2007).

178. Davey, R.A. et al. Decreased body weight in young Osterix-Cre transgenic mice results in delayed cortical bone expansion and accrual. *Transgenic research* **21**, 885-893 (2012).

179. Aszodi, A., Hunziker, E.B., Brakebusch, C. & Fassler, R. Beta1 integrins regulate chondrocyte rotation, G1 progression, and cytokinesis. *Genes Dev* **17**, 2465-2479 (2003).

180. Raducanu, A., Hunziker, E.B., Drosse, I. & Aszodi, A. Beta1 integrin deficiency results in multiple abnormalities of the knee joint. *J Biol Chem* **284**, 23780-23792 (2009).

181. Blumbach, K. et al. Dwarfism in mice lacking collagen-binding integrins alpha2beta1 and alpha11beta1 is caused by severely diminished IGF-1 levels. *J Biol Chem* **287**, 6431-6440 (2012).

182. Popova, S.N. et al. Alpha11 beta1 integrin-dependent regulation of periodontal ligament function in the erupting mouse incisor. *Molecular and cellular biology* **27**, 4306-4316 (2007).

183. Chang, D.D., Wong, C., Smith, H. & Liu, J. ICAP-1, a novel beta1 integrin cytoplasmic domain-associated protein, binds to a conserved and functionally important NPXY sequence motif of beta1 integrin. *J Cell Biol* **138**, 1149-1157 (1997).

184. Millon-Fremillon, A. et al. Cell adaptive response to extracellular matrix density is controlled by ICAP-1-dependent beta1-integrin affinity. *J Cell Biol* **180**, 427-441 (2008).

185. Bouvard, D. et al. Defective osteoblast function in ICAP-1-deficient mice. *Development* **134**, 2615-2625 (2007).

186. Schmidmaier, G., Schwabe, P., Strobel, C. & Wildemann, B. Carrier systems and application of growth factors in orthopaedics. *Injury* **39 Suppl 2**, S37-43 (2008).

187. Phelps, E.A. et al. Maleimide cross-linked bioactive PEG hydrogel exhibits improved reaction kinetics and cross-linking for cell encapsulation and in situ delivery. *Advanced materials* **24**, 64-70, 62 (2012).

188. Martino, M.M. et al. Engineering the growth factor microenvironment with fibronectin domains to promote wound and bone tissue healing. *Science translational medicine* **3**, 100ra189 (2011).

189. Atala, A., Kasper, F.K. & Mikos, A.G. Engineering complex tissues. *Science translational medicine* **4**, 160rv112 (2012).

190. Salinas, C.N. & Anseth, K.S. Mesenchymal stem cells for craniofacial tissue regeneration: designing hydrogel delivery vehicles. *J Dent Res* **88**, 681-692 (2009).

191. Patterson, J. & Hubbell, J.A. SPARC-derived protease substrates to enhance the plasmin sensitivity of molecularly engineered PEG hydrogels. *Biomaterials* **32**, 1301-1310 (2011).

192. Patterson, J. & Hubbell, J.A. Enhanced proteolytic degradation of molecularly engineered PEG hydrogels in response to MMP-1 and MMP-2. *Biomaterials* **31**, 7836-7845 (2010).

193. Lutolf, M.P. et al. Synthetic matrix metalloproteinase-sensitive hydrogels for the conduction of tissue regeneration: engineering cell-invasion characteristics. *Proc Natl Acad Sci U S A* **100**, 5413-5418 (2003).

194. Fiedler, J., Roderer, G., Gunther, K.P. & Brenner, R.E. BMP-2, BMP-4, and PDGF-bb stimulate chemotactic migration of primary human mesenchymal progenitor cells. *Journal of cellular biochemistry* **87**, 305-312 (2002).

195. Chen, C., Uludag, H., Wang, Z. & Jiang, H. Noggin suppression decreases BMP-2-induced osteogenesis of human bone marrow-derived mesenchymal stem cells in vitro. *Journal of cellular biochemistry* **113**, 3672-3680 (2012).

196. Lewandrowski, K.U., Nanson, C. & Calderon, R. Vertebral osteolysis after posterior interbody lumbar fusion with recombinant human bone morphogenetic

protein 2: a report of five cases. *The spine journal : official journal of the North American Spine Society* **7**, 609-614 (2007).

197. Knox, J.B., Dai, J.M., 3rd & Orchowski, J. Osteolysis in transforaminal lumbar interbody fusion with bone morphogenetic protein-2. *Spine* **36**, 672-676 (2011).

198. Kaneko, H. et al. Direct stimulation of osteoclastic bone resorption by bone morphogenetic protein (BMP)-2 and expression of BMP receptors in mature osteoclasts. *Bone* **27**, 479-486 (2000).

199. Okamoto, M., Murai, J., Yoshikawa, H. & Tsumaki, N. Bone morphogenetic proteins in bone stimulate osteoclasts and osteoblasts during bone development. *J Bone Miner Res* **21**, 1022-1033 (2006).

200. Kanakaris, N.K. & Giannoudis, P.V. Clinical applications of bone morphogenetic proteins: current evidence. *Journal of surgical orthopaedic advances* **17**, 133-146 (2008).

201. O'Brien, F.J., Harley, B.A., Yannas, I.V. & Gibson, L.J. The effect of pore size on cell adhesion in collagen-GAG scaffolds. *Biomaterials* **26**, 433-441 (2005).

202. Azad, V. et al. rhBMP-2 enhances the bone healing response in a diabetic rat segmental defect model. *Journal of orthopaedic trauma* **23**, 267-276 (2009).

203. Osbun, J.W. et al. A multicenter, single-blind, prospective randomized trial to evaluate the safety of a polyethylene glycol hydrogel (Duraseal Dural Sealant System) as a dural sealant in cranial surgery. *World neurosurgery* **78**, 498-504 (2012).

204. Cosgrove, G.R. et al. Safety and efficacy of a novel polyethylene glycol hydrogel sealant for watertight dural repair. *Journal of neurosurgery* **106**, 52-58 (2007).

205. Street, J. et al. Vascular endothelial growth factor stimulates bone repair by promoting angiogenesis and bone turnover. *Proc Natl Acad Sci U S A* **99**, 9656-9661 (2002).

206. Martino, M.M., Briquez, P.S., Ranga, A., Lutolf, M.P. & Hubbell, J.A. Heparin-binding domain of fibrin(ogen) binds growth factors and promotes tissue repair when incorporated within a synthetic matrix. *Proc Natl Acad Sci U S A* **110**, 4563-4568 (2013).